



## Review

## Mapping local climate zones for cities: A large review



Fan Huang <sup>a,1</sup>, Sida Jiang <sup>a,1</sup>, Wenzheng Zhan <sup>a,b,\*</sup>, Benjamin Bechtel <sup>c</sup>, Zihan Liu <sup>a</sup>, Matthias Demuzere <sup>c</sup>, Yuan Huang <sup>d</sup>, Yong Xu <sup>e</sup>, Lei Ma <sup>f</sup>, Wanjun Xia <sup>g</sup>, Jinling Quan <sup>h</sup>, Lu Jiang <sup>a</sup>, Jiameng Lai <sup>a</sup>, Chengguang Wang <sup>a</sup>, Fanhua Kong <sup>a</sup>, Huilin Du <sup>a</sup>, Shiqi Miao <sup>a</sup>, Yangyi Chen <sup>a</sup>, Jike Chen <sup>i</sup>

<sup>a</sup> Jiangsu Provincial Key Laboratory of Geographic Information Science and Technology, International Institute for Earth System Science, Nanjing University, Nanjing 210023, China

<sup>b</sup> Jiangsu Center for Collaborative Innovation in Geographical Information Resource Development and Application, Nanjing 210023, China

<sup>c</sup> Department of Geography, Ruhr-University Bochum, 44801 Bochum, Germany

<sup>d</sup> Department of Urban and Rural Planning, School of Architecture and Design, Southwest Jiaotong University, Chengdu 610000, China

<sup>e</sup> School of Geography and Remote Sensing, Guangzhou University, Guangzhou 510006, China

<sup>f</sup> School of Geography and Ocean Science, Nanjing University, Nanjing 210023, China

<sup>g</sup> Library, Southwest Jiaotong University, Chengdu 611756, China

<sup>h</sup> State Key Laboratory of Resources and Environmental Information System, Institute of Geographic Sciences and Natural Resources Research, Chinese Academy of Sciences, Beijing 100101, China

<sup>i</sup> School of Remote Sensing & Geomatics Engineering, Nanjing University of Information Science & Technology, Nanjing 210044, China

## ARTICLE INFO

## ABSTRACT

## Keywords:

Local climate zone (LCZ)  
LCZ mapping  
Remote sensing (RS)  
Geographic information system (GIS)  
Urban climate

The local climate zone (LCZ) system provides a universal classification mechanism for urban and natural landscapes and plays an increasingly important role in urban climate research. With the rapid development of various LCZ mapping methods, a thorough survey of the LCZ mapping literature is urgently needed to better understand current progress, challenges, and future directions. Accordingly, this study provided a comprehensive review of the LCZ mapping literature during 2012–2021, with a detailed analysis on literature statistics, research topics, LCZ cities, and active research groups. Furthermore, remote sensing (RS)-based LCZ mapping methods were elucidated from feature sets, classification units, training areas, classification algorithms, and accuracy assessment; geographic information system (GIS)-based LCZ mapping methods were elaborated from LCZ parameters, basic spatial units, classification algorithms, and accuracy assessment; and their combination methods

**Abbreviations:** Ah, Anthropogenic heat; AMDA, Adaptive Multisource Domain Adaptation; ANN, Artificial Neural Network; AR, Aspect Ratio; ASTER, Advanced Spaceborne Thermal Emission and Reflection Radiometer; BSF, Building Surface Fraction; CCF, Canonical Correlation Forest; CNN, Convolutional Neural Network; CRF, Conditional Random Field; DEM, Digital Elevation Model; DenseNet, Dense Convolutional Network; DFN, Dynamic Filter Network; DMSP-OLS, Defense Meteorological Satellite Program Operational Linescan System; DNN, Deep Neural Network; DSM, Digital Surface Model; DTM, Digital Terrain Model; ENLIGHT, ENabling the analysis of Global urban HeaT; GBM, Gradient Boosting Machine; GCN, Graph Convolution Network; GEE, Google Earth Engine; GFCH, Global Forest Canopy Height; GIS, Geographic Information System; GUF, Global Urban Footprint; HRE, Height of Roughness Elements; ICUC, International Conference on Urban Climate; IFSAR, Interferometric Synthetic Aperture Radar; IGARSS, International Geoscience and Remote Sensing Symposium; ISF, Impervious Surface Fraction; JURSE, Joint Urban Remote Sensing Event; LCZ, Local Climate Zone; MapUCE, Urban Climate, Human behavior, and Energy consumption: from LCZ mapping to simulation and urban planning; ML, Maximum Likelihood; MLP, Multi-layer Perceptron; MRF, Markov Random Field; MRS, Multi-Resolution Segmentation; MSCNN, Multi-Scale CNN; MSPPF-nets, Multi-Scale Input Spatial Pyramid Pooling Fusion Networks; NB, Naive Bayes; NDVI, Normalized Difference Vegetation Index; NN, Neural Network; OA, Overall Accuracy; OBIA, Object based Image Analysis; OSM, OpenStreetMap; PA, Producer Accuracy; PALSAR, Phased Array type L-band Synthetic Aperture Radar; PSF, Pervious Surface Fraction; RCM, Regional Climate Model; Re-ResNet, Recurrent Residual Network; ResNet, Residual Neural Network; RF, Random Forest; RNN, Recurrent Neural Network; RoF, Rotation Forest; ROSIS, Reflective Optics System Imaging Spectrometer; RS, Remote Sensing; SAD, Surface Admittance; SAL, Surface Albedo; SAR, Synthetic Aperture Radar; SOM, Self-Organization Map; SUEWS, Surface Urban Energy and Water Balance Scheme; SVF, Sky View Factor; SVM, Support Vector Machine; TRC, Terrain Roughness Class; UA, User Accuracy; UCM, Urban Canopy Model; URBAN-PATH, URBAN PATterns of Human thermal conditions; VGI, Volunteered Geographic Information; VIIRS, Visible Infrared Imaging Radiometer Suite; WA, Weighted Accuracy; WRF, Weather Research and Forecasting Model; WUDAPT, World Urban Database and Access Portal Tools; XGBoost, Extreme Gradient Boosting.

\* Corresponding author at: Nanjing University at Xianlin Campus, No. 163 Xianlin Avenue, Qixia District, Nanjing, Jiangsu Province 210023, China.

E-mail address: [zhanwenfeng@nju.edu.cn](mailto:zhanwenfeng@nju.edu.cn) (W. Zhan).

<sup>1</sup> Fan Huang and Sida Jiang contributed equally.

were summarized from two typical integration strategies. Finally, several challenges and future directions for LCZ mapping were discussed. The topics include exploiting multi-source RS and GIS data, determining appropriate LCZ mapping unit sizes, acquiring high-quality LCZ ground truth data, improving LCZ classification algorithms, optimizing LCZ parameters and subclasses, exploring the transferability of LCZ models, conducting global interannual LCZ mapping, and expanding the application of LCZs. The research community can quickly obtain abundant information on the LCZ mapping literature, understand the frameworks of different LCZ mapping methods, and inspire new directions for future research.

## 1. Introduction

Global climate change and rapid urbanization are placing cities worldwide under increasing risks of extreme climate events and natural disasters (IPCC, 2021). It is anticipated that by 2050, over two-thirds of the global population will reside in cities (United Nations, 2019), thus placing more people, particularly vulnerable groups such as the elderly and children, at greater risk of negative climate effects, such as heat stress (Tuholske et al., 2021; Zhao et al., 2021) and climate-sensitive infectious diseases (Alcayna et al., 2022). In response to the increasing severity of modern urban climate risks, extensive research has been conducted to gain a comprehensive understanding of urban climate through observations and simulations (Kleereker et al., 2017; Krayenhoff et al., 2018; Manoli et al., 2019; Masson et al., 2020; Sun et al., 2016; Zhao et al., 2021). Urban climate specifics are closely related to urban form and urban function. Traditionally, urban climate research adopts the simple ‘urban-rural’ dichotomy, ignoring intra-urban differences; however, a more detailed description of urban form and function is required for in-depth urban climate research (González et al., 2021).

Over the past decades, the research community has developed several urban classification schemes to study urban climate (Auer, 1978; Ellefsen, 1991; Grimmond and Oke, 1999; Lorian and Grimmond,

2012; Oke, 2004; Ren et al., 2011; Stewart and Oke, 2009). Although these classification schemes indeed promoted urban climate research to a certain extent, they have not yet formed a unified classification system applicable to global cities. To this end, Stewart and Oke (2012) formally proposed the Local Climate Zones (LCZs) classification system as a climate-based generic framework for urban climate research. LCZs are defined as “regions of uniform surface cover, structure, material, and human activity that span hundreds of meters to several kilometers horizontally” (Stewart and Oke, 2012). The standard LCZs consist of ten built types (LCZs 1–10), and seven land cover types (LCZs A–G, Fig. 1). Each LCZ has a specific range of climate-relevant physical parameters. Therefore, the LCZ system establishes a fundamental research framework for urban climate studies and standardizes the worldwide exchange of urban climate knowledge.

Numerous studies have conducted LCZ classification for field sites. In general, two approaches are employed, i.e., the three-step process given in Stewart and Oke (2012) and the visual interpretation method. First, the three-step process includes collecting site metadata, defining the thermal source area, and selecting the best-fit LCZ. The thermal source area for a field site is a circle of influence (or footprint) with a radius extending from meters to kilometers (Oke, 2004). This method has been widely used to classify field sites into LCZs in different cities (Amini-pouri et al., 2019; Emmanuel and Loconsole, 2015; Fenner et al., 2014;

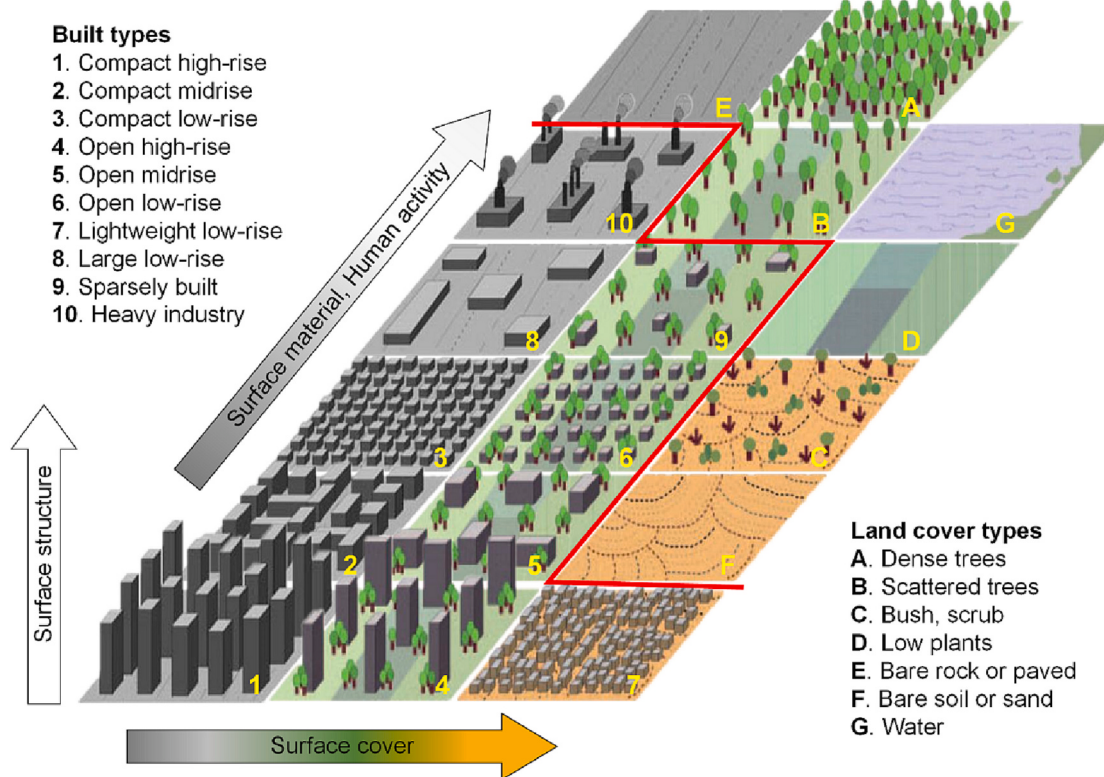


**Fig. 1.** The 17 standard Local Climate Zones (LCZs): 10 built types (LCZs 1–10) and 7 land cover types (LCZs A–G), modified from Stewart and Oke (2012). The red line divides built types and land cover types. (For interpretation of the references to colour in this figure legend, the reader is referred to the web version of this article.)

Lehnert et al., 2015; Lelovics et al., 2016; Liu et al., 2018; Middel et al., 2014; Müller et al., 2014; Savic et al., 2013; Siu and Hart, 2013; Stewart et al., 2014; Wang et al., 2016). Second, the visual interpretation method classifies field sites into LCZs based on expert knowledge by viewing satellite images and conducting field survey. This method requires expertise in remote sensing image recognition and familiarity with the local urban layout. Although the visual interpretation method can produce a reasonably accurate match between field sites and LCZs, the three-step method supports a more objective and reproducible classification (Stewart and Oke, 2019). However, both methods are limited to the site scale, which become time-consuming and labor-intensive when directly extended to the city scale. To overcome these limitations, remote sensing (RS) and geographic information system (GIS) tools have been employed for generating LCZ maps for cities.

In the past decade, various LCZ mapping methods have been proposed, yet the development of LCZ mapping is still in a disorderly fashion. To date, Quan and Bansal (2021) conducted a review of 16 representative GIS-based LCZ mapping studies, Ma et al. (2021b) provided a concise survey of RS-based per-pixel LCZ mapping methods, and Lehnert et al. (2021) presented a review of mapping LCZs and their applications in Europe. Although these papers have advanced our understanding of LCZ mapping research to some extent, there are still several limitations, such as incomplete survey of LCZ mapping literature and focusing only on a single category of LCZ mapping methods, making it difficult to gain a comprehensive understanding of LCZ mapping. With the rapid development of LCZ mapping research, a thorough review of the LCZ mapping literature is urgently needed to better understand current progress and challenges and to inform future directions. Accordingly, the present paper comprehensively reviews the total LCZ mapping literature from 2012 to 2021. We provide a statistical analysis of LCZ mapping literature, elaborate the frameworks of different LCZ mapping methods, and discussed several deficiencies, challenges, and future directions for LCZ mapping. This paper provides abundant information on LCZ mapping literature, allowing the research community to quickly grasp the theoretical and methodological frameworks, and

inspire new directions for LCZ mapping research.

## 2. Literature survey

A two-step procedure was used to screen the LCZ mapping literature: First, the peer-reviewed papers from 2012 to 2021 that contain ‘local climate zone(s)’ and/or ‘LCZ(s)’ in the title, abstract, or keywords were searched via Google Scholar, Web of Science, and Microsoft Academic. We categorized all these papers as LCZ papers. Note that doctoral dissertations and non-English journal papers were excluded due to the limitations in accessibility and comprehensibility. Second, we scrutinized each LCZ paper and labeled those that elaborate how to create LCZ maps for cities as LCZ mapping papers. Note that LCZ papers that directly use previous/existing LCZ maps were excluded, as were those that classify field sites rather than cities into LCZs. Accordingly, of the 394 LCZ papers surveyed, 248 were categorized as LCZ mapping papers. On this basis, we analyzed the literature from four aspects: literature statistics, research topics, LCZ cities, and active research groups.

### 2.1. Literature statistics

LCZ mapping has achieved significant progress in recent decade, which can be indicated by the number of papers published and citations. (1) *Number of LCZ mapping literature*: The number of LCZ mapping papers accounted for more than half of all LCZ papers per year (Fig. 2a). Specifically, although initially increasing slowly, the number of LCZ mapping papers rose dramatically after 2015 due to the initiative of the World Urban Database and Access Portal Tools (WUDAPT) project (Bechtel et al., 2015; Mills et al., 2015). With the wide application of multi-source RS and GIS data and the introduction of various machine learning algorithms, the number of LCZ mapping papers has continued to rise annually until 2020, followed by a slight decline in 2021. (2) *Number of literature citations*: The pioneering work of Stewart and Oke (2012) has received a steadily increasing number of citations annually (Fig. 2b). Meanwhile, several other representative LCZ mapping papers

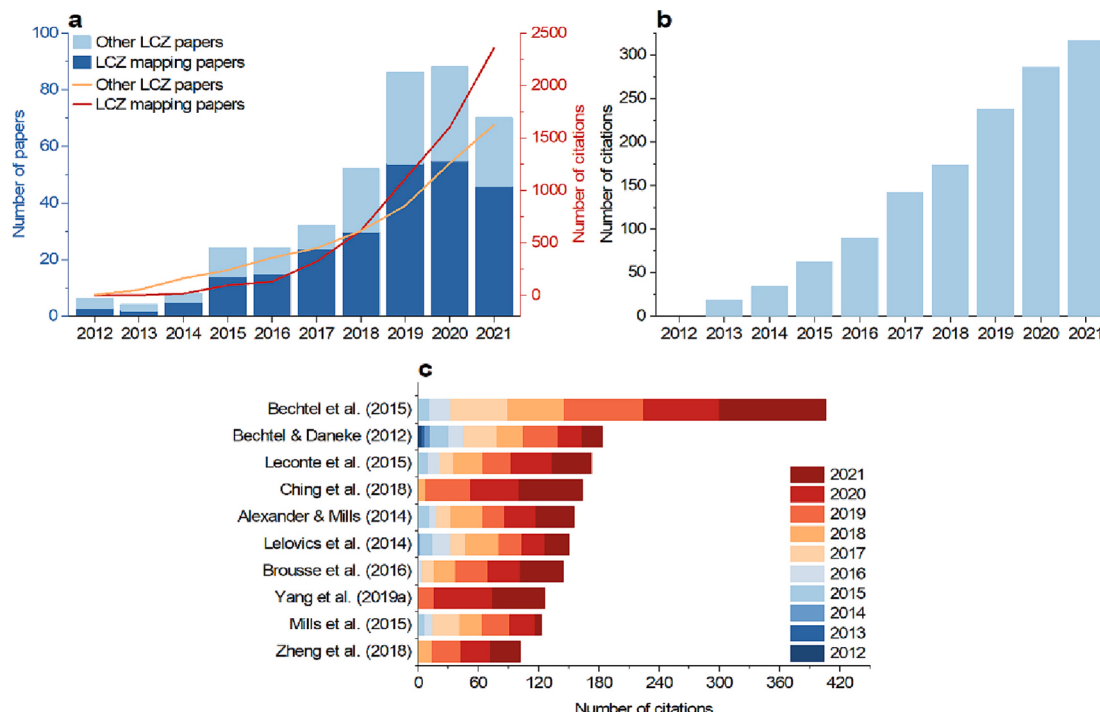


**Fig. 2.** (a) The number of LCZ mapping papers and citations from 2012 to 2021, (b) the number of annual citations of Stewart and Oke (2012), and (c) the top 10 highly cited LCZ mapping papers as of March 28, 2023. The LCZ mapping literature and citations were searched via Google Scholar, Web of Science, and Microsoft Academic.

have also been increasingly cited (Fig. 2c), such as the studies of Bechtel et al. (2015) and Lelovics et al. (2014), which are representative papers for RS-based LCZ mapping methods (see Section 3.1) and GIS-based LCZ mapping methods (see Section 3.2), respectively.

The number and type of journals or conference proceedings that published LCZ mapping papers have generally increased since 2012 (Fig. 3). The journals are mostly in the fields of remote sensing and urban climate research. The first LCZ mapping paper was published in the *IEEE Journal of Selected Topics in Applied Earth Observations and Remote Sensing* (Bechtel and Daneke, 2012). As of 2021, *Urban Climate*, *Remote Sensing*, and *IEEE Journal of Selected Topics in Applied Earth Observations and Remote Sensing* have published the most papers on LCZ mapping, and the *International Geoscience and Remote Sensing Symposium (IGARSS)*, *Joint Urban Remote Sensing Event (JURSE)*, and *International Conference on Urban Climatology (ICUC)* are among the top conference publishers on this topic. Furthermore, several journals and conferences have set special issues for LCZ, such as when *Remote Sensing* launched an LCZ-related special issue in 2015, as did the *ISPRS International Journal of Geo-Information* in 2021, and the *ICUC* published LCZ related sessions in 2015 and 2018. With the rapid development of LCZ mapping methods, several conferences have also focused on this technique. For example, the *IEEE Geoscience and Remote Sensing Society* organized

global competition for LCZ mapping based on remote sensing data, and *IGARSS* set a special topic for LCZ mapping in 2019.

## 2.2. Research topics

LCZ mapping research has incorporated a wide range of keywords over different periods (Fig. 4), which reflect the development of data sources and classification algorithms employed for LCZ mapping: (1) *Data sources*: The earliest RS data used for LCZ mapping is Landsat imagery, while many other RS data have also been employed, such as ASTER, Sentinel, SAR, and LiDAR data. Recently, Google Earth Engine (GEE) has been used to process multi-source RS data for LCZ mapping. In addition, GIS data such as building architecture, OpenStreetMap (OSM), and volunteered geographic information (VGI), have been used as well. (2) *LCZ classification methods*: Both RS- and GIS-based methods have been used for LCZ mapping. RS-based methods were developed from supervised classification, such as object-based image analysis (OBIA) and scene classification methods. The WUDAPT project uses random forest (RF) for LCZ classification, and since 2017, a variety of deep learning models have been introduced, including convolutional neural network (CNN), recurrent neural network (RNN), and deep neural networks (DNN).

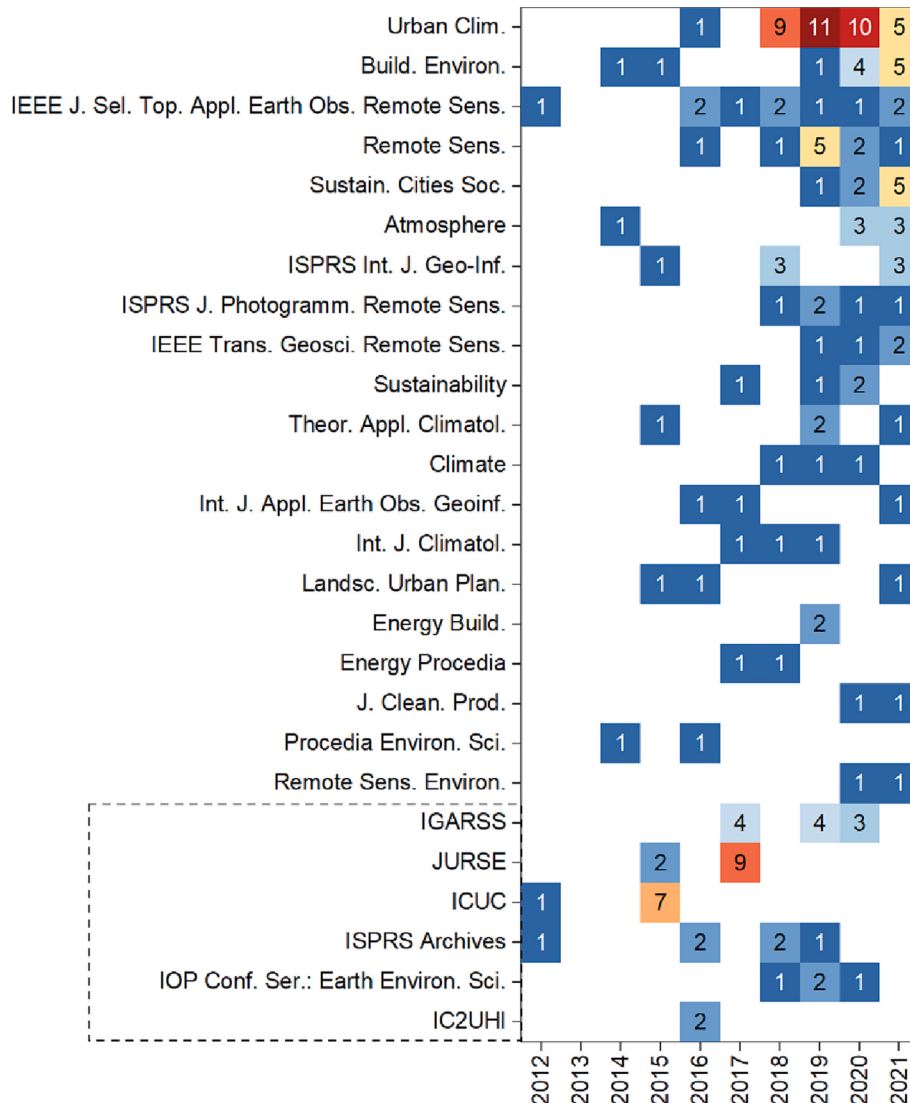


**Fig. 3.** The journals and conferences (bottom dashed box) ranked by the number of LCZ mapping papers (with two papers at least) published during 2012–2021. The corresponding literature is given in Table A1 in the Appendix.

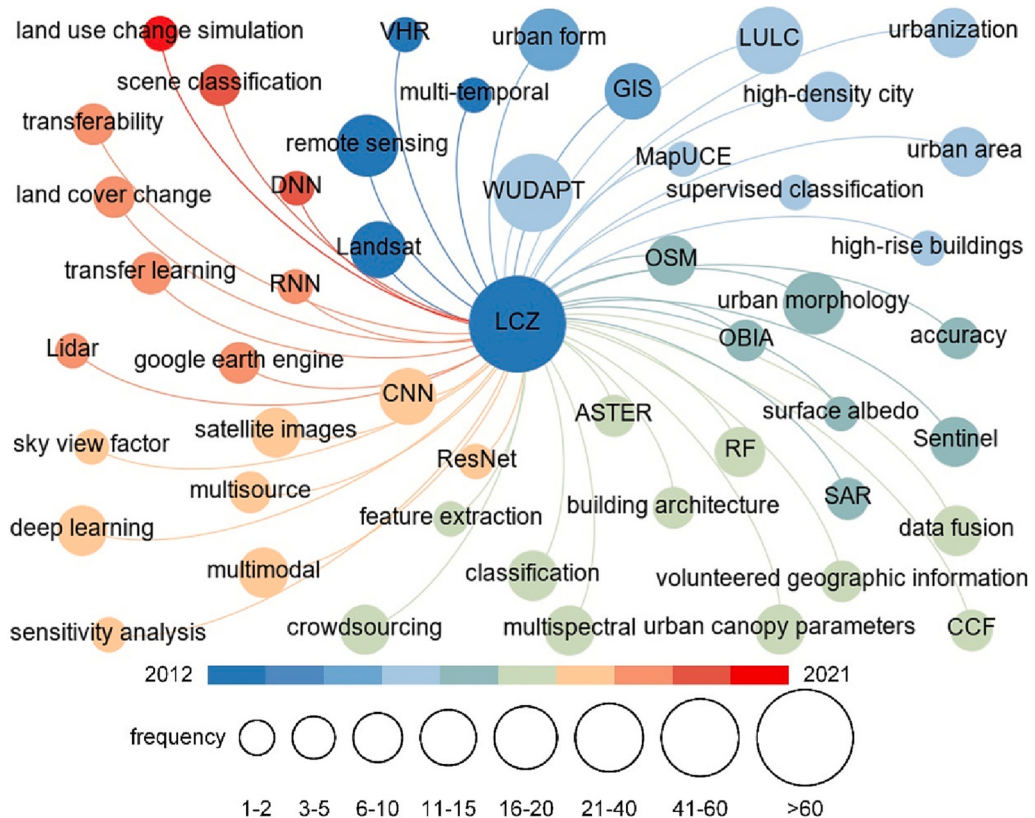


**Fig. 4.** The keyword occurrence network of LCZ mapping papers during 2012–2021. Node size represents keywords frequency, and colors represent the keyword's initial appearance year.

### 2.3. LCZ cities

Over the past decade, LCZ cities have expanded rapidly from a few cities to global cities. As the number of LCZ mapping literature increased significantly in 2015 and 2019 (Fig. 2a), we divide the development of LCZ cities into three stages: *Phase 1 (2012–2014)*: In the early stage, several pioneering studies extended LCZ classification of field sites to city-scale LCZ mapping. The early LCZ cities appeared in Europe, Asia, and South America, and were mostly restricted to a few megacities. *Phase 2 (2015–2018)*: The rapid growth of LCZ cities after 2015 is largely attributed to the WUDAPT project (Bechtel et al., 2015). In this period, LCZ cities increased a lot in Europe, Asia, and North America, which include many medium and small cities. *Phase 3 (2019–2022)*: During this period, LCZ cities increased significantly globally. Specifically, the number of LCZ cities in Europe and Asia continued to increase, while those in Africa, North America, and South America became more widespread. More recently, Zhu et al. (2022) has innovatively created the first-ever global dataset of LCZ maps for 1692 cities with a population  $>300,000$ ; the LCZ maps are freely available to the community (<https://mediatum.ub.tum.de/1633461>). Demuzere et al. (2022a) presented a global LCZ map covering the whole terrestrial areas (Fig. 5a); this dataset can be freely downloaded from <https://doi.org/10.5281/zenodo.6364594>. The two global products were produced using different data sources and classification algorithms. The former used a modified residual neural network model and Sentinel-1 and 2 data, while the latter used lightweight global random forest models and multiple earth observation data, including Landsat 8, Sentinel-1 and 2, PALSAR, VIIRS, and other data. Both products are produced at 100-m resolution and achieve acceptable accuracy comparable to city-specific mapping; either product could be used when needed.

### 2.4. Active research groups

Over 130 institutions worldwide have published LCZ mapping papers, mainly located in Germany, China, France, the US, and India. Here are some active research groups in LCZ mapping. In Germany, the research group of Dr. Benjamin Bechtel and Dr. Matthias Demuzere (Ruhr-University Bochum) and the research group of Dr. Xiaoxiang Zhu (Technical University of Munich) have made distinguished contributions to LCZ mapping. The Bechtel's group developed the first RS-based LCZ mapping method and initiated the well-known WUDAPT project that aims at mapping LCZs for global cities. The Zhu's group has carried out a series of pioneering studies on CNN-based LCZ classification methods. They built the first benchmark data set (So2Sat LCZ42) for global LCZ mapping (Zhu et al., 2020). More recently, they have created the first-ever global database of LCZ maps for 1692 cities (Zhu et al., 2022). In China, the research group of Dr. Chao Ren (The Chinese University of Hong Kong) has contributed substantially to both RS- and GIS-based LCZ mapping; their studies cover a wide range of topics related to LCZ mapping. Some other research groups such as those from Wuhan University and The University of Hong Kong have also done a lot of work on LCZ mapping. In addition, the research groups of Dr. Valéry Masson (National Center for Meteorological Research) and Dr. Julia Hidalgo (French National Centre for Scientific Research) in France, and the research groups of Dr. Tamás Gál (University of Szeged) and Dr. Stevan Savić (University of Novi Sad) in Hungary have also contributed greatly to GIS-based LCZ mapping.

### 3. LCZ mapping methods

In general, LCZ mapping methods fall into three categories: RS-based, GIS-based, and combined methods. More specifically, RS-based methods are essentially the supervised classification of remote sensing

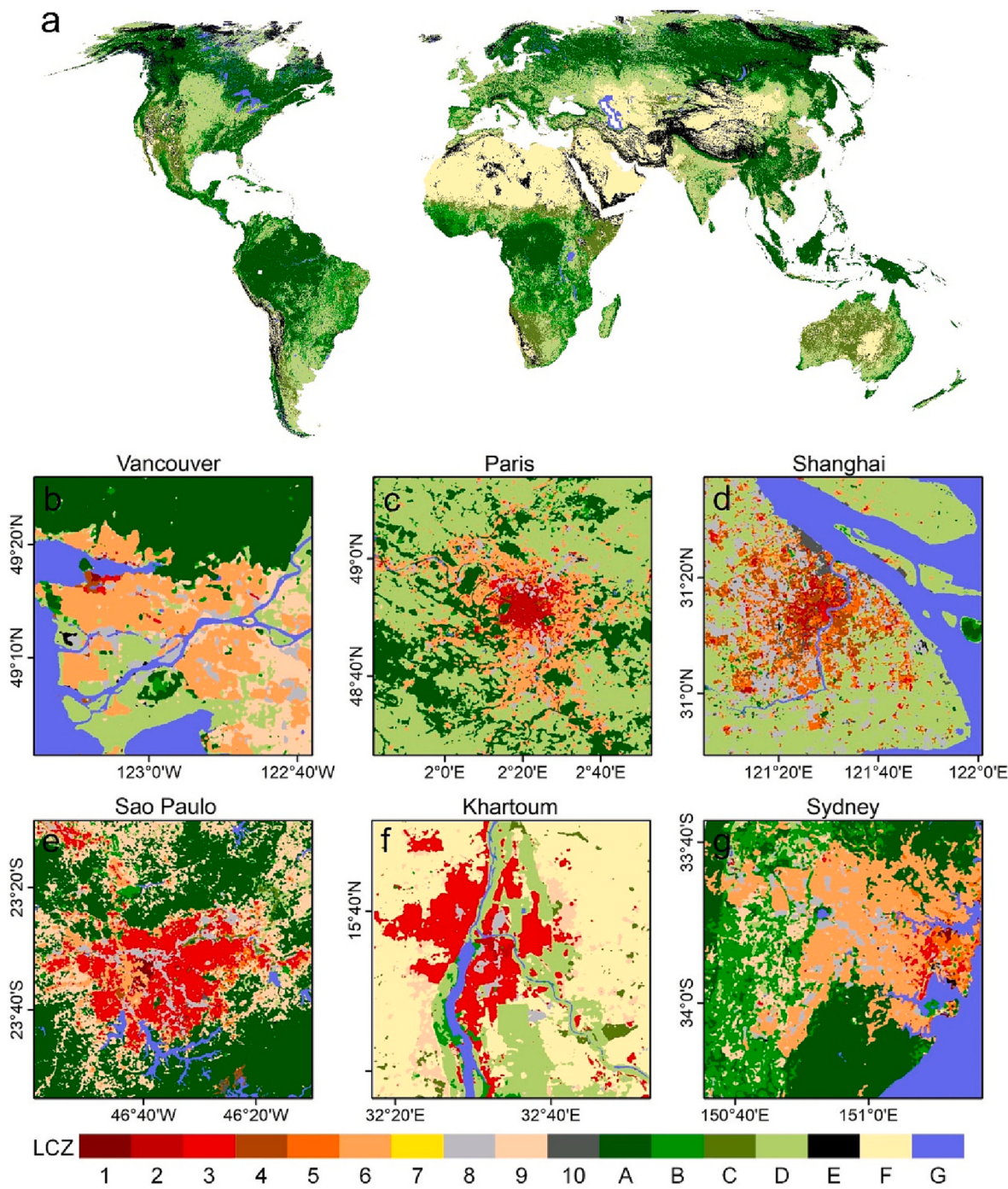


**Fig. 5.** (a) The global map of LCZs modified from Demuzere et al. (2022a). (b)-(g) LCZ maps of six typical cities download from the WUDAPT portal (<https://www.wudapt.org/lcz-maps>).

imagery; GIS-based methods can be broadly defined as those determine LCZ types based on physical parameters; and the combined method aims to integrate the advantages of the former two methods. Fig. 6 tracks the use of these three methods as well as the overall increase in their respective publications in the past decade. RS-based methods account for the largest proportion of LCZ mapping literature (66.2%), followed by GIS-based (24.1%), and combined methods (9.6%). Specifically, the number of RS-based LCZ mapping papers has undergone remarkable growth due to the initiation of the WUDAPT project (Bechtel et al., 2015), as well as the expanded application of multi-source RS and GIS data and machine learning algorithms in recent years. GIS-based LCZ mapping methods gained significant attention in 2015 following the

representative research of Lelovics et al. (2014). The number of GIS-based studies has increased annually during 2016–2019, followed by a little increase in recent years. As for combined methods, the number of papers published per year has overall increased slightly in recent years.

### 3.1. RS-based LCZ mapping methods

RS-based LCZ mapping methods can be further divided into pixel-level, object-level, and scene-level classification methods. This categorization has been commonly adopted in remote sensing image analysis (Blaschke, 2010; Cheng et al., 2017). The three categories of RS-based methods represent different classification paradigms. In short, pixel-

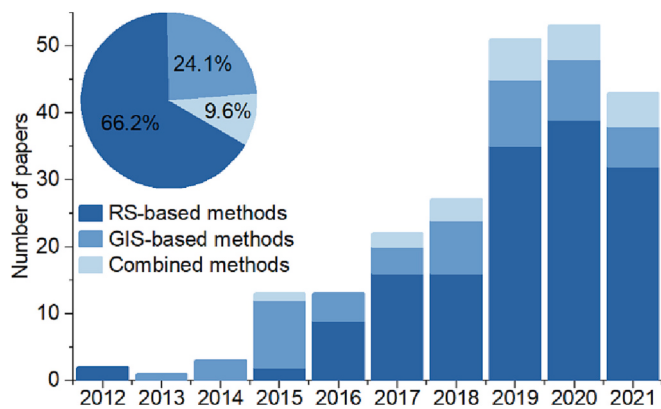


**Fig. 6.** The number and proportion of published literature on RS-based, GIS-based, and combined LCZ mapping methods during 2012–2021.

level LCZ classification divides each pixel of an image into a single LCZ; object-level LCZ classification partitions an image into meaningful semantic objects (i.e., LCZ objects) with each composed of groups of pixels; and scene-level LCZ classification labels each scene image (i.e., an image patch that contains an explicit semantic class) with a specific LCZ class. An exhaustive list of the literature on the three categories of RS-based LCZ mapping methods can be found in Table A2 in the Appendix.

Currently, RS-based LCZ mapping primarily focuses on pixel-level methods, which can be largely attributed to the WUDAPT LCZ mapping initiative that can be easily extended to cities worldwide (Bechtel et al., 2015; Mills et al., 2015). The WUDAPT LCZ mapping process includes selecting LCZ training areas from Google Earth based on expert knowledge, combining Landsat data and the RF model to classify LCZs, and iterating the above steps until an accurate LCZ map is generated

(Fig. 7a). Bechtel et al. (2019a) systematically evaluated the quality of WUDAPT Level-0 LCZ data, concluding that the overall accuracy reached an intermediate level of 50–60%. According to Ching et al. (2018), WUDAPT plans to develop more detailed, higher-level urban databases in the next phase. Considering the inefficiency of the WUDAPT LCZ mapping procedure performed on local computing facilities, Demuzere et al. (2021b) developed an automated online platform, the LCZ Generator (<https://lcz-generator.rub.de/>), to simplify the LCZ mapping process by employing GEE-based LCZ classification strategies, which will facilitate the accessibility and dissemination of LCZ maps and their metadata.

The typical workflows of the three categories of RS-based methods are illustrated in Fig. 7. The basic process of RS-based LCZ mapping methods generally consists of five steps: select feature sets, define classification units, collect training areas, classify LCZs, and evaluate classification results. Accordingly, five key components are required for RS-based methods: feature sets, classification units, training areas, classification algorithms, and accuracy assessment.

### 3.1.1. Feature sets

A feature set is a collection of spectral, textural, morphological, spatial, and temporal features derived from multi-source RS and GIS data to characterize surface structure, cover, radiative, and thermal properties. Currently, satellite data with spatial resolution higher than 100 m have been widely used for RS-based LCZ mapping. For example, pixel-level methods typically use Landsat data, whereas object- and scene-level methods generally use high-resolution satellite data (e.g., Sentinel-2 data). In addition, many other satellite data have also been used for LCZ mapping, such as Sentinel-1 (Bechtel et al., 2016b; Brousse et al., 2019; Demuzere et al., 2019a, 2020a; Hu et al., 2018; Kaloustian et al., 2017), ASTER (Xu et al., 2017b), RapidEye (Oxoli et al., 2018), PALSAR-2 (La et al., 2020), SPOT-6 and Pleiades (Simanjuntak et al., 2019), and DMSP-OLS nighttime light data (Demuzere et al., 2019a; Qiu

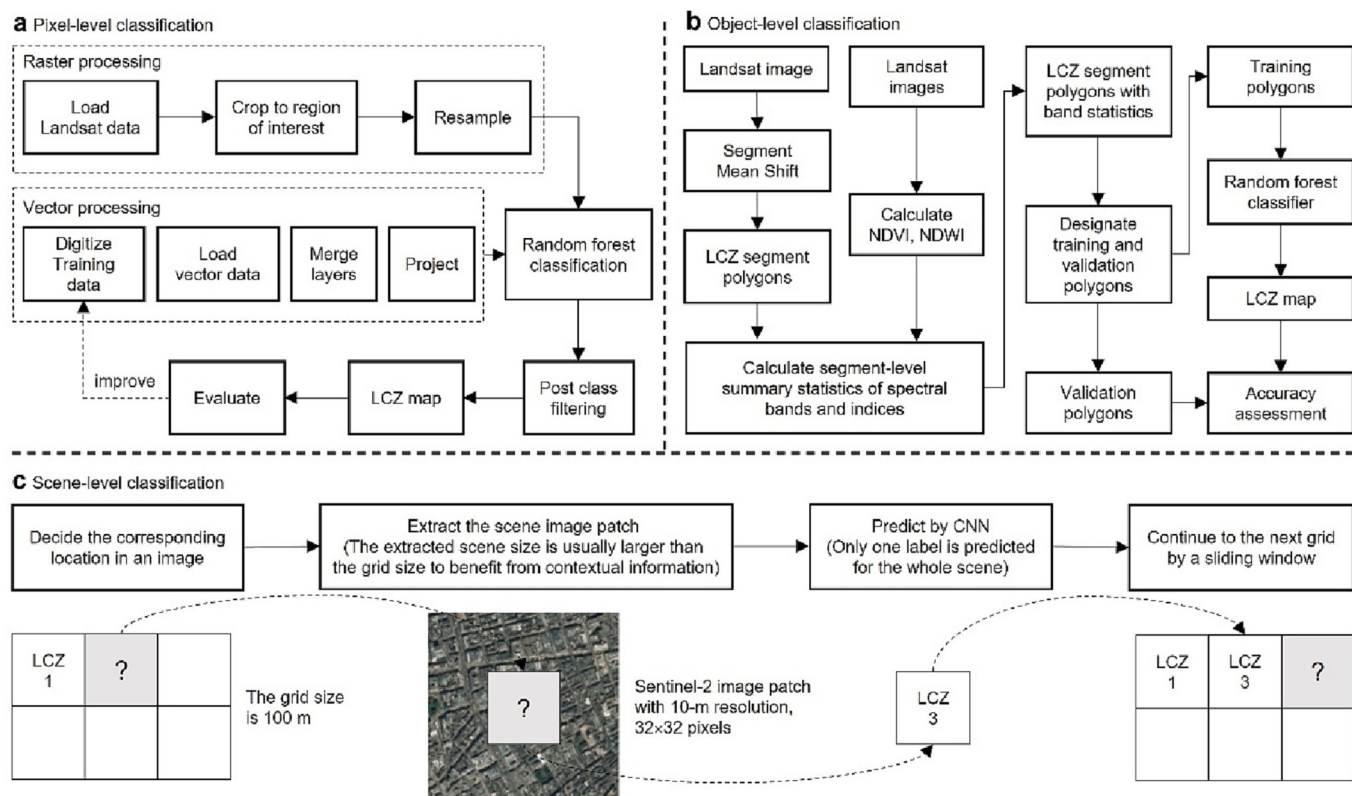


**Fig. 7.** The typical workflows of three typical RS-based LCZ mapping methods. (a) The pixel-level classification modified from Bechtel et al. (2015), (b) the object-level classification modified from Collins and Dronova (2019), and (c) the scene-level classification modified from Qiu et al. (2020b).

et al., 2018a).

Many studies have explored feature importance for LCZ classification. They reported a variety of feature importance rankings using multi-source data. Bechtel and Daneke (2012) found that the multispectral and thermal features derived from Landsat data outperformed those derived from IFSAR (Interferometric Synthetic Aperture Radar) data. Hu et al. (2018) compared the polarimetric, local statistical, textural, and morphological features extracted from Sentinel-1 data, revealing that the features related to the VH polarized data contributed the most to LCZ classification on the global scale. Xu et al. (2018) extracted spectral, thermal, spatial, and temporal features from Landsat-8 and digital surface model (DSM) data, finding that the spectral feature set was more important than the others. Demuzere et al. (2019a) analyzed features derived from Landsat-8 and Sentinel-1 data, among others, concluding that Sentinel-1 backscatter was the most important feature for LCZ classification in Europe. However, Demuzere et al. (2019b) found that the maximum NDVI was the most important feature on the global scale, followed by Sentinel-1 backscatter. Zhang et al. (2019a) compared the spectral, spatial, and textural features extracted from Landsat-8, Sentinel-2, etc., finding that NDVI and its morphological profiles have higher importance than other features. The morphological profile is used to extract spatial information of an image, which is constructed based on the repeated use of openings and closings by reconstruction with a structuring element of increasing size applied to the image (Ghamisi et al., 2015). Hay Chung et al. (2021) explored the relative importance of different features derived from Landsat-8, Sentinel-1 and 2, and VIIRS data, reporting that VIIRS average day/night band radiance was most important.

Meanwhile, many studies have evaluated the effect of different feature combinations on LCZ classification. For example, Xu et al. (2017b) tested six combinations of spectral and textural features extracted from Landsat and ASTER data, concluding that the dominant features varied by city. Qiu et al. (2018c) evaluated different combinations of features derived from Sentinel-2, Landsat-8, etc., suggesting that Landsat-8 and Sentinel-2 spectral reflectance should be jointly used for large-scale LCZ mapping. Demuzere et al. (2019b) compared four combinations of features derived from Landsat 8, Sentinel-1 and 2, etc., and found that the feature sets selected based on the RF algorithm's feature importance performed the best. La et al. (2020) compared six combinations of spectral and polarimetric features extracted from Sentinel-2 and PALSAR-2 data, concluding that the integration of polarimetric features substantially improved classification accuracy. Hay Chung et al. (2021) suggested that while increasing input features can generally improve LCZ classification, the features should be carefully chosen to avoid misleading information. Similarly, Shi and Ling (2021) also found that although adding some features can contribute to LCZ classification, it may be inappropriate to combine as many datasets as possible.

### 3.1.2. Classification units

RS-based methods typically use three categories of classification units (i.e., pixel, object, and scene). The classification unit sizes are determined in different ways. For pixel-level methods, most studies used the classification unit size of 100 m suggested by the WUDAPT project (Bechtel et al., 2015). The basis for choosing 100 m is twofold: The optimal scale for pixel-level classification should be higher than the defined LCZ scale because LCZs are irregular patches; and feasibility tests in different cities have shown that 100–150 m is an appropriate range considering typical urban block scales (Bechtel et al., 2015; Bechtel and Daneke, 2012). Alternatively, some studies adjusted the classification unit size according to specific city characteristics and application cases. For example, the native resolution (30 m) of Landsat images was used instead of resampling to 100 m (Shih et al., 2020; Zonato et al., 2020), which can interpret detailed spatial information and better distinguish different LCZs. Wang et al. (2018c) resampled the pixel size of Landsat data to 200 m based on previous research on

dividing local climate in the hot summer and cold winter region; this pixel size was also used by Tuia et al. (2017b) and Chen et al. (2021b). Tong et al. (2021) set the classification unit size to 300 m to match the resolution of the urban terrain model. Zhang et al. (2021b) tested pixel sizes from 30 to 240 m at 30-m intervals, and found that the classification accuracy is best at 60 m in Beijing.

For object-level methods, the object size depends on image segmentation, which is regulated by the scale parameter. The optimal scale parameter varies with the spatial resolution of satellite imagery. For example, Wei and Blaschke (2016) used an optimized scale of 50 to segment HJ-1B images. Collins and Dronova (2019) determined an appropriate scale parameter of 20 by testing the range of 2 to 60 for Landsat images. Liu et al. (2019) analyzed the sensitivity of LCZ classification accuracy to the segmentation scale, finding the optimal scale range of 40–80 (15–30) for the optical-SAR Sentinel data. Simanjuntak et al. (2019) set different scale parameters for different segmentation levels using very high-resolution images (i.e., Pleiades and SPOT-6), 10 for preliminary segmentation of land cover and 300 (500) for precise segmentation of trees (built-up areas). Ma et al. (2021b) set the scale parameter to 90 to segment Sentinel-2 images to avoid the under-segmentation phenomenon.

For scene-level methods, many studies determined the appropriate scene size by testing LCZ classification accuracy for a range of scene sizes. For example, Yoo et al. (2019) compared the scene sizes of 10 × 10 and 30 × 30 pixels (10 m resolution), reporting higher LCZ classification accuracy for the latter. Liu and Shi (2020) tested the scene sizes from 10 × 10 to 96 × 96 pixels (10 m resolution), finding that the sizes of 32 × 32 to 64 × 64 pixels were the most suitable. Kim et al. (2021) demonstrated that the scene sizes of 32 × 32 and 48 × 48 pixels (10 m resolution) were both suitable for LCZ classification. On the other hand, several studies used the benchmark So2Sat LCZ42 dataset with the scene size of 32 × 32 pixels (10 m resolution) for LCZ classification (Feng et al., 2019; Gawlikowski et al., 2020; Jing et al., 2019; Qiu et al., 2020b; Taubenböck et al., 2020; Zhu et al., 2020). In addition, some studies set scene size based on empirical knowledge, such as 640 × 640 pixels (horizontal field of view, 120°) of Google Street View (GSV) images (Xu et al., 2019), 16 × 16 pixels (15 m resolution) of Landsat-8 images (Huang et al., 2021b), and 64 × 64 pixels (8 m resolution) of Gaofen-3 data (Zhang et al., 2021a).

### 3.1.3. Training areas

LCZ training areas (also known as training data or samples) are usually collected manually from visual interpretation of Google Earth images or through field surveys. The quality of LCZ training areas depends heavily on prior knowledge and experience of participants. Bechtel et al. (2017b) and Verdonck et al. (2019a) investigated the human influence of crowdsourced training data on LCZ mapping. They found that LCZ mapping accuracy improved with the number of training data revisions, and suggested that a standard workflow is required to guide participants in collecting LCZ training areas. The WUDAPT project provides detailed guidelines for the selection of LCZ training areas (<https://www.wudapt.org/digitize-training-areas/>). In addition, Xu et al. (2021) explored the effects of inconsistent labeling and spatial autocorrelation of training areas on LCZ mapping. They found that the former reduced classification accuracy and the latter led to misinterpretation of classification results.

LCZ training areas usually suffer from class imbalance, i.e., some LCZ classes have abundant training samples, while for other LCZ types, the number of training samples is scarce. The class imbalance problem is detrimental to LCZ classification. For example, Xu et al. (2017a) found that the overall mapping accuracy was not satisfactory for some minor LCZ classes due to the unbalanced training data problem. Yokoya et al. (2018) pointed out that the class imbalance problem would pose additional challenges to some classification algorithms. Some studies have proposed effective methods to address the class imbalance problem. For example, Qiu et al. (2018c) demonstrated that balancing training

samples can improve the classification accuracy of small LCZ classes, but the performance of different balancing methods varied by LCZ. Liu and Shi (2020) found that a large image representation can achieve higher classification accuracy compared to a small image when the training samples are limited. Yu et al. (2021) attributed the high accuracy of their deep learning model when using small training samples to the model's robust feature representation. On the other hand, LCZ training areas may also suffer from spatial imbalance; that is, training areas are clustered in a certain part of the city rather than distributed across the city. This problem may lead to misclassification of LCZs, because for most LCZs, their spectral, textural, and morphological features can vary in different parts of the city.

### 3.1.4. Classification algorithms

Pixel-level LCZ classification has employed a wide variety of machine learning algorithms for per-pixel analysis. The random forest (RF) algorithm has been most widely used in pixel-level LCZ classification. This is mainly because most studies follow the WUDAPT LCZ mapping method, which uses the RF algorithm to classify LCZs. Many other machine learning algorithms have also been used for LCZ classification, including naive bayes (NB), support vector machine (SVM), neural network (NN), canonical correlation forest (CCF), conditional random field (CRF), Markov random field (MRF), subspace, and maximum likelihood (ML) algorithms (Bechtel et al., 2016b; Bechtel and Daneke, 2012; La et al., 2020; Nurwanda and Honjo, 2018; Tuia et al., 2017b; Xu et al., 2018; Zhang et al., 2019a; Zhao et al., 2019b). The winning teams of 2017 IEEE GRSS Data Fusion Contest used a variety of ensemble learning algorithms, including a combination of CCF and rotation forest (RoF) (Yokoya et al., 2017), and an ensemble of self-paced co-training, SVM, and multilayer perceptron (MLP) (Xu et al., 2017a). Overall, the performance of machine learning algorithms for pixel-level LCZ classification varies by city. For example, Bechtel and Daneke (2012) and Bechtel et al. (2016b) found that RF and NN outperformed NB and SVM in Hamburg and Khartoum, whereas Xu et al. (2017b) reported that RF and SVM performed slightly better than NN in Guangzhou and Wuhan. Xu et al. (2018) and Mushore et al. (2019) found that both RF and SVM accurately classified LCZs in Nanjing and Harare, with RF slightly more accurate. La et al. (2020) concluded that the subspace method performed better than SVM and MLC in Shanghai. Hay Chung et al. (2021) found that RF obtained higher accuracy compared with SVM and CART for LCZ mapping in Guangdong, Macao, and Hong Kong. It can be concluded from these studies that RF generally performs well for pixel-level LCZ classification.

Object-level LCZ classification typically uses image segmentation algorithms to generate object candidates, and then uses machine learning algorithms to classify them into LCZs. For example, Wei and Blaschke (2016) used multi-resolution segmentation (MRS) and self-organization map (SOM) to classify LCZs; dos Anjos et al. (2017) and Ma et al. (2021a) combined MRS and RF, and Simanjuntak et al. (2019) integrated MRS with rule-set classification. Several studies have further promoted object-level LCZ classification in recent years. For example, Collins and Dronova (2019) explored the potential of object-level LCZ classification using medium-resolution Landsat data instead of high-resolution satellite data. Liu et al. (2019) developed an object-based post-classification refinement method to integrate OBIA with CNN, which outperformed object-based SVM and RF methods. Zhou et al. (2021a) proposed an image standardization approach to integrate OBIA and CNN, which achieved higher classification accuracy than the sliding-window-based method.

Scene-level LCZ classification assigns a scene image to a specific LCZ based on feature representation learning (i.e., the process of converting the scene image into a discriminative feature space). Deep learning models have been widely used in scene-level LCZ classification due to their powerful feature representation capabilities. The most widely used deep learning models are CNNs, including ResNet (Qiu et al., 2018a), ResNeXt (Jing et al., 2019), Inception-v3 (Xu et al., 2019), DenseNet

(Feng et al., 2019; Yang et al., 2019b), VGGNet (Rosentreter et al., 2020), and other CNN architectures (Yoo et al., 2019). In recent years, some studies have developed novel deep learning architectures and compared the performance of different deep learning models in scene-level LCZ classification. For example, Feng et al. (2019) proposed an embracement DenseNet framework for LCZ classification, which outperformed the conventional DenseNet. Qiu et al. (2019a) proposed a recurrent residual network (*Re-ResNet*) architecture combining ResNet and RNN, which can learn a joint spectral-spatial-temporal feature representation in a unified framework. Qiu et al. (2020b) developed a Sen2LCZ-Net-MF architecture consisting of an end-to-end CNN and multilevel feature fusion, which outperformed other CNNs, including VGGNet, ResNet, ResNeXt, DenseNet, and Xception. Liu and Shi (2020) proposed a LCZNet architecture composed of residual learning and Squeeze-and-Excitation blocks, which outperformed the CNN of Rosentreter et al. (2020). Kim et al. (2021) built a MSMLA-Net architecture that integrates multi-scale and multi-level attention modules into a modified SE-ResNet, which outperformed Sen2LCZ-Net (Qiu et al., 2020b) and LCZNet (Liu and Shi, 2020). Yu et al. (2021) designed a hybrid framework that integrates ResNet with graph convolution network (GCN), which outperformed the CNNs of Rosentreter et al. (2020) and Yoo et al. (2019). Zhang et al. (2021a) developed a complex-valued CNN (SAR4LCZ-Net) that improves classification accuracy compared with the real-valued CNN with the same structure.

### 3.1.5. Accuracy assessment

The validation of RS-based LCZ mapping results is usually based on evaluation metrics calculated from the confusion matrix between LCZ classification results and validation data. Here we summarize three aspects: validation strategies, evaluation metrics, and classification accuracy.

The commonly used validation strategies include three methods: hold-out (or train-test split) methods, i.e., a part of LCZ ground truth data is selected as the training set, and the remaining is used for validation; bootstrapping methods, i.e., the training set is selected from LCZ ground truth data with replacement, while the remaining samples comprise the validation set; and cross-validation methods, i.e., LCZ ground truth data is randomly split up into  $k$  groups, of which one is the validation set and the rest for training, repeating until each group has been used for validation. For the three methods, the hold-out method has been mostly widely used (see Table A2) because it is simpler than the other two methods; however, it fails to measure the generalization performance of LCZ classification models. The bootstrapping method is usually preferable to the cross-validation method (Bechtel et al., 2019a), in part because the latter requires a considerable amount of LCZ ground truth data, which is difficult to guarantee, especially in small cities.

Traditional evaluation metrics usually include overall accuracy (OA, i.e., the percentage of correctly classified pixels), producer's accuracy (PA, i.e., the percentage of correctly classified pixels for class  $i$ ; or called recall), user's accuracy (UA, i.e., the percentage of pixels classified as class  $i$  that actually belong to class  $i$ ; or called precision), F1 score (i.e., a class-wise metric and calculated as the harmonic mean of UA and PA), kappa coefficient, and average accuracy (AA, i.e., the average of all PA). These metrics are calculated from the confusion matrix between LCZ classification results and validation data. Although OA is commonly used, Bechtel et al. (2017b) pointed out that high OA alone does not indicate a well generated LCZ map; therefore, the OA of urban LCZ classes only ( $OA_u$ ), and the OA of built versus natural classes only ( $OA_{bu}$ ) ignoring their internal differentiation, have also been used for accuracy assessment.

The traditional evaluation metrics derived from confusion matrices penalize all classification errors equally. This treatment may be insufficient for measuring LCZ classification accuracy, because some LCZ types are quite similar to each other in physical properties. To this end, Bechtel et al. (2017b) proposed a weighted accuracy (WA) metric to account for the similarity and dissimilarity between LCZ classes, which

measures LCZ classification accuracy in terms of the expected thermal impact. However, Johnson and Jozdani (2019) questioned the methodology and logic of the WA metric, and proposed another WA metric of LCZ dissimilarity based on physical parameters. Furthermore, Bechtel et al. (2020) and Johnson and Jozdani (2020) discussed the two WA metrics in more depth, which provide us with more details on how these two metrics were developed and further improved. Both the two metrics apply a greater penalization to the misclassification between more physically dissimilar LCZ classes, which complements the traditional measure metrics.

RS-based studies have reported a wide range of LCZ mapping accuracy. As far as the overall accuracy is concerned, Bechtel et al. (2019a) concluded that the overall accuracy of WUDPAT LCZ maps is moderate, ranging from 50%-60%. Ren et al. (2019) reported that the overall accuracy ranges from 60% to 89% for 20 cities in China. Demuzere et al. (2020a, 2019a) obtained an overall accuracy of above 80% for Europe and the continental US. Zhu et al. (2022) achieved an average accuracy between about 50% to >80% for 1692 cities across the globe. Demuzere et al. (2022a) achieved an overall accuracy of >70% for global LCZ mapping. Furthermore, the classification accuracy usually shows large discrepancy among different LCZs. Several studies have shown that the classification accuracy is low for some built types, such as LCZ 4 (Open high-rise) and LCZ 5 (Open midrise) (Demuzere et al., 2019a, 2020a), and LCZ 9 (Sparsely built) (Ren et al., 2019). Zhu et al. (2022) discovered three types of major confusions between LCZ classes: among low-rise classes (i.e., LCZ 3, LCZ 6, and LCZ 7), between heavy industry (LCZ 10) and large low-rise (LCZ 8), and among bush, scrub (LCZ C), low plants (LCZ D), and bare soil or sand (LCZ F). For the three categories of RS-based methods, object-level and scene-level classification methods commonly achieve higher accuracy compared with pixel-level methods (Liu and Shi, 2020; Rosentreter et al., 2020; Simanjuntak et al., 2019; Yoo et al., 2019).

### 3.2. GIS-based LCZ mapping methods

GIS-based LCZ mapping methods follow the three-step process given in Stewart and Oke (2012), and generally include four steps (Fig. 8): calculate LCZ parameters, define basic spatial units, classify LCZs, and evaluate classification results. Accordingly, GIS-based methods consist of four key components: LCZ parameters, basic spatial units, classification algorithms, and accuracy assessment.

#### 3.2.1. LCZ parameters

Stewart and Oke (2012) defined ten LCZ parameters associated with their reference ranges to characterize four categories of surface physical properties: surface structure (i.e., sky view factor-SVF, aspect ratio-AR, height of roughness elements-HRE, and terrain roughness class-TRC),

surface cover (i.e., building, impervious, and pervious surface fractions-BSF, ISF, and PSF), surface material (i.e., surface admittance and surface albedo-SAD and SAL), and human activity (i.e., anthropogenic heat output-Ah). In general, surface structure and cover parameters have been commonly used for LCZ classification, while surface material and human activity parameters are rarely employed due to lack of data (see Table A3). However, the rarely used parameters may still play an important role in LCZ classification.

Multi-source RS and GIS data have been used to calculate LCZ parameters. For surface structure parameters (i.e., SVF, AR, HRE, and TRC), SVF can be calculated using DSM (Bartesaghi Koc et al., 2017; Mitraka et al., 2015; Quan, 2019a; Zhao et al., 2019a; Zheng et al., 2018), building data (Chen et al., 2020b; Nassar et al., 2016), and Google Street View (Demuzere et al., 2019a, 2020a; Middel et al., 2018). Using building data, AR was calculated as the mean building height divided by the mean street width (Chen et al., 2020b; Zheng et al., 2018), or as the maximum height divided by the average width of ground surface (Zhao et al., 2019a). Several studies approximated HRE as the mean height of buildings weighted by the building footprints (Lelovics et al., 2014; Nassar et al., 2016; Quan, 2019a; Zheng et al., 2018). The Davenport classification method is typically used to determine TRC, using aerial imagery, topographic maps, and building data (Lelovics et al., 2014), Landsat 8 imagery (Chen et al., 2020b), and DSM and land cover data (Zhao et al., 2019a). Surface cover parameters (i.e., BSF, ISF, and PSF) are commonly calculated using land cover and building data (Lelovics et al., 2014; Nassar et al., 2016; Quan et al., 2017). For surface material parameters (i.e., SAD and SAL), RS multispectral data are generally used to characterize surface albedo (Lelovics et al., 2014).

#### 3.2.2. Basic spatial units

GIS-based methods typically employ two types of basic spatial units, i.e., parcel and grid units. The parcel unit uses line elements as boundaries, such as roads, streets, and rivers, whereas the grid unit divides the city into a net of square cells. The parcel unit generally refers to lot area polygons (Lelovics et al., 2014; Molnár et al., 2019; Savić et al., 2018; Skarbit et al., 2015, 2017; Unger et al., 2014), urban blocks (He et al., 2019; Jin et al., 2020; Kwok et al., 2019; Perera and Emmanuel, 2018; Quan, 2019a; Quan et al., 2017; Wu et al., 2018), urban islets (Bocher et al., 2018; Hidalgo et al., 2019; Plumejeaud-Perreau et al., 2015), and community units (Chang et al., 2021).

Different approaches have been used to determine the appropriate spatial unit size. For the parcel unit, the minimum radius is generally set to 200–500 m, as suggested by Stewart and Oke (2012). For example, Lelovics et al. (2014) set the minimum radius of lot area polygons to 250 m to acquire large homogeneous areas for establishing LCZs. The same criterion was adopted by Wu et al. (2018) to define the minimum radius

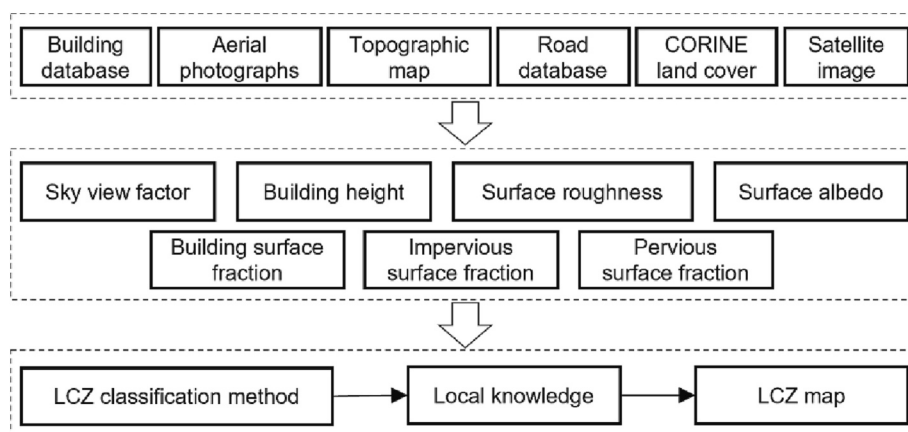


**Fig. 8.** The workflow of the typical GIS-based method modified from Lelovics et al. (2014).

of blocks; whereas Quan et al. (2017) and Jin et al. (2020) set the minimum radius of urban blocks to 200–500 m to reduce the influence of surrounding LCZs. For the grid unit, the appropriate size can be determined by three strategies: (1) *Based on empirical knowledge*: This method requires prior knowledge of urban form and its relationship to the local climate, which has been widely used to determine appropriate grid sizes (Agathangelidis et al., 2019; Cai et al., 2019; Geletić et al., 2016, 2019; Geletić and Lehnert, 2016; Kopp et al., 2021; Mitraka et al., 2015; Ru et al., 2021; Shi et al., 2018; Wang et al., 2018b). For example, Geletić and Lehnert (2016) selected 100 m as the appropriate grid size for three medium-sized cities in the Czech Republic, because the physical properties at this scale significantly affect local air temperature. Cai et al. (2019) used the grid size of 250 m for LCZ mapping in Chongqing, due to the significant correlation between urban morphology factors and LST at this scale. (2) *Test different grid sizes*: This method is straightforward and has also been widely used in RS-based LCZ mapping studies (see Section 3.1.2). For example, Hu et al. (2019) tested six grid sizes (i.e., 120, 180, 240, 270, 360, and 480 m) to select the optimal scale (240 m) for LCZ classification in Nanjing. (3) *Based on the spatial autocorrelation of building height*: The basis of this method is that building height plays a key role in classifying LCZ built types and there is significant spatial autocorrelation in uniform urban morphology. The appropriate grid size determined by this method was 300 m in Hong Kong (Zheng et al., 2018), 270 m in San Antonio (Zhao et al., 2019a), and 200 m in Chenzhou (Chen et al., 2020b).

### 3.2.3. Classification algorithms

GIS-based methods have used various classification algorithms to identify LCZ types. The most widely used approach is to match the calculated LCZ parameters with their reference ranges using decision-making algorithms (Agathangelidis et al., 2019; Bartesaghi Koc et al., 2017; Chen et al., 2020b; Geletić and Lehnert, 2016; Nassar et al., 2016; Perera and Emmanuel, 2018; Quan, 2019a; Unal Cilek and Cilek, 2021; Wang et al., 2018b; Zhao et al., 2019a). Different decision-making algorithms were designed based on the selected LCZ parameters. Some studies have also used other classification algorithms to determine LCZ classes, such as the score assignment (Jin et al., 2020; Lelovics et al., 2014; Unger et al., 2014), multidimensional linear interpolation (Quan et al., 2017), NB (Hammerberg et al., 2018), RF (Hu et al., 2019), and k-means algorithms (Hidalgo et al., 2019; Kwok et al., 2019; Zhan et al., 2018). After the preliminary classification, post-processing is usually performed to refine LCZ classification. The typical practice is spatial aggregation that merges unclassified, small, or isolated LCZs into adjacent dominant/large/similar LCZs. For example, Lelovics et al. (2014) explored how to merge lot area polygons based on the relative locations and spatial extensions of merged LCZ polygons. In addition, Geletić and Lehnert (2016) merged small LCZs into the prevailing LCZ of the neighborhood; Wu et al. (2018) used a majority filter to determine the dominant LCZ when a small LCZ was surrounded by larger LCZ clusters; and Jin et al. (2020) merged small LCZ blocks into adjacent larger blocks of similar LCZ classes.

### 3.2.4. Accuracy assessment

Not all GIS-based studies performed accuracy assessment. This is because GIS-based methods use a set of physical parameters that quantitatively describe LCZ properties to match the “correct” or best-fit LCZ class; that is, GIS-based LCZ mapping results are implicitly correct if the LCZ parameters are calculated accurately. Nonetheless, some GIS-based studies have evaluated LCZ mapping results, and the validation strategies are different from those of RS-based studies. Quan and Bansal (2021) summarized that the validation of GIS-based LCZ mapping results is typically based on expert knowledge and temperature observations. The validation based on temperature observations lacks objective criteria, since one can hardly tell whether the LCZ classification results are correct based on the thermal differentiation of LCZ classes. In contrast, the validation based on expert knowledge is a common practice

in some GIS-based studies. For example, Geletić and Lehnert (2016) evaluated the agreement of their classification results with those defined based on expert knowledge and found that the agreement was in 79–89% of cases. Kotharkar and Bagade (2018) conducted site visits and photographic survey to confirm the LCZ classification results as well as to recheck the ambiguous LCZs. Quan (2019a) randomly selected sample blocks of the LCZ map for visual inspection based on Google Earth images and photographs of field observations and concluded that the overall correspondence was over 90% for most classes. Chen et al. (2020b) randomly selected sample grids to test LCZ classification results and achieved an overall accuracy of 67.3%. It should be noted that the validation based on expert knowledge is essentially a subjective judgement of LCZ classes, which may lead to uncertainty.

### 3.3. Combined LCZ mapping methods

Different strategies have been developed to integrate RS- and GIS-based methods, which can be broadly divided into two categories (Fig. 9 and Table A4): (1) “*Coarse-to-fine*” classification methods: This category uses RS-based methods to preliminarily classify LCZs, complemented by GIS-based methods to refine LCZ classification. Some studies used GIS-based post-processing to refine RS-based classification. For example, Gál et al. (2015) integrated the two methods by adding the GIS-based LCZ aggregation process to the RS-based method. Alternatively, several studies used LCZ parameters to assist in RS-based LCZ classification. For example, Lopes et al. (2017) and Fonte et al. (2019) used BSF and ISF information, and Zhou et al. (2020a) incorporated building height, BSF, and PSF parameters, to improve the WUDAPT LCZ classification. (2) “*Built type and land cover type separation*” classification methods: A common practice is to identify land cover types of LCZs based on RS-based methods, while using GIS-based methods to classify built types of LCZs, which has been widely used for LCZ classification (Du et al., 2020a; Han et al., 2020; Kotharkar and Bagade, 2018; Shi et al., 2018; Wang et al., 2018b; Wicki and Parlow, 2017; Yang et al., 2019a, 2020b, 2021; Zhao et al., 2019a; Zheng et al., 2018; Zhou et al., 2021b).

### 3.4. Comparison between RS- and GIS-based methods

LCZ maps generated by RS- and GIS-based methods have been compared in several cities (Gál et al., 2015; Geletić and Lehnert, 2016; Hammerberg et al., 2018; He et al., 2019; Hidalgo et al., 2019; Quan, 2019a; Shi et al., 2018; Wang et al., 2018b). In addition to the different classification processes, the two categories of LCZ mapping methods also differ in LCZ classification accuracy and LCZ types. (1) *Difference in classification accuracy*: Some studies reported that GIS-based methods can obtain higher accuracy and more spatial details for LCZ built types than the WUDAPT method (Hidalgo et al., 2019; Quan, 2019a; Wang et al., 2018b). For example, Wang et al. (2018b) found that the overall accuracy of GIS-based method (72%) is higher than that of the WUDAPT method (58%) in Hongkong, where the GIS-based method was more accurate for the classification of built types, but the WUDAPT method performed better in classifying land cover types. (2) *Difference in LCZ types*: In general, LCZ types determined by RS-based methods depend on labeled LCZ training samples, which are selected from the standard LCZ classes defined in Stewart and Oke (2012). By contrast, some GIS-based studies reported that the calculated LCZ parameters did not match their reference ranges, and thus, new LCZ classes or LCZ subclasses were introduced (Perera and Emmanuel, 2018; Quan, 2019a). Previous studies have demonstrated that RS- and GIS-based methods may differ in LCZ types and their spatial coverage; for example, the agreement of LCZ classification results between the two methods was only 67% in Vienna (Hammerberg et al., 2018) and 51% in Brno (Geletić and Lehnert, 2016).

## 4. Discussion

Although great progress has been achieved in LCZ mapping methods,

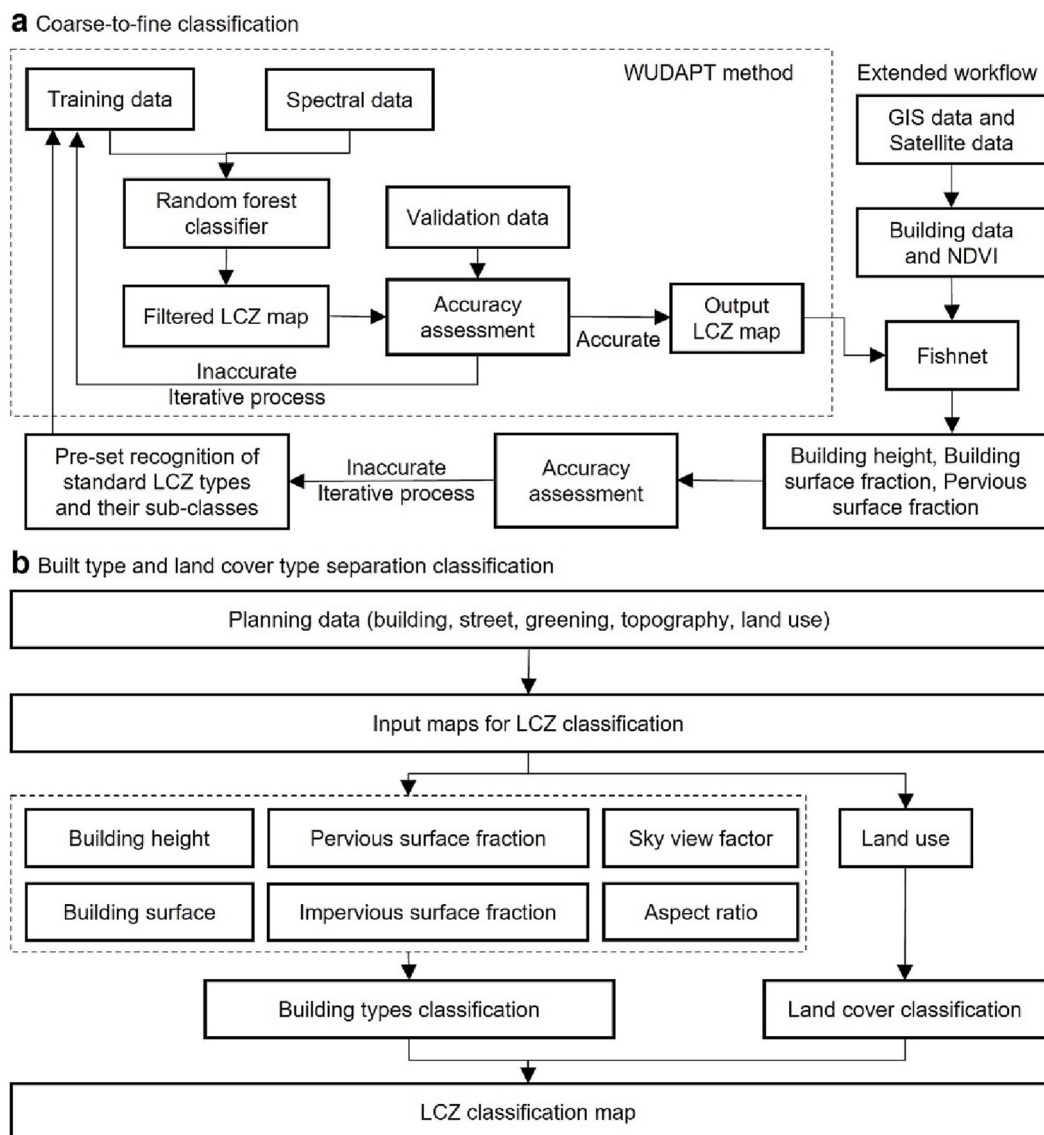


**Fig. 9.** The workflow of two typical combined methods. (a) The “coarse-to-fine” classification modified from Zhou et al. (2020a) and (b) the “built type and land cover type separation” classification modified from Zheng et al. (2018).

there are still many aspects to be further explored to improve LCZ mapping. We further discuss some challenges and future directions regarding data sources, LCZ mapping unit sizes, LCZ ground truth data, LCZ parameters and subclasses, classification algorithms/rules, transferability of LCZ models, global interannual LCZ mapping, and application of LCZs.

#### 4.1. Exploiting multi-source RS and GIS data

High-resolution and high-precision data characterizing surface cover, structure, material, and human activity are the basis for LCZ mapping. Although a wide variety of RS and GIS data have been used (see Sections 3.1.1 and 3.2.1), several challenges remain in using multi-source data, such as which data is needed, how to acquire and process data, how to deal with inconsistent data quality and feature redundancy, and how to integrate multi-source data. These challenges need to be addressed properly in future research. Here we analyze three issues in data sources for LCZ mapping.

First, a wealth of RS and GIS data that provide useful urban form and function information have been seldom used so far. Very high-resolution satellite data such as IKONOS, QuickBird, Worldview, Pleiades, and

Gaofen imagery, can provide detailed and accurate surface coverage, but have only been used tentatively for LCZ mapping. The leading volunteered geographic information, OpenStreetMap (OSM), exhibits great potential for LCZ mapping (Fonte et al., 2019; Varentsov et al., 2020), but has yet to be fully exploited. Social sensing data collected by crowdsourcing, web crawlers, or social networks, such as points of interest, mobile phone positioning data, social media check-in data, vehicle trajectory data, etc., have been demonstrated feasible for urban function recognition (Cao et al., 2020; Du et al., 2020b; Tu et al., 2018; Xing and Meng, 2018; Zhang et al., 2019b), which can be used for LCZ mapping (Mhedhbi et al., 2019). LCZ mapping studies should explore the potential of many other suitable and accessible RS and GIS data.

Second, there is a lack of detailed building height information in many cities, likely leading to the misclassification of built-type LCZs (Ren et al., 2019). Satellite remote sensing technology provides an effective means for mapping building heights on a large scale. For example, multiple satellite-based Synthetic Aperture Radar (SAR) and Light Detection and Ranging (LiDAR) data have been used to retrieve high-resolution building heights, such as TerraSAR-X data (Sun et al., 2022), TanDEM-X data (Geis et al., 2019), Ice, Cloud, and land Elevation Satellite-2 (ICESat-2) data (Lao et al., 2021), and Sentinel-1 data (Li

et al., 2020). High-resolution optical imagery can also be used to estimate building heights, such as IKONOS data (Shao et al., 2011), Google Earth images (Liasis and Stavrou, 2016; Qi et al., 2016), and street view images (Yan and Huang, 2022). Satellite-derived high-resolution building height data is now available for many cities. For example, Frantz et al. (2021) combined Sentinel-1 and Sentinel-2 data to map building heights at 10-m resolution for entire Germany. Cao and Huang (2021) estimated building heights at 2.5-m resolution for 42 Chinese cities using high-resolution ZY-3 multi-view images, and Huang et al. (2022) estimated building heights at 30-m resolution for all cities in China using Advanced Land Observing Satellite (ALOS) AW3D30 data. Future studies could use the satellite data and methods described above to retrieve high-resolution building heights for other cities.

Third, using multi-source data inevitably introduces feature redundancy. While some high-resolution RS and GIS data can provide abundant geometric, textural, and spectral features, they likely introduce redundant information, e.g., excessive detail, confusing objects, and complex spectral features, which may be detrimental to LCZ classification. Some studies have demonstrated that the importance of features varies across cities (see Section 3.1.1). For example, some studies recommended using multi-seasonal data for LCZ classification (Bechtel et al., 2015; Huang et al., 2021b; Qiu et al., 2019a), because land surface properties may change significantly with season for most LCZ classes. However, Demuzere et al. (2019b) found that the inclusion of multi-seasonal information was ambiguous for LCZ classification in different cities. Accordingly, the selection and combination of features extracted from multi-source data for LCZ mapping requires further investigation.

#### 4.2. Determining appropriate LCZ mapping unit sizes

LCZ mapping units refer to pixel, object, and scene units for RS-based methods (see Section 3.1.2), and parcel and grid units for GIS-based methods (see Section 3.2.2). Mapping unit size is a key factor in generating LCZ maps; nevertheless, how to determine appropriate mapping unit sizes needs further exploration.

Five factors need to be considered when determining appropriate LCZ mapping unit sizes: (1) *LCZ scale*: Stewart and Oke (2012) defined LCZs as hundreds of meters to several kilometers in horizontal scale, and suggested that each LCZ should have a minimum diameter of 400–1000 m (i.e., a radius of 200–500 m) to minimize the influence from neighboring LCZs. The definition of LCZs allows a certain range of appropriate scales for mapping (Bechtel et al., 2015). (2) *City characteristics*: Globally, cities span vastly different geographic and climatic settings, urban form and layout, and development modes, all of which add variability to the size of LCZ mapping units. Moreover, LCZs appear in various forms in different cities instead of being arranged in square grids; thus, the classification unit should be smaller than the average size of LCZ polygons. (3) *Spatial resolution of multi-source data*: For remote sensing image classification, low-resolution imagery suffers from mixed pixels while high-resolution imagery results in fragmented objects, both of which make LCZs difficult to classify. The classification unit of LCZs is preferably larger than the sufficiently high pixel resolution of satellite imagery that can identify the interior composition within a single LCZ. (4) *Classification algorithms*: For RS-based methods, the classification units should contain the typical characteristics of LCZs that are required by machine learning algorithms to accurately recognize LCZs. For GIS-based methods, the basic spatial units should be applicable to minimize within-class but maximize between-class variances of LCZ parameters. (5) *Application requirements*: The LCZ system has been used in a wide range of fields (see Section 4.9), which probably require different levels of LCZ-based information. For example, LCZ-based information has been incorporated into a variety of regional climate models (RCMs), such as the Weather Research and Forecasting Model (WRF) coupled with urban canopy models (UCMs). Therefore, the application cases of LCZ maps need to be considered before determining an appropriate mapping unit size.

Both empirical and quantitative methods have been used to determine the size of LCZ mapping units (see Sections 3.1.2 and 3.2.2). Empirical methods determine the appropriate unit size by comprehensively considering the above-mentioned factors based on expert knowledge. For example, the WUDAPT project uses a pixel size of 100 m to generate LCZ maps, which has been commonly accepted by the research community. Nevertheless, a uniform mapping unit size may not be suitable for all cities in the world due to the great diversity of cities and the varying spatial configurations of LCZs from city to city. Alternatively, quantitative methods usually determine the appropriate mapping unit size by testing a range of sizes. In general, quantitative methods can achieve higher accuracy than empirical methods, but testing a range of mapping unit sizes is time-consuming, especially when extended to global cities. Combining the advantages of empirical and quantitative methods could be beneficial for determining the appropriate size of LCZ mapping units. Here is an example process for combining the two methods: First, quantitative methods are used to determine the optimal size of LCZ mapping units for a collection of typical cities. These cities are representative of different city styles or characteristics, such as geographic and climatic contexts, city size, urban form, development levels, etc. Second, the appropriate mapping unit size for a target city is determined by matching the city characteristics to similar typical cities based on expert knowledge.

Although appropriate mapping unit sizes can produce LCZ maps with acceptable accuracy, some misclassified, small, isolated, or unclassified LCZs are sometimes retained. Moreover, LCZs are naturally irregular parcels in shape rather than square polygons generated from pixel-, scene-, and grid-based classification units. In such context, spatial aggregation of LCZs (i.e., merging LCZ polygons) is needed to refine LCZ mapping results, even when generated based on an appropriate mapping unit size. GIS-based methods generally include a spatial aggregation step, while RS-based methods do not. Although most GIS-based studies follow some aggregation rules proposed by Lelovics et al. (2014) to merge LCZ polygons based on relative position and similarity, there are still large differences among different studies. Moreover, some merging rules may lead to uncertainty. For example, merging a small LCZ B (scattered trees) into the nearby larger LCZ 6 (open low-rise) may create misclassification when the true LCZ may be LCZ 9 (sparsely built). This problem is in turn related to the question of the most suitable LCZ mapping unit size. Accordingly, it is necessary to design standard and reasonable spatial aggregation schemes by synthesizing existing rules and strategies. Alternatively, users can create new LCZ subclasses to represent combinations of different LCZs (Stewart and Oke, 2012), such as merging LCZ 8 (large low-rise) with LCZ B (scattered trees) into a new subclass LCZ 8<sub>B</sub> (large low-rise with scattered trees). See Section 4.5 for more discussion on LCZ subclasses.

#### 4.3. Acquiring high-quality LCZ ground truth data

LCZ ground truth data is crucial for training classification models and validating LCZ mapping results (see Sections 3.1.3, 3.1.5, and 3.2.4). Several challenges with LCZ ground truth data need to be addressed in future research.

First, the quality of LCZ ground truth data is difficult to guarantee. Bechtel et al. (2017b) concluded that the quality of crowdsourced LCZ training areas collected through human interpretation was poor to moderate in most cases, while untrained operators had more difficulty identifying representative examples of LCZs. Stehman and Foody (2019) pointed out three imperfections in reference data for land cover mapping: data error (i.e., incorrect class labels), class ambiguity (i.e., a single class label does not adequately characterize the ground truth), and inconsistent class labelling (i.e., different interpreters assign different classes to the same sample). These issues are also present in LCZ ground truth data; however, labeling LCZs through visual interpretation is more challenging, especially for built types. This is because real urban forms are typically heterogeneous (e.g., great variation in spatial

arrangements and structural patterns) and exhibit greater diversity than idealized homogeneous LCZs. Therefore, acquiring high-quality LCZ ground truth data requires knowledge of LCZ concepts, expertise in remote sensing image analysis, familiarity with urban morphology, and specialized training.

Second, there are few benchmark LCZ data sets. Zhu et al. (2020) built the first benchmark data set (So2Sat LCZ42) for global LCZ mapping, which includes a total of 400,673 Sentinel-1 and Sentinel-2 image patches collected from 52 cities around the world. This data set was created by 15 domain experts following a meticulously designed workflow and a rigorous label-quality assessment process, achieving an overall confidence of 85%. Thus far, the benchmark So2Sat LCZ42 data set has been widely used for LCZ mapping (Feng et al., 2019; Jing et al., 2019; Qiu et al., 2018a, 2020b; Taubenböck et al., 2020; Yang et al., 2019b; Zhu et al., 2022). LCZ benchmark data sets play a key role in training deep feature learning models. Given the great diversity of cities worldwide and the high complexity of scene images (e.g., different sizes, shapes, colors, and rotations), high-quality LCZ benchmark data sets need to be created at global scales using multiple high-resolution satellite imagery. Several key issues should be addressed for building benchmark LCZ data sets, such as how to design labeling workflows and quality assessment processes.

#### 4.4. Improving LCZ classification algorithms

Although RS-based and GIS-based LCZ mapping methods have employed a wide range of classification algorithms or rules (see Sections 3.1.4 and 3.2.3), there are still many aspects to be improved further.

For RS-based LCZ mapping methods, the research focus is shifting from pixel-level classification methods to object-level and scene-level classification methods; meanwhile, deep learning represents the fastest growing trend in LCZ classification. Compared with pixel-level classification, both object-level and scene-level classification have exhibited greater potential for LCZ mapping, especially in cities with heterogeneous landscapes. The core task of object-level LCZ classification is image segmentation, where MRS algorithms have been most widely used. Since the performance of MRS is regulated by scale, shape, and compactness parameters, it is critical to optimize these parameters and evaluate segmentation quality. Given the discrepancy between irregular objects obtained from image segmentation and rectangular classification units required for deep learning (e.g., CNNs), how to integrate image segmentation and deep learning needs to be further explored for object-level LCZ classification. On the other hand, the most important part of scene-level LCZ classification is feature representation. Significant challenges in scene classification include great intraclass diversity, high interclass similarity, large variance of object/scene scales, and coexistence of multiple ground objects (Cheng et al., 2020). Given these challenges, it is essential to develop more advanced deep feature learning models to discover intricate structures and discriminative information in high-dimensional data. For GIS-based LCZ mapping methods, the design of decision rules is usually based on the selected LCZ parameters. Using all the ten LCZ parameters may be inefficient; moreover, redundant LCZ parameters could add complexity and uncertainty to rule-based decision-making algorithms. Therefore, identifying key LCZ parameters based on city characteristics is crucial for designing effective decision rules.

Future studies could also focus on the following two aspects. The first is to explore the advantages and disadvantages of RS-based and GIS-based methods. The two methods have only been compared in a few cities (see Section 3.4), where their LCZ classification results have not been thoroughly analyzed, and their performance in classifying some LCZs remains controversial. Therefore, surveys of more cities are needed to gain further insights into the pros and cons of the two methods. The second is to explore how to integrate RS-based and GIS-based methods. Although several strategies have been proposed to integrate the two methods (see Section 3.3), the development of combined methods is still

in the exploratory phase. The two categories of methods were developed from opposite paradigms; the former is a “top-down” approach while the latter is a “bottom-up” approach (Hidalgo et al., 2019). Therefore, more attention needs to be paid to exploring how to integrate the two methodological frameworks by considering their complementarity.

#### 4.5. Optimizing LCZ parameters and subclasses

The LCZ system is designed inherently universal while its descriptive and explanatory powers are sometimes limited (Stewart and Oke, 2012). Perera and Emmanuel (2018) pointed out that the LCZ framework is inherently reductionist that cannot capture all the nuances of urban forms in the world, and thus needs some degree of local customization. Many other GIS-based studies have also argued that the LCZ framework needs to be adjusted in terms of LCZ parameters and LCZ subclasses (Chen et al., 2020b; He et al., 2019; Quan, 2019a; Yang et al., 2019a; Zhao et al., 2019a).

LCZ parameters are the main basis for GIS-based LCZ mapping. However, there are several issues with LCZ parameters, e.g., it is difficult to obtain all the ten LCZ parameters due to lack of data; the reference ranges of some LCZ parameters overlap among similar LCZ classes; and the calculated LCZ parameters cannot match their reference ranges. To deal with these issues, LCZ parameters could be optimized from two aspects: (1) *Adjust reference ranges*: When the calculated LCZ parameters deviate from their reference ranges, or the reference ranges are too wide compared to the calculated values, adjusting reference ranges of LCZ parameters through statistical analysis of extensive urban data collected from various cities with different backgrounds, could be beneficial. (2) *Add auxiliary parameters*: Several LCZ parameters are rarely used due to lack of data, such as surface admittance and anthropogenic heat output, which hinders LCZ classification. The introduction of new LCZ parameters will be primarily based on the availability of data that directly or indirectly characterize urban form and function, as well as the ability to distinguish LCZ classes. For example, some satellite-derived biophysical parameters that contribute to LCZ classification, such as NDVI, NDWI, and nighttime light (Demuzere et al., 2019a; Qiu et al., 2018a; Shi and Ling, 2021; Yang et al., 2020b; Zhao et al., 2023), could be used as LCZ parameters.

Stewart and Oke (2012) suggested that LCZ subclasses can be created when an LCZ class deviates from the standard set; new subclasses represent combinations of built types, land cover types, and land cover properties. Many GIS-based studies have created various LCZ subclasses to characterize heterogeneous urban forms. However, whether and how to use LCZ subclasses remain to be explored. LCZ subclasses could be created based on the following two parameters: (1) *Area ratio of mixed LCZs*: For example, when the area ratio of LCZ B (scattered trees) in LCZ 5 (open midrise) reaches a certain threshold, LCZ 5<sub>B</sub> (mixed open midrise with scattered trees) can be used. (2) *Building height variance*: For example, LCZ 2<sub>4</sub> (mixed compact midrise and open high-rise) can be created when the variance of building heights within LCZ 2 (compact midrise) containing LCZ 4 (open high-rise) reaches a certain threshold. Appropriate thresholds for these parameters may vary across cities. Although LCZ subclasses can add flexibility to the LCZ system, Stewart and Oke (2012) recommended careful use of LCZ subclasses as too many or complex subclasses can hinder comparison and clarity.

#### 4.6. Exploring the transferability of LCZ models

The transferability of LCZ models (also known as transferability of LCZ training data) refers to LCZ classification of the target city using training samples collected from other cities. Although the transferability of LCZ models has been explored in recent years (Demuzere et al., 2019b; Liu and Shi, 2020; Rosentreter et al., 2020; Yoo et al., 2019), progress has been limited since most LCZ models were not designed for this purpose. There are three key factors relevant to the transferability of LCZ models: data features, city characteristics, and machine learning

algorithms.

Data features play an important role in the transferability of LCZ models. Although a massive amount of RS and GIS data have been used for LCZ mapping, how data features affect the performance of LCZ model transferability is still largely unknown. Demuzere et al. (2019b) investigated the transferability of LCZ models based on different combinations of features. They found that spectral indices were more relevant than single band spectral reflectance, and more importantly, the results based on the top ten features selected from the RF feature importance ranking outperformed those using all available features. This indicates that a reduced set of well-selected features can be generic enough to classify cities across climates and ecoregions. Therefore, feature selection and combination are crucial for the transferability of LCZ models, which deserve further investigation.

City characteristics such as geographic and climatic contexts, urban form and function, and development mode would affect the transferability of LCZ models. Since each city has its own characteristics, it is difficult for LCZ models to use training samples from other cities. Demuzere et al. (2019b) conducted city-to-city and all-to-one experiments to explore the role of city characteristics on LCZ model transferability. The all-to-one experiments used all-but-one city data to train the classifier and evaluate the performance on the remaining city. Their experiments showed that LCZ classification accuracy can be considerably improved if the training data came from the same ecoregion or from a combination of multiple cities. This indicates that the transferability of LCZ models tends to be easier to achieve among cities with similar characteristics. Future research could explore which aspects of city characteristics contribute more to LCZ model transferability.

The transferability of LCZ models is essentially a domain adaptation problem (Liu and Shi, 2020; Yokoya et al., 2018). Tuia et al. (2016) systematically reviewed four categories of domain adaptation methods for remote sensing image analysis, i.e., invariant feature selection, representation matching, adaptation of classifiers, and selective sampling, which could be introduced to tackle the LCZ model transferability problem. In recent years, many studies have explored the use of advanced machine learning algorithms to achieve the transferability of LCZ models. For example, the 2017 IEEE GRSS Data Fusion Contest was aimed at developing robust generalized LCZ classification models that can perform well on new cities unseen during training (Tuia et al., 2017a). The winning teams used a variety of ensemble methods to fuse results from different machine learning models and achieved acceptable classification accuracy (Yokoya et al., 2018). Elshamli et al. (2020) proposed a scalable yet simple adaptive multisource domain adaptation (AMDA) framework to address the transferability of LCZ training data. For future studies, effective domain adaptation methods that combine data features, city characteristics, and deep learning models, need to be developed to improve the transferability of LCZ models.

#### 4.7. Conducting global interannual LCZ mapping

Global interannual LCZ mapping will provide detailed and consistent information on urban form and function for urban climate studies. To date, LCZ mapping has been extended from single-city scales to regional scales, e.g., the Yangtze River Delta (Cai et al., 2018), the Pearl River Delta (Wang et al., 2019), and the Great Bay Area (Chen et al., 2021a; Hay Chung et al., 2021), continental scales, e.g., Europe (Demuzere et al., 2019a) and the continental US (Demuzere et al., 2020a), and global scales (Demuzere et al., 2022b; Zhu et al., 2022). On the other hand, interannual LCZ maps have also been generated to reveal urban expansion and intra-urban restructuring (Chen et al., 2021a; Collins and Dronova, 2019; Demuzere et al., 2020b; Huang et al., 2021a; Khamchiangta and Dhakal, 2021; Vandamme et al., 2019; Wang et al., 2019; Zhang et al., 2021b; Zhao et al., 2023), helping to assess the impact of urbanization on local climate and environment, as well as guide sustainable urban development. These recent research advances suggest that global interannual LCZ mapping is emerging as an important

research trend.

LCZ mapping on global and interannual scales is a tremendous undertaking since it is time-consuming, labor-intensive, and cost-expensive. Faced with this challenge, the research community could make efforts in the following areas: (1) *Take full advantage of Google Earth Engine (GEE)*: The GEE platform not only provides global, long-term, multi-source remote sensing data, but also supports online processing and data visualization (Gorelick et al., 2017). In recent years, GEE has been increasingly used for LCZ mapping (Brousse et al., 2019, 2020a; Chen et al., 2021a; Demuzere et al., 2019b, 2020a, 2021; Hay Chung et al., 2021; Middel et al., 2018; Shi and Ling, 2021; Zhao et al., 2023). It can be anticipated that GEE will play a more important role in global interannual LCZ mapping. (2) *Develop deep learning-based LCZ models*: Deep feature learning models have shown remarkable ability to improve the transferability of LCZ models, which can largely reduce the time and labor costs of manual selecting LCZ training data for each individual city, thereby promoting global LCZ mapping. (3) *Exploit the potential of crowdsourcing*: Crowdsourcing provides an easy and effective way to collect LCZ metadata for creating LCZ maps. The experiments by Bechtel et al. (2017b) and Verdonck et al. (2019a) showed that crowdsourced training data is acceptable for LCZ mapping. Some other crowdsourced information has also been used to assist LCZ mapping; for example, Mhedhbi et al. (2019) gathered architectural information on buildings by crowdsourcing using Facebook social network. Future studies could exploit the potential of crowdsourcing for large-scale LCZ mapping. (4) *Enhance collaboration among research communities and projects*: Many LCZ-based projects have been conducted around the world. For example, the MapUCE (Urban Climate, Human behavior, and Energy consumption: from LCZ mapping to simulation and urban planning) project is tasked with developing a generic, automated method for generating LCZ maps for all cities in France (Masson et al., 2015). The URBAN-PATH (URBAN PATHerns of Human thermal conditions) project has been proposed to evaluate urban thermal and human comfort conditions based primarily on LCZs in Szeged and Novi Sad, Hungary (Unger et al., 2015). The WUDAPT project is community-based project to collect LCZ metadata and create LCZ maps around the world (Bechtel et al., 2015). Additionally, the ENLIGHT (ENabling the analYsIs of Global urban HeaT) project is directed at global LCZ mapping and urban heat island analysis (Demuzere et al., 2021). We look forward to more LCZ-related projects and more collaborations among different research teams worldwide to promote LCZ mapping and applications.

#### 4.8. Expanding the application of LCZs

The LCZ system has been used in a wide range of research fields including, but not limited to, urban heat islands (Bechtel et al., 2019b; Budhiraja et al., 2019; Dian et al., 2020; Giridharan and Emmanuel, 2018; Liu et al., 2020b; Quan, 2019b; Zhao et al., 2020a), heat wave/risk, heat stress, and thermal comfort (Aminipouri et al., 2019; Das and Das, 2020a; Geletić et al., 2018; Giannaros et al., 2023; Kotharkar et al., 2021; Lau et al., 2019; Milošević et al., 2016; Patel et al., 2022; Savić et al., 2018; Top et al., 2020; Unger et al., 2018; Verdonck et al., 2019b), urban design and planning (Liu et al., 2020a; Maharoof et al., 2020; Perera and Emmanuel, 2018; Vandamme et al., 2019), urban meteorology (Dunjić et al., 2021; Patel et al., 2020; Tse et al., 2018; Yang et al., 2020d), urban pollution (Shi et al., 2019b), human health (Brousse et al., 2019, 2020a), building energy consumption (Shi et al., 2019a), anthropogenic heat (Rathnayake et al., 2020), building carbon emissions (Sharifi et al., 2018; Wu et al., 2018), land cover change (Chen et al., 2021a; Khamchiangta and Dhakal, 2021; Wang et al., 2019), and thermal anisotropy (Jiang et al., 2021; Krayenhoff and Voogt, 2016).

Despite its wide range of applications, the LCZ system is basically used in spatial statistical analysis and urban climate modeling. Spatial statistical analysis based on the LCZ classification scheme is generally performed in two ways. The first is to analyze the spatial variation of target variables between and within LCZ classes. The most typical

research is to investigate intra- and inter-class temperature differences of LCZs (Chen et al., 2020b; Du et al., 2020a; Fenner et al., 2017; Geletič et al., 2016; Jiang et al., 2022; Lehnert et al., 2018; Li et al., 2021; Meier et al., 2017; Stewart et al., 2014; Unal Cilek and Cilek, 2021; Yang et al., 2020c). Some studies have also explored inter- and intra-LCZ variability in other surface and atmospheric parameters, such as NDVI (Ferreira and Duarte, 2019), wind speed (Zhao et al., 2020c), humidity (Yang et al., 2020d), and heat advection (Brousse et al., 2022). The second is to analyze the relationship between target variables and LCZs (or LCZ parameters). For example, Shih et al. (2020) used an ordinary least squares regression model to explain LST variation at the neighborhood level resulting from LCZ types and greenspace coherence. Sapena et al. (2021) used multiple linear regression models to quantify the relationship between LCZ-based urban spatial pattern metrics and socio-economic variables. Future studies could explore more broadly the spatial patterns and correlations of observed variables involved in surface and atmospheric processes that occur across LCZs.

The LCZ system provides detailed urban morphological and material properties, which can improve urban parameterization of regional climate models (RCMs). To date, LCZ-based information has been incorporated into various RCMs, such as the WRF model (Brousse et al., 2016; Molnár et al., 2019; Mu et al., 2020; Mughal et al., 2019, 2020; Patel et al., 2020; Pellegatti Franco et al., 2019; Ribeiro et al., 2021; Vogel et al., 2022; Zhou et al., 2022), the COSMO-CLM model (Brousse et al., 2020b; Varentsov et al., 2020), the MesoNH-SURFEX-TEB-BEM coupling model (Kwok et al., 2020), the urban energy balance calculation model (Jin et al., 2020), and the surface urban energy and water balance scheme (SUEWS) model (Alexander et al., 2015). Most of these studies reported improved model performance by incorporating LCZs. Given the discrepancy in scale between LCZs and RCMs, fine-scale LCZs are normally upscaled to the coarse scales of RCMs by spatial aggregation. For example, Bechtel et al. (2015) suggested that it is appropriate to conduct LCZ mapping at a finer scale and then aggregate LCZ-based urban canopy parameters (UCPs) to a coarser scale for modeling. The WUDAPT project provides useful tools to inject LCZ-based UCPs into RCMs, such as the WUDAPT-TO-WRF, WUDAPT-TO-COSMO-CLM, and WUDAPT-TO-UMEP tools (<https://www.wudapt.org/>). Future research could further explore the potential of integrating LCZ information into RCMs for urban climate and environmental modeling.

LCZs are climatic in nature; however, the definition of LCZs does not tell what climate each LCZ represents. LCZs have specific geometric, surface cover, thermal, radiative, and metabolic properties, which impact the local climate. Stewart and Oke (2012) elucidated that “Each LCZ has a characteristic screen height temperature regime that is most apparent over dry surfaces, on calm, clear nights, and in areas of simple relief.” In fact, meteorological variables (e.g., temperature, humidity, and wind) in the urban canopy layer show distinct characteristic regimes between and within LCZ classes. It is difficult to directly link each LCZ to a specific local climate. Nevertheless, further understanding of the climatic signatures of LCZs can be gained by carrying out in situ observations and model simulations based on LCZs in extensive cities. For example, van de Walle et al. (2021) demonstrated the importance of combining local fieldwork (e.g., the acquisition of building material properties in the city and the placement of sensors in a variety of LCZs) with regional climate modeling for LCZ-based urban climate research. With the expanding application of LCZs in urban research, a wealth of new knowledge on urban climate and environment could be gained, which serves sustainable urban development.

## 5. Summary

LCZ mapping research has achieved great advance in the past decade. This paper systematically reviewed the research progress of different LCZ mapping methods. Specifically, we comprehensively surveyed the LCZ mapping literature during 2012–2021, provided a statistical analysis of the LCZ mapping literature, elaborated the

frameworks of different LCZ mapping methods, and discussed challenges and future directions for LCZ mapping.

The LCZ mapping literature has increased significantly since 2012; meanwhile, LCZ mapping has been extended from single-city to global scales. LCZ mapping methods can be broadly categorized into RS-based, GIS-based, and combined methods. RS-based methods can be further divided into pixel-, object-, and scene-level classification methods. RS-based methods are much more widely used compared with GIS-based and combined methods. RS-based methods generally consist of five steps: select feature sets, define classification units, collect training areas, classify LCZs, and evaluate classification results. GIS-based methods usually include four steps: calculate LCZ parameters, define basic spatial units, classify LCZs, and evaluate classification results. For RS-based methods, we elaborated on commonly used feature sets and feature importance analysis; pixel, object, and scene classification units; considerations for collecting LCZ training areas; machine learning algorithms employed by pixel-, object-, and scene-level classification and differences in model performance; and validation strategies, evaluation metrics, and classification accuracy. For GIS-based methods, we elaborated on LCZ parameters calculated using multi-source data; parcel and grid spatial units; classification algorithms and post-processing rules; and validation strategies and classification accuracy. For combined methods, we summarized two typical strategies, namely “coarse-to-fine” and “built type-land cover type separation” for integrating RS- and GIS-based methods.

Several challenges and future directions for LCZ mapping have been discussed, including data sources, LCZ mapping unit size, LCZ ground truth data, LCZ classification algorithms, LCZ parameters and subclasses, transferability of LCZ models, global interannual LCZ mapping, and application of LCZs. The corresponding key points are summarized as follows: (1) A wealth of RS and GIS data that provide useful information on urban form and function need to be further exploited for LCZ mapping. How to deal with inconsistent data quality and feature redundancy of multi-source data requires further exploration. (2) Determining an appropriate LCZ mapping unit size needs to consider LCZ scale, city characteristics, spatial resolution of multi-source data, classification algorithms, and application requirements. (3) Acquiring high-quality LCZ ground truth data requires knowledge of LCZ concepts, expertise in remote sensing image analysis, familiarity with urban morphology, and specialized training. Benchmark LCZ data sets need to be created at global scales using multiple high-resolution satellite imageries. (4) Developing deep learning models plays an important role in improving RS-based LCZ mapping methods, especially for object- and scene-level classification. How to effectively integrate RS- and GIS-based LCZ mapping methods needs to be further explored. (5) LCZ parameters could be optimized by adjusting their reference ranges and adding auxiliary parameters, and LCZ subclasses could be created based on the area ratio and building height variance of mixed LCZs. (6) Effective domain adaptation methods that combine data features, city characteristics, and deep learning models, need to be developed to improve the transferability of LCZ models. (7) Global interannual LCZ mapping is emerging as an important research trend that can benefit from GEE, deep learning, crowdsourcing, and collaboration among research communities. (8) The application of LCZs needs to be expanded in the analysis of spatial patterns and correlations of observed surface and atmospheric variables, as well as in urban climate and environmental modeling.

Our comprehensive review of LCZ mapping provides the research community with a wealth of information on current progress, challenges, and future directions. With the collaboration of participants from different research fields, LCZ mapping will be further promoted and its application will be further expanded in the future. LCZ mapping contributes to creating standardized spatial databases of urban form and function for cities worldwide, advancing scientific knowledge of urban climate and environment, and formulating adaptation and mitigation strategies for sustainable urban development.

## CRediT authorship contribution statement

**Fan Huang:** Writing – original draft. **Sida Jiang:** Writing – original draft. **Wenfeng Zhan:** Conceptualization, Writing – original draft, Writing – review & editing. **Benjamin Bechtel:** Writing – review & editing. **Zihan Liu:** Writing – review & editing. **Matthias Demuzere:** Writing – review & editing. **Yuan Huang:** Writing – review & editing. **Yong Xu:** Writing – review & editing. **Lei Ma:** Writing – review & editing. **Wanjun Xia:** Writing – review & editing. **Jinling Quan:** Writing – review & editing. **Lu Jiang:** Writing – review & editing. **Jiameng Lai:** Writing – review & editing. **Chenguang Wang:** Writing – review & editing. **Fanhua Kong:** Writing – review & editing. **Huilin Du:** Writing – review & editing. **Shiqi Miao:** Writing – review & editing. **Yangyi Chen:** Writing – review & editing. **Jike Chen:** Writing – review & editing.

## Appendix A

### Table A1

The journals and conferences that has published at least two LCZ mapping papers during 2012–2021.

Journals and conferences (abbreviation)	LCZ mapping literature
Urban Climate (Urban Clim.)	(Bechtel et al., 2019a; Beck et al., 2018; Bocher et al., 2018; Brousse et al., 2016, 2019; Cai et al., 2018; Chen et al., 2020a; Ching et al., 2019; Choudhury et al., 2021; Das and Das, 2020a; Demuzere et al., 2019b; Du et al., 2020a; Emery et al., 2021; Fernández et al., 2021; Fonte et al., 2019; Hidalgo et al., 2019; Huang et al., 2021a; Khamchiangta and Dhakal, 2021; Kotharkar and Bagade, 2018; La et al., 2020; Mhedbibi et al., 2019; Mouzourides et al., 2019; Mushore et al., 2019; Ochola et al., 2020; Oliveira et al., 2020; Patel et al., 2020; Perera and Emmanuel, 2018; Richard et al., 2018; Rodler and Leduc, 2019; Wang et al., 2018b, 2019; Yang et al., 2020c; Zheng et al., 2018; Zhou et al., 2020a; Ziaul and Pal, 2018; Zonato et al., 2020)
Building and Environment (Build. Environ.)	(Anjos et al., 2020; Cai et al., 2021; Chen et al., 2021a; Geletič et al., 2019; Hay Chung et al., 2021; Jin et al., 2020; Leconte et al., 2015; Ma et al., 2021a; McRae et al., 2020; Quan and Bansal, 2021; Villadiego and Velay-Dabat, 2014; Wang et al., 2020)
IEEE Journal of Selected Topics in Applied Earth Observations and Remote Sensing (IEEE J. Sel. Top. Appl. Earth Obs. Remote Sens.)	(Bartesaghi Koc et al., 2018; Bechtel et al., 2016b; Bechtel and Daneke, 2012; Danylo et al., 2016; Hu et al., 2019; Qiu et al., 2020b; Xu et al., 2017b; Yokoya et al., 2018; Yu et al., 2021; Zhou et al., 2021a)
Remote Sensing (Remote Sens.)	(Bechtel et al., 2020; Collins and Dronova, 2019; Geletič et al., 2016; Johnson and Jozdani, 2019; Li et al., 2021; Liu et al., 2019; Qiu et al., 2018a; Vandamme et al., 2019; Yoo et al., 2020; Zhao et al., 2019b)
Sustainable Cities and Society (Sustain. Cities Soc.)	(Khoshnoodmotagh et al., 2021; Shih et al., 2020; Unal Cilek and Cilek, 2021; Wang et al., 2021a; Yang et al., 2019a, 2021; Zhou et al., 2020b, 2021b)
Atmosphere	(Alexander and Mills, 2014; Dimitrov et al., 2021; Ma et al., 2021b; Mandelmilch et al., 2020; Varentsov et al., 2020; Zhang et al., 2021b; Zhao et al., 2020c)
ISPRS International Journal of Geo-Information (ISPRS Int. J. Geo-Inf.)	(Bechtel et al., 2015; Hu et al., 2018; Kopp et al., 2021; Lehnert et al., 2021; Nurwanda and Honjo, 2018; Oxoli et al., 2018; Stredová et al., 2021)
ISPRS Journal of Photogrammetry and Remote Sensing (ISPRS J. Photogramm. Remote Sens.)	(Kim et al., 2021; Liu and Shi, 2020; Qiu et al., 2019a; Wang et al., 2018a; Yoo et al., 2019)
IEEE Transactions on Geoscience and Remote Sensing (IEEE Trans. Geosci. Remote Sens.)	(Elshamli et al., 2020; Ru et al., 2021; Zhang et al., 2019a, 2021a)
Sustainability	(Cai et al., 2019; Chen et al., 2020b; Manandhar et al., 2019; Wang et al., 2017)
Theoretical and Applied Climatology (Theor. Appl. Climatol.)	(Chen et al., 2019; Leconte et al., 2017; Molnár et al., 2019; van de Walle et al., 2021)
Climate	(Agathangelidis et al., 2019, 2020; Gonçalves et al., 2018)
International Journal of Applied Earth Observation and Geoinformation (Int. J. Appl. Earth Obs. Geoinf.)	(Nassar et al., 2016; Verdonck et al., 2017; Xu et al., 2021)
International Journal of Climatology (Int. J. Climatol.)	(Hammerberg et al., 2018; Kwok et al., 2019; Skarbit et al., 2017)
Landscape and Urban Planning (Landsc. Urban Plan.)	(Alexander et al., 2016; Emmanuel and Loconsole, 2015; Kabano et al., 2021)
Energy and Buildings (Energy Build.)	(Bokwa et al., 2019; Pokhrel et al., 2019)
Energy Procedia	(Quan et al., 2017; Wu et al., 2018)
Journal of Cleaner Production (J. Clean. Prod.)	(Wang et al., 2021b; Yang et al., 2020b)
Procedia Environmental Sciences (Procedia Environ. Sci.)	(Cai et al., 2016; Thomas et al., 2014)
Remote Sensing of Environment (Remote Sens. Environ.)	(Chang et al., 2021; Rosenreiter et al., 2020)
IEEE International Geoscience and Remote Sensing Symposium (IGARSS)	(dos Anjos et al., 2017; Feng et al., 2019, 2020; Gawlikowski et al., 2020; Jing et al., 2019; Qiu et al., 2019b; Sukhanov et al., 2017; Xu et al., 2017a; Yang et al., 2019b; Yokoya et al., 2017; Zhao et al., 2020b)
Joint Urban Remote Sensing Event (JURSE)	(Bartesaghi Koc et al., 2017; Bechtel et al., 2017a; Cai et al., 2017; Chen et al., 2017; Kaloustian et al., 2017; Lopes et al., 2017; Mitraka et al., 2015; Shih, 2017; Skarbit et al., 2015; Tuia et al., 2017b; Xu et al., 2017c)
International Conference on Urban Climatology (ICUC)	(Bokwa et al., 2015; Gál et al., 2015; Lau et al., 2015; Masson et al., 2015; Mills et al., 2015; Picone and Campo, 2015; Plumejeaud-Perreau et al., 2015; Zheng et al., 2015)
The International Archives of the Photogrammetry, Remote Sensing and Spatial Information Sciences (ISPRS Archives)	(Bechtel et al., 2012, 2016a; Estacio et al., 2019; Leichter et al., 2018; Qiu et al., 2018c; Wei and Blaschke, 2016)
IOP Conference Series: Earth and Environmental Science (IOP Conf. Ser.: Earth Environ. Sci.)	(Berlessova and Konstantinov, 2020; Nurwanda, 2018; Pradhesta et al., 2019; Semenova et al., 2019)

## Declaration of Competing Interest

The authors declare that they have no known competing financial interests or personal relationships that could have appeared to influence the work reported in this paper.

## Data availability

Data will be made available on request.

## Acknowledgments

This research was supported by the National Natural Science Foundation of China (42001270 and 42171306). We are also grateful for the financial support from the National Youth Talent Support Program of China.

(continued on next page)

**Table A1 (continued)**

Journals and conferences (abbreviation)	LCZ mapping literature
International Conference on Countermeasures to Urban Heat Islands (IC2UHI)	(Ren et al., 2016a, 2016b)

**Table A2**

The literature information of RS-based LCZ mapping methods. The symbol ‘–’ indicates that the information is not explicitly provided in the literature.

Literature	Primary data sources	Classification unit size	Classification algorithms	Validation strategies (Evaluation metrics)
Pixel-level classification methods				
(Bechtel and Daneke, 2012)	Landsat 5, Landsat 7, IFSAR data	100 m	NB, NN, SVM, RF	Hold-out (OA, UA, PA, Kappa)
(Bechtel et al., 2015)	Landsat 5, Landsat 8	100 to 120 m	RF	(OA, UA, PA, Kappa)
(Bechtel et al., 2016b)	Landsat 8, Sentinel-1	120 m	NB, RF, SVM, MLP	Hold-out (OA, PA, UA, Kappa)
(Brousse et al., 2016)	Landsat 8	–	WUDAPT	–
(Cai et al., 2016)	Landsat 8	–	WUDAPT	Hold-out (OA, PA, UA, Kappa)
(Danylo et al., 2016)	Landsat 8	120 m	RF	Hold-out (OA, PA, UA, Kappa)
(Kaloustian and Bechtel, 2016)	Landsat 8, Sentinel-2	100 m	RF	Bootstrapping (OA, Kappa)
(Skarbit and Gál, 2016)	–	–	WUDAPT	–
(Budhiraja et al., 2017)	Landsat 8	–	WUDAPT	–
(Cai et al., 2017)	Landsat 8	100 m	RF	Hold-out (OA, UA, PA, Kappa)
(Chen et al., 2017)	Landsat 8	–	WUDAPT	–
(Kaloustian et al., 2017)	Landsat 8, Sentinel-1, Sentinel-2	100 m	RF	Bootstrapping (OA, Kappa)
(Shih, 2017)	Landsat 8	–	WUDAPT	–
(Sukhanov et al., 2017)	Landsat 8, Sentinel-2, OSM	100 m	CNN, RF, GBM	Cross-validation (OA, Kappa)
(Tuia et al., 2017b)	Rapid-eye, Cartosat-1, OSM	200 m	MRF	Hold-out (OA, AA, Kappa)
(Verdonck et al., 2017)	Landsat 8	30, 100 m	RF	Bootstrapping (OA, F1)
(Wang et al., 2017)	Landsat 8	100 m	WUDAPT	–
(Xu et al., 2017a)	Landsat 8, Sentinel-2, OSM	–	XGBoost, SVM, MLP	(OA, Kappa)
(Xu et al., 2017b)	Landsat 8, ASTER	30 m	RF, NN, SVM	Hold-out (OA, Kappa)
(Xu et al., 2017c)	Landsat 8	120 m	RF	Hold-out (OA, UA, PA, Kappa)
(Yokoya et al., 2017)	Landsat 8, OSM	100 m	CCF, RoF	Hold-out (OA, UA, PA, Kappa)
(Beck et al., 2018)	Landsat 8	100 m	WUDAPT	–
(Cai et al., 2018)	Landsat 8	100 m	RF	Hold-out (OA, UA, PA, Kappa)
(Chieppa et al., 2018)	Landsat 8	–	WUDAPT	–
(Hu et al., 2018)	Landsat 8, Sentinel-1	100 m	CCF	Hold-out (OA, UA, PA, Kappa)
(Nurwanda and Honjo, 2018)	Landsat 5, Landsat 8	–	ML	(OA, UA, PA, k)
(Nurwanda, 2018)	–	–	–	–
(Oxoli et al., 2018)	Landsat 8, Sentinel-2, Rapid-eye	–	RF	Hold-out (OA, UA, PA, k)
(Richard et al., 2018)	Landsat 8	–	WUDAPT	–
(Wang et al., 2018a)	Landsat 8	100 m	RF	Hold-out (OA, UA, PA, k)
(Wang et al., 2018c)	Landsat 8	200 m	WUDAPT	–
(Xu et al., 2018)	Landsat 8, DSM	30 m	RF, SVM	Hold-out (OA, UA, PA)
(Ziaul and Pal, 2018)	Landsat 5, Landsat 8	100 m	RF	Hold-out (OA, UA, PA, Kappa)
(Bechtel et al., 2019a)	Landsat 8, Sentinel-2	100 m	WUDAPT	Bootstrapping (OA, WA, Kappa)
(Bokwa et al., 2019)	–	–	WUDAPT	–
(Brousse et al., 2019)	Landsat 8, Sentinel-1, DMSP-OLS nighttime lights	–	WUDAPT	Bootstrapping (OA, OA <sub>u</sub> , OA <sub>bu</sub> , WA, F1)
(Chen et al., 2019)	Landsat 8	100 m	WUDAPT	–
(Demuzere et al., 2019b)	Landsat 8, Sentinel-1, DMSP-OLS nighttime lights, GFCH, GTOPO30, DSM, DEM	100 m	RF	Bootstrapping (OA, OA <sub>u</sub> , OA <sub>bu</sub> , WA, F1)
(Demuzere et al., 2019a)	–	–	–	–
(Eldesoky et al., 2019)	Landsat 8, digital topographic database	30 m	WUDAPT	Bootstrapping (OA, OA <sub>u</sub> , PA, Kappa)
(Khamchiangta and Dhakal, 2019)	Landsat 8	–	WUDAPT	(OA, Kappa)

(continued on next page)

**Table A2 (continued)**

Literature	Primary data sources	Classification unit size	Classification algorithms	Validation strategies (Evaluation metrics)
(Mouzourides et al., 2019)	Landsat 8	100 m	RF	Hold-out (OA, Kappa)
(Mughal et al., 2019)	Landsat 8, building height data	–	WUDAPT	Hold-out (OA, Kappa)
(Mushore et al., 2019)	Landsat 8	30 m	SVM, RF	Hold-out (OA, UA, PA, Kappa)
(Pokhrel et al., 2019)	Landsat 8	100 m	WUDAPT	–
(Pradhesta et al., 2019)	Landsat 8	–	WUDAPT	–
(Ren et al., 2019)	Landsat 8, Sentinel-1	100 m	WUDAPT	Hold-out (OA, OA <sub>u</sub> , WA)
(Gholami and Beck, 2019)	Landsat 8	100 m	WUDAPT	–
(Semenova et al., 2019)	Landsat 7	–	WUDAPT	–
(Shi et al., 2019c)	Landsat 8	100 m	WUDAPT	Hold-out (OA, Kappa)
(Vandamme et al., 2019)	Landsat 7, Landsat 8	100 m	RF	Bootstrapping (OA, F1)
(Wang et al., 2019)	Landsat 5, Landsat 8	100 m	RF	Hold-out (OA, UA, PA, Kappa)
(Zhang et al., 2019a)	Landsat 8, Sentinel-2, OSM	100 m	CCF	Hold-out (OA, UA, PA, Kappa)
(Zhao et al., 2019b)	Landsat 8	100 m	CRF, RF, SVM, NB	Bootstrapping (OA, Kappa)
(Anjos et al., 2020)	Landsat 8	100 m	RF	Hold-out (OA, UA, PA, Kappa)
(Bande et al., 2020a)	Landsat 8	–	WUDAPT	–
(Bande et al., 2020b)	Landsat	–	WUDAPT	–
(Berlessova and Konstantinov, 2020)	Landsat	–	WUDAPT	–
(Brousse et al., 2020a)	–	100 m	RF	Bootstrapping (OA, WA, F1)
(Chen et al., 2020a)	Landsat 8	–	WUDAPT	Hold-out (OA)
(Colli et al., 2020)	Landsat 8	–	WUDAPT	–
(Das and Das, 2020b)	Landsat 5, Landsat 8	100 m	WUDAPT	Hold-out (OA, UA, PA, Kappa)
(Demuzere et al., 2020a)	Landsat 8, Sentinel-1, DMSP-OLS, nighttime lights, GFCH, USGS/GTOPO30, DSM, DEM	100 m	RF	Bootstrapping (OA, OA <sub>u</sub> , OA <sub>bu</sub> , WA, F1)
(Demuzere et al., 2020b)	Landsat 5, Landsat 7, Landsat 8	–	WUDAPT	–
(Droste et al., 2020)	–	–	WUDAPT	–
(Fricke et al., 2020)	Landsat 8	100 m	WUDAPT	–
(La et al., 2020)	Sentinel-2, PALSAR-2	10 m	Subspace, SVM, ML	Hold-out (OA, UA, PA, Kappa)
(Manandhar et al., 2019)	Landsat 8	–	WUDAPT	–
(McRae et al., 2020)	Landsat 8	100 m	WUDAPT	–
(Mu et al., 2020)	Landsat 8	–	WUDAPT	–
(Ochola et al., 2020)	Landsat 8	100 m	RF	Hold-out (OA, UA, PA, Kappa)
(Patel et al., 2020)	Landsat 8	100 m	RF	Hold-out (OA, UA, PA, Kappa)
(Shevchenko et al., 2020)	Landsat 8	–	WUDAPT	–
(Shih et al., 2020)	Landsat 8	30 m	WUDAPT	–
(Varentsov et al., 2020)	Landsat 8, Sentinel-1, Sentinel-2, GFCH, DTM, DEM, DSM	100 m	RF	Bootstrapping (OA, OA <sub>u</sub> , OA <sub>bu</sub> , WA, F1)
(Wang et al., 2020)	–	–	WUDAPT	–
(Yang et al., 2020a)	Landsat	100 m	WUDAPT	Hold-out (OA, UA, PA, Kappa)
(Zhao et al., 2020c)	–	–	WUDAPT	–
(Zhou et al., 2020b)	Landsat 8	100 m	RF	Hold-out (OA, UA, PA, Kappa)
(Zonato et al., 2020)	Landsat	30 m	WUDAPT	–
(Aslam et al., 2021)	Landsat 8	100 m	WUDAPT	Cross-validation
(Chen et al., 2021a)	Sentinel-1, Sentinel-2	–	RF	–
(Chen et al., 2021b)	Landsat 8	200 m	WUDAPT	–
(Choudhury et al., 2021)	Landsat 8	100 m	WUDAPT	Hold-out (OA, Kappa)
(Hay Chung et al., 2021)	Landsat 8, Sentinel-1, Sentinel-2	100 m	RF, SVM, CART	Hold-out (OA, OA <sub>u</sub> , OA <sub>nat</sub> , UA, PA, F1)
(Dutta et al., 2021)	Landsat 8	15 m	ML	Hold-out (OA, UA, PA, Kappa)
(Emery et al., 2021)	Landsat 8	100 m	WUDAPT	–
(Fernández et al., 2021)	Landsat 8	–	WUDAPT	–
(Gál et al., 2021)	Landsat	–	WUDAPT	–
(Huang et al., 2021a)	–	–	WUDAPT	–
(Jamali et al., 2021)	Landsat 8	100 m	WUDAPT	Hold-out (OA, Kappa)
(Kabano et al., 2021)	Landsat 8	100 m	RF	Hold-out (OA, Kappa)
(Khamchiangta and Dhakal, 2021)	Landsat	–	WUDAPT	–
(Khoshnoodmotlagh et al., 2021)	Landsat	100 m	WUDAPT	Hold-out (OA, Kappa)
(Li et al., 2021)	Landsat 8	–	WUDAPT	Hold-out (OA, OA <sub>u</sub> , OA <sub>nat</sub> )

(continued on next page)

**Table A2 (continued)**

Literature	Primary data sources	Classification unit size	Classification algorithms	Validation strategies (Evaluation metrics)
(Liang et al., 2021)	Landsat 8	100 m	WUDAPT	–
(Pokhrel and González-Cruz, 2021)	–	–	WUDAPT	–
(Shi and Ling, 2021)	Sentinel-1, Sentinel-2, OSM, nighttime light	–	RF	Hold-out (OA, OA <sub>bu</sub> , OA <sub>nat</sub> , UA, PA)
(Tong et al., 2021)	Landsat 8	300 m	WUDAPT	–
(Wang et al., 2021a)	Landsat 8	–	ML	Hold-out (OA, UA, PA, Kappa)
(Wang et al., 2021b)	Landsat 8	100 m	WUDAPT	Hold-out (OA, Kappa)
(Xu et al., 2021)	Landsat	100 m	RF, ResNet	Bootstrapping (OA, OA <sub>bu</sub> , OA <sub>nat</sub> , WA, F1)
(Zhang et al., 2021b)	Landsat 5, 7, 8	From 30 to 240 m at 30-m intervals	RF	Hold-out (OA, Kappa)
Object-level classification methods				
(Wei and Blaschke, 2016)	HJ-1B	Scale parameter: 50	MRS, SOM	–
(dos Anjos et al., 2017)	Landsat 8, Sentinel-2	Scale parameter: 20	MRS, RF	Bootstrapping (OA, Kappa)
(Collins and Dronova, 2019)	Landsat 5, 8	Scale parameter: 20	Segment Mean Shift tool in ArcGIS, RF	Bootstrapping (OA, PA, UA)
(Liu et al., 2019)	Sentinel-1, Sentinel-2, ROSIS data	Scale parameter: 30, 20, 8	MRS, SVM, RF, CNN	Hold-out (OA, AA, Kappa)
(Simanjuntak et al., 2019)	Pleiades, SPOT-6, OSM	Scale parameter: 10, 300, 500	MRS, Rule-set classification	Hold-out (OA, PA, UA, Kappa)
(Ma et al., 2021a)	Sentinel-2	Scale parameter: 100	MRS, RF	Hold-out (OA, PA, UA, Kappa)
(Ma et al., 2021b)	–	Scale parameter: 90	–	Hold-out (OA)
(Zhou et al., 2021a)	Sentinel-2, OSM, DSM, DEM	–	CNN	Hold-out (OA, UA, PA, Kappa)
Scene-level classification methods				
(Leichter et al., 2018)	Sentinel-2, Twitter data	Scene size: 250 × 250 pixels (10 m resolution)	CNN	Hold-out (F1, recall, precision)
(Qiu et al., 2018a)	Sentinel-2, Landsat 8, GUF, OSM, VIIRS nighttime light, So2Sat LCZ42 data set	Scene size: 32 × 32 pixels (10 m resolution)	ResNet	Cross-validation (OA, AA, Kappa, WA)
(Qiu et al., 2018b)	Sentinel-2, So2Sat LCZ42 data set	–	–	–
(Qiu et al., 2018c)	Sentinel-2, GUF, OSM, So2Sat LCZ42 dataset	–	–	–
(Feng et al., 2019)	Sentinel-1, Sentinel-2, So2Sat LCZ42 data set	Scene size: 32 × 32 pixels (10 m resolution)	Inception and Densenet based embranchment CNN	Hold-out (precision)
(Jing et al., 2019)	Sentinel-1, Sentinel-2, So2Sat LCZ42 data set	Scene size: 32 × 32 pixels (10 m resolution)	ResNeXt	Hold-out (OA)
(Qiu et al., 2019a)	Sentinel-2, So2Sat LCZ42 data set	Scene size: 32 × 32 pixels (10 m resolution)	Re-ResNet	Cross-validation (OA, Kappa)
(Qiu et al., 2020a)	–	Scene size: 32 × 32 pixels (10 m resolution)	ResNet	Bootstrapping (OA, PA, UA)
(Xu et al., 2019)	Google Street View	Scene size: 640 × 640 pixels	Inception-v3	–
(Yang et al., 2019b)	Sentinel-2, So2Sat LCZ42 data set	Scene size: 32 × 32 pixels (10-m resolution)	MSPPF-nets	Hold-out (precision, recall, F1)
(Yoo et al., 2019)	Landsat 8	Scene size: 10 × 10 and 30 × 30 pixels (10 m resolution)	Keras open-source library	Hold-out (OA, PA, UA, F1)
(Elshamli et al., 2020)	Landsat 8, Sentinel-2	Scene size: 20 × 20 pixels (30 m resolution)	DNN-based AMDA framework	Hold-out (OA)
(Feng et al., 2020)	Sentinel-1, Sentinel-2, So2Sat LCZ42 data set	Scene size: 32 × 32 pixels (10 m resolution)	DFN	Hold-out (accuracy, precision)
(Gawlikowski et al., 2020)	Sentinel-1, Sentinel-2, So2Sat LCZ42 dataset	Scene size: 32 × 32 pixels (10 m resolution)	CNN-based fusion network	Hold-out (OA, AA, Kappa)
(Kim et al., 2020)	Sentinel-2	Scene size: 32 × 32 pixels (10 m resolution)	MSCNN	Hold-out (OA, Kappa, F1)
(Liu and Shi, 2020)	Sentinel-2	Scene size: 10 × 10, 16 × 16, 32 × 32, 64 × 64 (10 m resolution)	LCZNet	Hold-out (OA, AA, Kappa)
(Qiu et al., 2020b)	Sentinel-2, So2Sat LCZ42 data set	Scene size: 32 × 32 pixels (10 m resolution)	Sen2LCZ-Net-MF	Hold-out (OA, AA, WA, Kappa)
(Qiu et al., 2022)	–	–	multi-task learning (MTL)-based CNN	–
(Rosentreter et al., 2020)	Sentinel-2	Scene size: 32 × 32 pixels (10 m resolution)	VGGNet	Hold-out (OA, PA, UA)
(Taubenböck et al., 2020)	Sentinel-2, So2Sat LCZ42 data set	Scene size: 32 × 32 pixels (10 m resolution)	Re-ResNet	–
(Yoo et al., 2020)	Sentinel-2, OpenStreetMap	Scene size: 55 × 55, 33 × 33 (10 m resolution)	Keras open-source library	Hold-out (OA, OA <sub>bu</sub> , OA <sub>nat</sub> , F1)
(Zhao et al., 2020b)	So2Sat LCZ42 data set	Scene size: 32 × 32 pixels (10 m resolution)	CNN, circled similarity propagation-based domain adaptation (CPDA) method	Bootstrapping (OA)
(Huang et al., 2021b)	Landsat 8	Scene size: 16 × 16 pixels (15 m resolution)	CNN	Hold-out (OA, PA, UA, F1)
(Kim et al., 2021)	Sentinel-2, OSM, DSM, LULC map, So2Sat LCZ42 data set	Scene size: 32 × 32, 48 × 48 pixels (10 m resolution)	MSMLA-Net	Hold-out (OA, OA <sub>bu</sub> , OA <sub>nat</sub> , WA, F1)
(Yu et al., 2021)	Landsat 8, Sentinel-2	–	ResNet, GCN	Hold-out (OA, Kappa, AA)

(continued on next page)

**Table A2 (continued)**

Literature	Primary data sources	Classification unit size	Classification algorithms	Validation strategies (Evaluation metrics)
(Zhang et al., 2021a)	Gaofen-3, So2Sat LCZ42 data set	Scene size: 64 × 64 pixels (5-m resolution)	CNN	Hold-out (OA, Kappa, AA)

**Table A3**

The standard LCZ parameters used by GIS-based LCZ mapping methods.

Literature	LCZ parameters									
	SVF	AR	BSF	ISF	PSF	HRE	TRC	SAD	SAL	Ah
<b>Parcel-based methods</b>										
(Perera et al., 2013)	✓	✓	✓	✓	✓	✓	✓	✓	✓	✓
(Lelovics et al., 2014)	✓		✓	✓	✓	✓	✓		✓	✓
(Thomas et al., 2014)	✓	✓	✓	✓	✓	✓				
(Unger et al., 2014)	✓		✓	✓	✓	✓				
(Leconte et al., 2015)	✓	✓	✓	✓	✓	✓	✓			✓
(Ndetto and Matzarakis, 2015)	✓	✓	✓	✓	✓	✓	✓			
(Plumejeaud-Perrreau et al., 2015)	✓	✓								✓
(Secerov et al., 2015)	✓			✓	✓	✓	✓		✓	
(Skarbit et al., 2015)	✓			✓	✓	✓	✓		✓	
(Quan et al., 2017)		✓				✓	✓			
(Skarbit et al., 2017)	✓		✓	✓	✓	✓	✓			
(Gonçalves et al., 2018)	✓			✓				✓		
(Perera and Emmanuel, 2018)	✓	✓	✓	✓	✓	✓	✓	✓	✓	✓
(Savić et al., 2018)	✓		✓	✓	✓	✓	✓	✓	✓	
(Wu et al., 2018)	✓	✓	✓	✓	✓	✓	✓			
(Hidalgo et al., 2019)						✓				
(Chen and Huang, 2019)	✓	✓	✓	✓	✓	✓	✓	✓		
(Kwok et al., 2019)						✓				
(Quan, 2019a)	✓		✓	✓	✓	✓	✓			
(Rodler and Leduc, 2019)	✓	✓	✓	✓	✓	✓	✓			
(Jin et al., 2020)	✓	✓	✓	✓	✓	✓	✓	✓		
(Mandelmilch et al., 2020)	✓	✓	✓	✓	✓	✓	✓			
(Cai et al., 2021)				✓	✓	✓	✓			
(Chang et al., 2021)			✓		✓	✓	✓			
<b>Grid-based methods</b>										
(Lau et al., 2013)	✓		✓			✓				
(Mitroka et al., 2015)	✓		✓	✓	✓	✓			✓	
(Zheng et al., 2015)			✓			✓				
(Nassar et al., 2016)	✓		✓	✓	✓	✓	✓			
(Geletič and Lehnert, 2016)			✓	✓	✓	✓	✓			
(Geletič et al., 2016)			✓	✓	✓	✓	✓			
(Zhongli and Hanqiu, 2016)			✓	✓	✓	✓	✓			
(Bartesaghi Koc et al., 2017)	✓			✓	✓	✓	✓			
(Hammerberg et al., 2018)		✓	✓	✓	✓	✓	✓			
(Bartesaghi Koc et al., 2018)	✓			✓	✓	✓	✓			
(Zhan et al., 2018)	✓		✓	✓	✓	✓	✓	✓		
(Agathangelidis et al., 2019)		✓		✓	✓	✓	✓			
(Cai et al., 2019)	✓			✓	✓	✓	✓			
(Estacio et al., 2019)	✓		✓	✓	✓	✓	✓	✓		
(Hu et al., 2019)			✓	✓	✓	✓	✓			
(Geletič et al., 2019)			✓	✓	✓	✓	✓			
(Agathangelidis et al., 2020)			✓	✓	✓	✓	✓			
(Chen et al., 2020b)	✓	✓	✓	✓	✓	✓	✓			
(Somuncu and Yüksel, 2020)			✓				✓			
(Dimitrov et al., 2021)								✓		
(Štredová et al., 2021)			✓	✓	✓	✓	✓			

**Table A4**

The division of combined LCZ mapping methods.

Literature	Classification methods
(Gál et al., 2015)	coarse-to-fine
(Lopes et al., 2017)	coarse-to-fine
(Fonte et al., 2019)	coarse-to-fine
(He et al., 2019)	coarse-to-fine
(Zhou et al., 2020a)	coarse-to-fine
(Wicki and Parlow, 2017)	built type-land cover type separation
(Kotharkar and Bagade, 2018)	built type-land cover type separation

(continued on next page)

**Table A4 (continued)**

Literature	Classification methods
(Wang et al., 2018b)	built type-land cover type separation
(Zheng et al., 2018)	built type-land cover type separation
(Molnár et al., 2019)	built type-land cover type separation
(Mu et al., 2019)	built type-land cover type separation
(Yang et al., 2019a)	built type-land cover type separation
(Zhao et al., 2019a)	built type-land cover type separation
(Du et al., 2020a)	built type-land cover type separation
(Han et al., 2020)	built type-land cover type separation
(Yang et al., 2020b)	built type-land cover type separation
(Yang et al., 2020c)	built type-land cover type separation
(Unal Cilek and Cilek, 2021)	built type-land cover type separation
(Gilabert et al., 2021)	built type-land cover type separation
(Ru et al., 2021)	built type-land cover type separation
(Yang et al., 2021)	built type-land cover type separation
(Zhou et al., 2021b)	built type-land cover type separation

## References

- Agathangelidis, I., Cartalis, C., Santamouris, M., 2020. Urban morphological controls on surface thermal dynamics: a comparative assessment of major European cities with a focus on Athens Greece. *Climate* 8, 131. <https://doi.org/10.3390/cli8110131>.
- Agathangelidis, I., Cartalis, C., Santamouris, M., 2019. Integrating urban form, function, and energy fluxes in a heat exposure indicator in view of intra-urban Heat Island assessment and climate change adaptation. *Climate* 7, 75. <https://doi.org/10.3390/cli7060075>.
- Alcayna, T., Fletcher, I., Gibb, R., Tremblay, L., Funk, S., Rao, B., Lowe, R., 2022. Climate-sensitive disease outbreaks in the aftermath of extreme climatic events: a scoping review. *One Earth* 5, 336–350. <https://doi.org/10.1016/j.oneear.2022.03.011>.
- Alexander, P., Mills, G., 2014. Local climate classification and Dublin's urban Heat Island. *Atmosphere (Basel)* 5, 755–774. <https://doi.org/10.3390/atmos5040755>.
- Alexander, P.J., Fealy, R., Mills, G.M., 2016. Simulating the impact of urban development pathways on the local climate: a scenario-based analysis in the greater Dublin region, Ireland. *Landscape Urban Plan.* 152, 72–89. <https://doi.org/10.1016/j.landurbplan.2016.02.006>.
- Alexander, P.J., Mills, G., Fealy, R., 2015. Using LCZ data to run an urban energy balance model. *Urban Clim.* 13, 14–37. <https://doi.org/10.1016/j.ulclim.2015.05.001>.
- Aminipour, M., Rayner, D., Lindberg, F., Thorsson, S., Knudby, A.J., Zickfeld, K., Middel, A., Krayenhoff, E.S., 2019. Urban tree planting to maintain outdoor thermal comfort under climate change: the case of Vancouver's local climate zones. *Build. Environ.* 158, 226–236. <https://doi.org/10.1016/j.buildenv.2019.05.022>.
- Anjos, M., Targino, A.C., Krecl, P., Oukawa, G.Y., Braga, R.F., 2020. Analysis of the urban heat island under different synoptic patterns using local climate zones. *Build. Environ.* 185, 107268 <https://doi.org/10.1016/j.buildenv.2020.107268>.
- Aslam, A., Rana, I.A., Bhatti, S.S., 2021. The spatiotemporal dynamics of urbanisation and local climate: A case study of Islamabad, Pakistan. *Environ. Impact Assess. Rev.* 91, 106666 <https://doi.org/10.1016/j.eiar.2021.106666>.
- Auer, A.H., 1978. Correlation of land use and cover with meteorological anomalies. *J. Appl. Meteorol.* 17, 636–643. [https://doi.org/10.1175/1520-0450\(1978\)017<0636:coluac>2.0.co;2](https://doi.org/10.1175/1520-0450(1978)017<0636:coluac>2.0.co;2).
- Bande, L., Manandhar, P., Ghazal, R., Marpu, P., 2020a. Characterization of local climate zones using ENVI-met and site data in the City of Al-Ain, UAE. *Int. J. Sustain. Dev. Plan.* 15, 751–760. <https://doi.org/10.18280/ijstdp.150517>.
- Bande, L., Manandhar, P., Marpu, P., Battah, M., 2020. Local climate zones definition in relation to ENVI-met in the City of Dubai, UAE. *IOP Conf. Ser. Mater. Sci. Eng.* 829, 012013 <https://doi.org/10.1088/1757-899X/829/1/012013>.
- Bartesaghi Koc, C., Osmond, P., Peters, A., Irger, M., 2018. Understanding land surface temperature differences of local climate zones based on airborne remote sensing data. *IEEE J. Sel. Top. Appl. Earth Obs. Remote Sens.* 11, 2724–2730. <https://doi.org/10.1109/JSTARS.2018.2815004>.
- Bartesaghi Koc, C., Osmond, P., Peters, A., Irger, M., 2017. Mapping Local Climate Zones for urban morphology classification based on airborne remote sensing data. In: 2017 Joint Urban Remote Sensing Event (JURSE). IEEE, Dubai, United Arab Emirates, pp. 1–4. <https://doi.org/10.1109/JURSE.2017.7924611>. Mar 5–7.
- Bechtel, B., Alexander, P., Böhner, J., Ching, J., Conrad, O., Feddema, J., Mills, G., See, L., Stewart, I., 2015. Mapping local climate zones for a worldwide database of the form and function of cities. *ISPRS Int. J. Geoinf.* 4, 199–219. <https://doi.org/10.3390/ijgi4010199>.
- Bechtel, B., Alexander, P.J., Beck, C., Böhner, J., Brousse, O., Ching, J., Demuzere, M., Fonte, C., Gál, T., Hidalgo, J., Hoffmann, P., Middel, A., Mills, G., Ren, C., See, L., Sismanidis, P., Verdonck, M.-L., Xu, G., Xu, Y., 2019a. Generating WUDAPT level 0 data – current status of production and evaluation. *Urban Clim.* 27, 24–45. <https://doi.org/10.1016/j.ulclim.2018.10.001>.
- Bechtel, B., Conrad, O., Tamminga, M., Verdonck, M.L., van Coillie, F., Tuia, D., Demuzere, M., See, L., Lopes, P., Fonte, C.C., Xu, Y., Ren, C., Mills, G., Kaloustian, N., Cassone, A., 2017a. Beyond the urban mask. In: 2017 Joint Urban Remote Sensing Event (JURSE). IEEE, Dubai, United Arab Emirates, pp. 1–4. <https://doi.org/10.1109/JURSE.2017.7924557>.
- Bechtel, B., Daneke, C., 2012. Classification of local climate zones based on multiple earth observation data. *IEEE J. Sel. Top. Appl. Earth Obs. Remote Sens.* 5, 1191–1202. <https://doi.org/10.1109/JSTARS.2012.2189873>.
- Bechtel, B., Demuzere, M., Mills, G., Zhan, W., Sismanidis, P., Small, C., Voogt, J., 2019b. SUHI analysis using local climate Zones—A comparison of 50 cities. *Urban Clim.* 28, 100451 <https://doi.org/10.1016/j.ulclim.2019.01.005>.
- Bechtel, B., Demuzere, M., Sismanidis, P., Fenner, D., Brousse, O., Beck, C., van Coillie, F., Conrad, O., Keramitsoglou, I., Middel, A., Mills, G., Niyogi, D., Otto, M., See, L., Verdonck, M.-L., 2017b. Quality of crowdsourced data on urban Morphology—The human influence experiment (HUMINEX). *Urban Sci.* 1, 15. <https://doi.org/10.3390/urbansci1020015>.
- Bechtel, B., Demuzere, M., Stewart, I.D., 2020. A Weighted Accuracy Measure for Land Cover Mapping: Comment on Johnson et al. Local Climate Zone (LCZ) Map Accuracy Assessments Should Account for Land Cover Physical Characteristics that Affect the Local Thermal Environment. *Remote Sens.* 2019, 11, 2420. *Remote Sens. (Basel)* 12, 1769. <https://doi.org/10.3390/rs12111769>. July 23–28.
- Bechtel, B., Langkamp, T., Böhner, J., Daneke, C., Obenbrügge, J., Schempp, S., 2012. Classification and modelling of urban micro-climates using multisensorial and multitemporal remote sensing data. *Int. Arch. Photogramm. Remote Sens. Spatial Inform. Sci.* 39, 463–468.
- Bechtel, B., Pesaresi, M., See, L., Mills, G., Ching, J., Alexander, P.J., Feddema, J.J., Florczyk, A.J., Stewart, I., 2016. Towards consistent mapping of urban structures – global human settlement layer and local climate zones. *International Archives of the Photogrammetry, Remote Sensing and Spatial Information Sciences XLI-B8*, 1371–1378. <https://doi.org/10.5194/isprs-archives-XLI-B8-1371-2016>.
- Bechtel, B., See, L., Mills, G., Foley, M., 2016b. Classification of local climate zones using SAR and multispectral data in an arid environment. *IEEE J. Sel. Top. Appl. Earth Obs. Remote Sens.* 9, 3097–3105. <https://doi.org/10.1109/JSTARS.2016.2531420>.
- Beck, C., Straub, A., Breitner, S., Cyrys, J., Philipp, A., Rathmann, J., Schneider, A., Wolf, K., Jacobbeit, J., 2018. Air temperature characteristics of local climate zones in the Augsburg urban area (Bavaria, southern Germany) under varying synoptic conditions. *Urban Clim.* 25, 152–166. <https://doi.org/10.1016/j.ulclim.2018.04.007>.
- Berlessova, A.A., Konstantinov, P.I., 2020. Local climate zones in the city of nur-sultan (Kazakhstan) and their connections with urban heat island and thermal comfort. *IOP Conf. Ser. Earth Environ. Sci.* 611, 012060 <https://doi.org/10.1088/1755-1315/611/1/012060>.
- Blaschke, T., 2010. Object based image analysis for remote sensing. *ISPRS J. Photogramm. Remote Sens.* 65, 2–16. <https://doi.org/10.1016/j.isprsjprs.2009.06.004>.
- Bocher, E., Petit, G., Bernard, J., Palominos, S., 2018. A geoprocessing framework to compute urban indicators: the MApUCE tools chain. *Urban Clim.* 24, 153–174. <https://doi.org/10.1016/j.ulclim.2018.01.008>.
- Bokwa, A., Dobrovolny, P., Gal, T., Geletic, J., Gulyas, A., Hajto, M.J., Hollosi, B., Kielar, R., Lehner, M., Skarbit, N., 2015. Modelling the impact of climate change on heat load increase in Central European cities. In: 9th International Conference on Urban Climates (ICUC9), 2015.07.20–24, Toulouse, France.
- Bokwa, A., Geletic, J., Lehner, M., Žuvela-Aloise, M., Hollosi, B., Gál, T., Skarbit, N., Dobrovolny, P., Hajto, M.J., Kielar, R., Walawender, J.P., Šťastný, P., Holec, J., Ostapowicz, K., Burianová, J., Garaj, M., 2019. Heat load assessment in central european cities using an urban climate model and observational monitoring data. *Energy Build.* 201, 53–69. <https://doi.org/10.1016/j.enbuild.2019.07.023>.
- Brousse, O., Georganos, S., Demuzere, M., Dujardin, S., Lennert, M., Linard, C., Snow, R.W., Thiery, W., van Lipzig, N.P.M., 2020a. Can we use local climate zones for predicting malaria prevalence across sub-saharan african cities? *Environ. Res. Lett.* 15, 124051 <https://doi.org/10.1088/1748-9326/abc996>.
- Brousse, O., Georganos, S., Demuzere, M., Vanhuyse, S., Wouters, H., Wolff, E., Linard, C., van Lipzig, N.P.-M., Dujardin, S., 2019. Using local climate zones in sub-saharan Africa to tackle urban health issues. *Urban Clim.* 27, 227–242. <https://doi.org/10.1016/j.ulclim.2018.12.004>.

- Brousse, O., Martilli, A., Foley, M., Mills, G., Bechtel, B., 2016. WUDAPT, an efficient land use producing data tool for mesoscale models? Integration of urban LCZ in WRF over Madrid. *Urban Clim.* 17, 116–134. <https://doi.org/10.1016/j.ulclim.2016.04.001>.
- Brousse, O., Simpson, C., Walker, N., Fenner, D., Meier, F., Taylor, J., Heaviside, C., 2022. Evidence of horizontal urban heat advection in London using six years of data from a citizen weather station network. *Environ. Res. Lett.* 17, 044041 <https://doi.org/10.1088/1748-9326/ac5c0f>.
- Brousse, O., Wouters, H., Demuzere, M., Thierry, W., van de Walle, J., Leipzig, N.P.M., 2020b. The local climate impact of an african city during clear-sky conditions—Implications of the recent urbanization in Kampala (Uganda). *Int. J. Climatol.* 40, 4586–4608. <https://doi.org/10.1002/joc.6477>.
- Budhiraja, B., Gawuc, L., Agrawal, G., 2019. Seasonality of surface urban Heat Island in Delhi City region measured by local climate zones and conventional indicators. *IEEE J. Sel. Top. Appl. Earth Obs. Remote Sens.* 12, 5223–5232. <https://doi.org/10.1109/JSTARS.2019.2955133>.
- Budhiraja, B., Pathak, P., Agrawal, G., 2017. Spatio-temporal variability of urban heat islands in local climate zones of Delhi-NCR. In: Heldens, W., Chrysoulakis, N., Erbertseder, T., Zhang, Y. (Eds.), *Remote Sensing Technologies and Applications in Urban Environments II*. SPIE, p. 37. <https://doi.org/10.1117/12.2280253>.
- Cai, M., Ren, C., Xu, Y., 2017. Investigating the relationship between Local Climate Zone and land surface temperature. In: 2017 Joint Urban Remote Sensing Event (JURSE). IEEE, Dubai, United Arab Emirates, pp. 1–4. <https://doi.org/10.1109/JURSE.2017.7924622>. Mar 5–7.
- Cai, M., Ren, C., Xu, Y., Dai, W., Wang, X.M., 2016. Local climate zone study for sustainable megacities development by using improved WUDAPT methodology – a case study in Guangzhou. *Proc. Environ. Sci.* 36, 82–89. <https://doi.org/10.1016/j.proenv.2016.09.017>.
- Cai, M., Ren, C., Xu, Y., Lau, K.K.-L., Wang, R., 2018. Investigating the relationship between local climate zone and land surface temperature using an improved WUDAPT methodology – a case study of Yangtze River Delta, China. *Urban Clim.* 24, 485–502. <https://doi.org/10.1016/j.ulclim.2017.05.010>.
- Cai, Z., Tang, Y., Chen, K., Han, G., 2019. Assessing the heat vulnerability of different local climate zones in the old areas of a chinese megacity. *Sustainability* 11, 2032. <https://doi.org/10.3390/su11072032>.
- Cai, Z., Tang, Y., Zhan, Q., 2021. A cooled city? Comparing human activity changes on the impact of urban thermal environment before and after city-wide lockdown. *Build. Environ.* 195, 107729. <https://doi.org/10.1016/j.buildenv.2021.107729>.
- Cao, R., Tu, W., Yang, C., Li, Q., Liu, J., Zhu, J., Zhang, Q., Li, Q., Qiu, G., 2020. Deep learning-based remote and social sensing data fusion for urban region function recognition. *ISPRS J. Photogramm. Remote Sens.* 163, 82–97. <https://doi.org/10.1016/j.isprsjprs.2020.02.014>.
- Cao, Y., Huang, X., 2021. A deep learning method for building height estimation using high-resolution multi-view imagery over urban areas: a case study of 42 chinese cities. *Remote Sens. Environ.* 264, 112590 <https://doi.org/10.1016/j.rse.2021.112590>.
- Chang, Y., Xiao, J., Li, X., Middel, A., Zhang, Y., Gu, Z., Wu, Y., He, S., 2021. Exploring diurnal thermal variations in urban local climate zones with ECOSTRESS land surface temperature data. *Remote Sens. Environ.* 263, 112544 <https://doi.org/10.1016/j.rse.2021.112544>.
- Chen, F., Huang, Y., 2019. A new comparative analysis of local urban morphology based on local climate zones: a study using mobile surveys in chengdu testbed. In: *Urban Form and Social Context: From Traditions to Newest Demands*, pp. 752–765. <https://elib.sfu-kras.ru/handle/2311/111751>.
- Chen, G., Xie, J., Li, W., Li, X., Hay Chung, L.C., Ren, C., Liu, X., 2021a. Future “local climate zone” spatial change simulation in Greater Bay Area under the shared socioeconomic pathways and ecological control line. *Build. Environ.* 203, 108077 <https://doi.org/10.1016/j.buildenv.2021.108077>.
- Chen, X., Xu, Y., Yang, J., Wu, Z., Zhu, H., 2020a. Remote sensing of urban thermal environments within local climate zones: a case study of two high-density subtropical chinese cities. *Urban Clim.* 31, 100568 <https://doi.org/10.1016/j.ulclim.2019.100568>.
- Chen, Y., Zheng, B., Hu, Y., 2020. Mapping local climate zones using ArcGIS-based method and exploring land surface temperature characteristics in Chenzhou, China. *Sustainability* 12, 2974. <https://doi.org/10.3390/su12072974>.
- Chen, Y.-C., Cheng, F.-Y., Yang, C.-P., Lin, T.-P., 2021b. Explore the accuracy of the pedestrian level temperature estimated by the combination of LCZ with WRF urban canopy model through the microclimate measurement network. In: *The 4th International Electronic Conference on Atmospheric Sciences*. MDPI, Basel Switzerland, p. 14. <https://doi.org/10.3390/ecas2021-10349>.
- Chen, Y.-C., Lin, T.-P., Shih, W.-Y., 2017. Modeling the urban thermal environment distributions in Taipei Basin using Local Climate Zone (LCZ). In: 2017 Joint Urban Remote Sensing Event (JURSE). IEEE, Dubai, United Arab Emirates, pp. 1–4. <https://doi.org/10.1109/JURSE.2017.7924531>. Mar 5–7.
- Chen, Y.-C., Lo, T.-W., Shih, W.-Y., Lin, T.-P., 2019. Interpreting air temperature generated from urban climatic map by urban morphology in Taipei. *Theor. Appl. Climatol.* 137, 2657–2662. <https://doi.org/10.1007/s00704-018-02764-x>.
- Cheng, G., Han, J., Lu, X., 2017. Remote sensing image scene classification: benchmark and state of the art. *Proc. IEEE* 105, 1865–1883. <https://doi.org/10.1109/JPROC.2017.2675998>.
- Cheng, G., Xie, X., Han, J., Guo, L., Xia, G.-S., 2020. Remote sensing image scene classification meets deep learning: challenges, methods, benchmarks, and opportunities. *IEEE J. Sel. Top. Appl. Earth Obs. Remote Sens.* 13, 3735–3756. <https://doi.org/10.1109/JSTARS.2020.3005403>.
- Chieppa, J., Bush, A., Mitra, C., 2018. Using “Local climate zones” to detect urban Heat Island on two small cities in Alabama. *Earth Interact.* 22, 1–22. <https://doi.org/10.1175/EI-D-17-0020.1>.
- Ching, J., Aliaga, D., Mills, G., Masson, V., See, L., Neophytou, M., Middel, A., Baklanov, A., Ren, C., Ng, E., Fung, J., Wong, M., Huang, Y., Martilli, A., Brousse, O., Stewart, I., Zhang, X., Shehata, A., Miao, S., Wang, X., Wang, W., Yamagata, Y., Duarte, D., Li, Y., Feddema, J., Bechtel, B., Hidalgo, J., Roustan, Y., Kim, Y., Simon, H., Kropp, T., Bruse, M., Lindberg, F., Grimmond, S., Demuzere, M., Chen, F., Li, C., Gonzales-Cruz, J., Bornstein, B., He, Q., Hanna, A., Erell, E., Tapper, N., Mall, R.K., Niyogi, D., 2019. Pathway using WUDAPT’s Digital Synthetic City tool towards generating urban canopy parameters for multi-scale urban atmospheric modeling. *Urban Clim.* 28, 100459. <https://doi.org/10.1016/j.ulclim.2019.100459>.
- Ching, J., Mills, G., Bechtel, B., See, L., Feddema, J., Wang, X., Ren, C., Brousse, O., Martilli, A., Neophytou, M., Mouzourides, P., Stewart, I., Hanna, A., Ng, E., Foley, M., Alexander, P., Aliaga, D., Niyogi, D., Shreevastava, A., Bhalachandran, P., Masson, V., Hidalgo, J., Fung, J., Andrade, M., Baklanov, A., Dai, W., Milcinski, G., Demuzere, M., Brunsell, N., Pesaresi, M., Miao, S., Mu, Q., Chen, F., Theeuwes, N., 2018. WUDAPT: an urban weather, climate, and environmental modeling infrastructure for the anthropocene. *Bull. Am. Meteorol. Soc.* 99, 1907–1924. <https://doi.org/10.1175/BAMS-D-16-0236.1>.
- Choudhury, D., Das, A., Das, M., 2021. Investigating thermal behavior pattern (TBP) of local climatic zones (LCZs): a study on industrial cities of Asansol-Durgapur development area (ADDA), eastern India. *Urban Clim.* 35, 100727. <https://doi.org/10.1016/j.ulclim.2020.100727>.
- Colli, M.F., Correa, É.N., Martinez, C.F., 2020. Aplicación del método WUDAPT en la ciudad de Mendoza-Argentina Para definir zonas Climáticas locales. *Rev. Urbano* 23, 18–31. <https://doi.org/10.22320/07183607.2020.23.42.02>.
- Collins, J., Dronova, I., 2019. Urban landscape change analysis using local climate zones and object-based classification in the salt Lake metro region, Utah, USA. *Remote Sens.* 11, 1615. <https://doi.org/10.3390/rs11131615>.
- Danylo, O., See, L., Bechtel, B., Schepaschenko, D., Fritz, S., 2016. Contributing to WUDAPT: local climate zone classification of two cities in Ukraine. *IEEE J. Sel. Top. Appl. Earth Obs. Remote Sens.* 9, 1841–1853. <https://doi.org/10.1109/JSTARS.2016.2539977>.
- Das, M., Das, A., 2020a. Exploring the pattern of outdoor thermal comfort (OTC) in a tropical planning region of eastern India during summer. *Urban Clim.* 34, 100708. <https://doi.org/10.1016/j.ulclim.2020.100708>.
- Das, M., Das, A., 2020. Assessing the relationship between local climatic zones (LCZs) and land surface temperature (LST) – A case study of Sriniketan-Santiniketan Planning Area (SSPA), West Bengal, India. *Urban Clim.* 32, 100591. <https://doi.org/10.1016/j.ulclim.2020.100591>.
- Demuzere, M., Bechtel, B., Middel, A., Mills, G., 2019a. Mapping Europe into local climate zones. *PLoS One* 14, e0214474. <https://doi.org/10.1371/journal.pone.0214474>.
- Demuzere, M., Bechtel, B., Mills, G., 2019b. Global transferability of local climate zone models. *Urban Clim.* 27, 46–63. <https://doi.org/10.1016/j.ulclim.2018.11.001>.
- Demuzere, M., Hankey, S., Mills, G., Zhang, W., Lu, T., Bechtel, B., 2020a. Combining expert and crowd-sourced training data to map urban form and functions for the continental US. *Sci. Data* 7, 264. <https://doi.org/10.1038/s41597-020-00605-z>.
- Demuzere, M., Kittner, J., Bechtel, B., 2021. LCZ generator: a web application to create local climate zone maps. *Front. Environ. Sci.* 9, 112. <https://doi.org/10.3389/fenvs.2021.637455>.
- Demuzere, M., Kittner, J., Martilli, A., Mills, G., Moede, C., Stewart, I.D., van Vliet, J., Bechtel, B., 2022a. A global map of local climate zones to support earth system modelling and urban-scale environmental science. *Earth Syst. Sci. Data* 14, 3835–3873. <https://doi.org/10.5194/essd-14-3835-2022>.
- Demuzere, M., Kittner, J., Martilli, A., Mills, G., Moede, C., Stewart, I.D., van Vliet, J., Bechtel, B., 2022b. A global map of local climate zones to support earth system modelling and urban scale environmental science. *Earth Syst. Sci. Data Discuss.* 2022, 1–57. <https://doi.org/10.5194/essd-2022-92>.
- Demuzere, M., Miura, T., Redivo, C.P., Feddema, J., Setton, E., 2020b. Multi-temporal LCZ maps for Canadian functional urban areas. *OSF Preprints*. <https://doi.org/10.31219/osf.io/h5tm6>.
- Dian, C., Pongrácz, R., Dezső, Z., Bartholy, J., 2020. Annual and monthly analysis of surface urban heat island intensity with respect to the local climate zones in Budapest. *Urban Clim.* 31, 100573. <https://doi.org/10.1016/j.ulclim.2019.100573>.
- Dimitrov, S., Popov, A., Iliev, M., 2021. An Application of the LCZ Approach in Surface Urban Heat Island Mapping in Sofia, Bulgaria. *Atmosphere (Basel)* 12, 1370. <https://doi.org/10.3390/atmos12111370>.
- dos Anjos, C.S., Lacerda, M.G., do Livramento Andrade, L., Salles, R.N., 2017. Classification of urban environments using feature extraction and random forest. In: *2017 IEEE International Geoscience and Remote Sensing Symposium (IGARSS)*. IEEE, pp. 1205–1208. <https://doi.org/10.1109/IGARSS.2017.8127174>.
- Droste, A.M., Heusinkveld, B.G., Fenner, D., Steeneveld, G., 2020. Assessing the potential and application of crowdsourced urban wind data. *Q. J. R. Meteorol. Soc.* 146, 2671–2688. <https://doi.org/10.1002/qj.3811>.
- Du, P., Chen, J., Bai, X., Han, W., 2020a. Understanding the seasonal variations of land surface temperature in Nanjing urban area based on local climate zone. *Urban Clim.* 33, 100657. <https://doi.org/10.1016/j.ulclim.2020.100657>.
- Du, S., Du, S., Liu, B., Zhang, X., Zheng, Z., 2020b. Large-scale urban functional zone mapping by integrating remote sensing images and open social data. *GIsci Remote Sens.* 57, 411–430. <https://doi.org/10.1080/15481603.2020.1724707>.
- Dunjić, J., Milošević, D., Kojić, M., Savić, S., Lužanin, Z., Šćerov, I., Arsenović, D., 2021. Air humidity characteristics in “Local climate zones” of Novi Sad (Serbia) based on long-term data. *ISPRS Int. J. Geoinf.* 10, 810. <https://doi.org/10.3390/ijgi10120810>.

- Dutta, K., Basu, D., Agrawal, S., 2021. Evaluation of seasonal variability in magnitude of urban heat islands using local climate zone classification and surface albedo. *Int. J. Environ. Sci. Technol.* 1–22. <https://doi.org/10.1007/s13762-021-03602-w>.
- Eldešoky, A.H.M., Colaninno, N., Morello, E., 2019. Improving local climate zones automatic classification based on physic-morphological urban features. In: XIII CTV 2019 Proceedings: XIII International Conference on Virtual City and Territory: "Challenges and Paradigms of the Contemporary City": UPC, Barcelona, October 2–4, 2019. Centre de Política de Sol i Valoracions, CPSV / Universitat Politècnica de Catalunya, UPC, Barcelona, pp. 0–3. <https://doi.org/10.5821/ctv.8663>.
- Ellefsen, R., 1991. Mapping and measuring buildings in the canopy boundary layer in ten U.S. Cities. *Energy Build.* 16, 1025–1049. [https://doi.org/10.1016/0378-7788\(91\)90097-M](https://doi.org/10.1016/0378-7788(91)90097-M).
- Elshamli, A., Taylor, G.W., Areibi, S., 2020. Multisource domain adaptation for remote sensing using deep neural networks. *IEEE Trans. Geosci. Remote Sens.* 58, 3328–3340. <https://doi.org/10.1109/TGRS.2019.2953328>.
- Emery, J., Pohl, B., Crétat, J., Richard, Y., Pergaud, J., Rega, M., Zito, S., Dudek, J., Vairet, T., Joly, D., Thévenin, T., 2021. How local climate zones influence urban air temperature: Measurements by bicycle in Dijon, France. *Urban Clim.* 40, 101017. <https://doi.org/10.1016/j.ulclim.2021.101017>.
- Emmanuel, R., Loconsole, A., 2015. Green infrastructure as an adaptation approach to tackling urban overheating in the Glasgow Clyde Valley region, UK. *Landsc. Urban Plan.* 138, 71–86. <https://doi.org/10.1016/j.landurbplan.2015.02.012>.
- Estacio, I., Babaan, J., Pecson, N.J., Blanco, A.C., Escoto, J.E., Alcantara, C.K., 2019. GIS-based mapping of local climate zones using fuzzy logic and cellular automata. *Int. Arch. Photogramm. Remote Sens. Spatial Inform. Sci.* XLII-4/W19, 199–206. <https://doi.org/10.5194/isprs-archives-XLII-4-W19-199-2019>.
- Feng, P., Lin, Y., Guan, J., Dong, Y., He, G., Xia, Z., Shi, H., 2019. Embankment CNN based local climate zone classification using SAR and multispectral remote sensing data. In: IGARSS 2019 - 2019 IEEE International Geoscience and Remote Sensing Symposium. IEEE, pp. 6344–6347. <https://doi.org/10.1109/IGARSS.2019.8898703>.
- Feng, P., Lin, Y., He, G., Guan, J., Wang, J., Shi, H., 2020. A dynamic end-to-end fusion filter for local climate zone classification using SAR and multi-spectrum remote sensing data. In: IGARSS 2020 - 2020 IEEE International Geoscience and Remote Sensing Symposium. IEEE, pp. 4231–4234. <https://doi.org/10.1109/IGARSS39084.2020.9324427>.
- Fenner, D., Meier, F., Bechtel, B., Otto, M., Scherer, D., 2017. Intra and inter 'local climate zone' variability of air temperature as observed by crowdsourced citizen weather stations in Berlin, Germany. *Meteorol. Z.* 26, 525–547. <https://doi.org/10.1127/metz/2017/0861>.
- Fenner, D., Meier, F., Scherer, D., Polze, A., 2014. Spatial and temporal air temperature variability in Berlin, Germany, during the years 2001–2010. *Urban Clim.* 10, 308–331. <https://doi.org/10.1016/j.ulclim.2014.02.004>.
- Fernández, M.E., Picone, N., Gentili, J.O., Campo, A.M., 2021. Analysis of the urban energy balance in Bahía Blanca (Argentina). *Urban Clim.* 37, 100856. <https://doi.org/10.1016/j.ulclim.2021.100856>.
- Ferreira, L.S., Duarte, D.H.S., 2019. Exploring the relationship between urban form, land surface temperature and vegetation indices in a subtropical megacity. *Urban Clim.* 27, 105–123. <https://doi.org/10.1016/j.ulclim.2018.11.002>.
- Fonte, C.C., Lopes, P., See, L., Bechtel, B., 2019. Using OpenStreetMap (OSM) to enhance the classification of local climate zones in the framework of WUDAPT. *Urban Clim.* 28, 100456. <https://doi.org/10.1016/j.ulclim.2019.100456>.
- Frantz, D., Schug, F., Okujeni, A., Navacchi, C., Wagner, W., van der Linden, S., Hostert, P., 2021. National-scale mapping of building height using Sentinel-1 and Sentinel-2 time series. *Remote Sens. Environ.* 252, 112128. <https://doi.org/10.1016/j.rse.2020.112128>.
- Fricke, C., Pongrácz, R., Gál, T., Savić, S., Unger, J., 2020. Using local climate zones to compare remotely sensed surface temperatures in temperate cities and hot desert cities. *Moravian Geographical Reports* 28, 48–60. <https://doi.org/10.2478/mgr-2020-0004>.
- Gál, T., Bechtel, B., Unger, J., 2015. Comparison of two different local climate zone mapping methods. In: 9th International Conference on Urban Climates, pp. 1–6.
- Gál, T., Skarbit, N., Molnár, N., Unger, J., 2021. Projections of the urban and intra-urban scale thermal effects of climate change in the 21st century for cities in the Carpathian Basin. *Hungarian Geograph. Bull.* 70, 19–33. <https://doi.org/10.15201/hungeobull.70.1.2>.
- Gawlikowski, J., Schmitt, M., Kruspe, A., Zhu, X.X., 2020. On the fusion strategies of sentinel-1 and sentinel-2 data for local climate zone classification. In: IGARSS 2020 - 2020 IEEE International Geoscience and Remote Sensing Symposium. IEEE, pp. 2081–2084. <https://doi.org/10.1109/IGARSS39084.2020.9324234>.
- Geis, C., Leichtle, T., Wurm, M., Pelizari, P.A., Standfus, I., Zhu, X.X., So, E., Siedentop, S., Esch, T., Taubenbock, H., 2019. Large-area characterization of urban Siedentop – Mapping of built-up height and density using TanDEM-X and Sentinel-2 data. *IEEE J. Sel. Top. Appl. Earth Obs. Remote Sens.* 12, 2912–2927. <https://doi.org/10.1109/JSTARS.2019.2917755>.
- Geletić, J., Lehner, M., 2016. GIS-based delineation of local climate zones: the case of medium-sized central European cities. *Moravian Geograph. Rep.* 24, 2–12. <https://doi.org/10.1515/mgr-2016-0012>.
- Geletić, J., Lehner, M., Dobrovolný, P., 2016. Land surface temperature differences within local climate zones, based on two central European cities. *Remote Sens.* 8, 788. <https://doi.org/10.3390/rs8100788>.
- Geletić, J., Lehner, M., Savić, S., Milošević, D., 2019. Inter-/intra-zonal seasonal variability of the surface urban heat island based on local climate zones in three central European cities. *Build. Environ.* 156, 21–32. <https://doi.org/10.1016/j.buildenv.2019.04.011>.
- Geletić, J., Lehner, M., Savić, S., Milošević, D., 2018. Modelled spatiotemporal variability of outdoor thermal comfort in local climate zones of the city of Brno, Czech Republic. *Sci. Total Environ.* 624, 385–395. <https://doi.org/10.1016/j.scitotenv.2017.12.076>.
- Ghamisi, P., Dalla Mura, M., Benediktsson, J.A., 2015. A survey on spectral-spatial classification techniques based on attribute profiles. *IEEE Trans. Geosci. Remote Sens.* 53, 2335–2353. <https://doi.org/10.1109/TGRS.2014.2358934>.
- Gholami, R., Beck, C., 2019. Towards the determination of driving factors of varying LST-LCZ relationships: a case study over 25 cities. *Geograph. Pannon.* 23, 289–307. <https://doi.org/10.5937/gp23-24238>.
- Giannaros, C., Agathangelidis, I., Papavasileiou, G., Galanaki, E., Kotroni, V., Lagouvardos, K., Giannaros, T.M., Cartalis, C., Matzarakis, A., 2023. The extreme heat wave of July–August 2021 in the Athens urban area (Greece): atmospheric and human-biometeorological analysis exploiting ultra-high resolution numerical modeling and the local climate zone framework. *Sci. Total Environ.* 857, 159300. <https://doi.org/10.1016/j.scitotenv.2022.159300>.
- Gilabert, J., Deluca, A., Lauwaet, D., Ballester, J., Corbera, J., Llasat, M.C., 2021. Assessing heat exposure to extreme temperatures in urban areas using the local climate zone classification. *Nat. Hazards Earth Syst. Sci.* 21, 375–391. <https://doi.org/10.5194/nhess-21-375-2021>.
- Giridharan, R., Emmanuel, R., 2018. The impact of urban compactness, comfort strategies and energy consumption on tropical urban heat island intensity: a review. *Sustain. Cities Soc.* 40, 677–687. <https://doi.org/10.1016/j.scs.2018.01.024>.
- Gonçalves, A., Ornella, G., Castro Ribeiro, A., Maia, F., Rocha, A., Feliciano, M., 2018. Urban cold and Heat Island in the City of Bragança (Portugal). *Climate* 6, 70. <https://doi.org/10.3390/cli6030070>.
- González, J.E., Ramamurthy, P., Bornstein, R.D., Chen, F., Bou-Zeid, E.R., Ghandehari, M., Luwall, J., Mitra, C., Niyogi, D., 2021. Urban climate and resiliency: a synthesis report of state of the art and future research directions. *Urban Clim.* 38, 100858. <https://doi.org/10.1016/j.ulclim.2021.100858>.
- Gorelick, N., Hancher, M., Dixon, M., Ilyushchenko, S., Thau, D., Moore, R., 2017. Google earth engine: planetary-scale geospatial analysis for everyone. *Remote Sens. Environ.* 202, 18–27. <https://doi.org/10.1016/j.rse.2017.06.031>.
- Grimmond, C.S.B., Oke, T.R., 1999. Aerodynamic properties of urban areas derived from analysis of surface form. *J. Appl. Meteorol.* 38, 1262–1292. [https://doi.org/10.1175/1520-0450\(1999\)038<1262:APUOAD>2.0.CO;2](https://doi.org/10.1175/1520-0450(1999)038<1262:APUOAD>2.0.CO;2).
- Hammerberg, K., Brousse, O., Martilli, A., Mahdavi, A., 2018. Implications of employing detailed urban canopy parameters for mesoscale climate modelling: a comparison between WUDAPT and GIS databases over Vienna, Austria. *Int. J. Climatol.* 38, e1241–e1257. <https://doi.org/10.1002/joc.5447>.
- Han, J., Liu, J., Liu, L., Ye, Y., 2020. Spatiotemporal changes in the urban Heat Island intensity of distinct local climate zones: case study of Zhongshan District, Dalian, China. *Complexity* 2020, 1–9. <https://doi.org/10.1155/2020/8820338>.
- Hay Chung, L.C., Xie, J., Ren, C., 2021. Improved machine-learning mapping of local climate zones in metropolitan areas using composite earth observation data in Google earth engine. *Build. Environ.* 199, 107879. <https://doi.org/10.1016/j.buildenv.2021.107879>.
- He, S., Zhang, Y., Gu, Z., Su, J., 2019. Local climate zone classification with different source data in Xi'an, China. *Indoor Built Environ.* 28, 1190–1199. <https://doi.org/10.1177/1420326X18796545>.
- Hidalgo, J., Dumas, G., Masson, V., Petit, G., Bechtel, B., Bocher, E., Foley, M., Schoetter, R., Mills, G., 2019. Comparison between local climate zones maps derived from administrative datasets and satellite observations. *Urban Clim.* 27, 64–89. <https://doi.org/10.1016/j.ulclim.2018.10.004>.
- Hu, J., Ghamsari, P., Zhu, X., 2018. Feature extraction and selection of Sentinel-1 dual-pol data for global-scale local climate zone classification. *ISPRS Int. J. Geoinf.* 7, 379. <https://doi.org/10.3390/ijgi7090379>.
- Hu, J., Yang, Y., Pan, X., Zhu, Q., Zhan, W., Wang, Y., Ma, W., Su, W., 2019. Analysis of the spatial and temporal variations of land surface temperature based on local climate zones: a case study in Nanjing, China. *IEEE J. Sel. Top. Appl. Earth Obs. Remote Sens.* 12, 4213–4223. <https://doi.org/10.1109/JSTARS.2019.2926502>.
- Huang, H., Chen, P., Xu, X., Liu, C., Wang, J., Liu, C., Clinton, N., Gong, P., 2022. Estimating building height in China from ALOS AW3D30. *ISPRS J. Photogramm. Remote Sens.* 185, 146–157. <https://doi.org/10.1016/j.isprsjprs.2022.01.022>.
- Huang, K., Leng, J., Xu, Y., Li, X., Cai, M., Wang, R., Ren, C., 2021a. Facilitating urban climate forecasts in rapidly urbanizing regions with land-use change modeling. *Urban Clim.* 36, 100806. <https://doi.org/10.1016/j.ulclim.2021.100806>.
- Huang, X., Liu, A., Li, J., 2021b. Mapping and analyzing the local climate zones in China's 32 major cities using landsat imagery based on a novel convolutional neural network. *Geo-spatial Inform. Sci.* 24, 528–557. <https://doi.org/10.1080/10095020.2021.1892459>.
- IPCC, 2021. Climate Change 2021: The Physical Science Basis. Cambridge University Press, Cambridge, United Kingdom and New York, NY, USA. <https://doi.org/10.1017/9781009157896>.
- Jamali, F.S., Khaledi, S., Razavian, M.T., 2021. Seasonal impact of urban parks on land surface temperature (LST) in semi-arid city of Tehran. *Int. J. Urban Sustain. Dev.* 13, 248–264. <https://doi.org/10.1080/19463138.2021.1872083>.
- Jiang, L., Zhan, W., Hu, L., Huang, F., Hong, F., Liu, Z., Lai, J., Wang, C., 2021. Assessment of different kernel-driven models for daytime urban thermal radiation directionalities simulation. *Remote Sens. Environ.* 263, 112562. <https://doi.org/10.1016/j.rse.2021.112562>.
- Jiang, S., Zhan, W., Dong, P., Wang, C., Li, J., Miao, S., Jiang, L., Du, H., Wang, C., 2022. Surface air temperature differences of intra- and inter-local climate zones across diverse timescales and climates. *Build. Environ.* 222, 109396. <https://doi.org/10.1016/j.buildenv.2022.109396>.
- Jin, L., Pan, X., Liu, L., Liu, L., Liu, J., Gao, Y., 2020. Block-based local climate zone approach to urban climate maps using the UDC model. *Build. Environ.* 186, 107334. <https://doi.org/10.1016/j.buildenv.2020.107334>.

- Jing, H., Feng, Y., Zhang, W., Zhang, Y., Wang, S., Fu, K., Chen, K., 2019. Effective classification of local climate zones based on multi-source remote sensing data. In: IGARSS 2019 - 2019 IEEE International Geoscience and Remote Sensing Symposium. IEEE, pp. 2666–2669. <https://doi.org/10.1109/IGARSS.2019.8898475>.
- Johnson, B.A., Jozdani, S.E., 2020. Confusion Matrices Help Prevent Reader Confusion: Reply to Bechtel, B., et al. A Weighted Accuracy Measure for Land Cover Mapping: Comment on Johnson et al. Local Climate Zone (LCZ) Map Accuracy Assessments Should Account for Land Cover Physical Characteristics that Affect the Local Thermal Environment. *Remote Sens.* 2019, 11, 2420. *Remote Sens. (Basel)* 12, 1771. <https://doi.org/10.3390/rs12111771>.
- Johnson, B.A., Jozdani, S.E., 2019. Local climate zone (LCZ) map accuracy assessments should account for land cover physical characteristics that affect the local thermal environment. *Remote Sens.* 11, 2420. <https://doi.org/10.3390/rs11202420>.
- Kabano, P., Lindley, S., Harris, A., 2021. Evidence of urban heat island impacts on the vegetation growing season length in a tropical city. *Landscape. Urban Plan.* 206, 103989. <https://doi.org/10.1016/j.landurbplan.2020.103989>.
- Kaloustian, N., Bechtel, B., 2016. Local climatic zoning and urban Heat Island in Beirut. *Proc. Eng.* 169, 216–223. <https://doi.org/10.1016/j.proeng.2016.10.026>.
- Kaloustian, N., Tamminga, M., Bechtel, B., 2017. Local climate zones and annual surface thermal response in a Mediterranean city. In: 2017 Joint Urban Remote Sensing Event (JURSE). IEEE, pp. 1–4. <https://doi.org/10.1109/JURSE.2017.7924597>.
- Khamchiangta, D., Dhakal, S., 2021. Future urban expansion and local climate zone changes in relation to land surface temperature: Case of Bangkok Metropolitan Administration, Thailand. *Urban Clim.* 37, 100835. <https://doi.org/10.1016/j.ulclim.2021.100835>.
- Khamchiangta, D., Dhakal, S., 2019. Physical and non-physical factors driving urban heat island: Case of Bangkok Metropolitan Administration, Thailand. *J. Environ. Manage.* 248, 109285. <https://doi.org/10.1016/j.jenvman.2019.109285>.
- Khosnoodmotlagh, S., Daneshi, A., Gharari, S., Verrelst, J., Mirzaei, M., Omrani, H., 2021. Urban morphology detection and it's linking with surface temperature: A case study for Tehran Metropolis, Iran. *Sustain. Cities Soc.* 74, 103228. <https://doi.org/10.1016/j.scs.2021.103228>.
- Kim, M., Jeong, D., Choi, H., Kim, Y., 2020. Developing High Quality Training Samples for Deep Learning Based Local Climate Zone Classification in Korea. Mar 5-7.
- Kim, M., Jeong, D., Kim, Y., 2021. Local climate zone classification using a multi-scale, multi-level attention network. *ISPRS J. Photogramm. Remote Sens.* 181, 345–366. <https://doi.org/10.1016/j.isprsjprs.2021.09.015>.
- Kleerekerop, L., Taleghani, M., van den Dobbelsteen, A., Hordijk, T., 2017. Urban measures for hot weather conditions in a temperate climate condition: a review study. *Renew. Sust. Energ. Rev.* 75, 515–533. <https://doi.org/10.1016/j.rser.2016.11.019>.
- Kopp, J., Frajer, J., Novotná, M., Preis, J., Dolejš, M., 2021. Comparison of ecohydrological and climatological zoning of the cities: case study of the City of Pilsen. *ISPRS Int. J. Geoinf.* 10, 350. <https://doi.org/10.3390/ijgi10050350>.
- Kotharkar, R., Bagade, A., 2018. Local climate zone classification for Indian cities: a case study of Nagpur. *Urban Clim.* 24, 369–392. <https://doi.org/10.1016/j.ulclim.2017.03.003>.
- Kotharkar, R., Ghosh, A., Kotharkar, V., 2021. Estimating summertime heat stress in a tropical Indian city using local climate zone (LCZ) framework. *Urban Clim.* 36, 100784. <https://doi.org/10.1016/j.ulclim.2021.100784>.
- Krayenhoff, E., Voogt, J., 2016. Daytime thermal anisotropy of urban neighbourhoods: morphological causation. *Remote Sens.* 8, 108. <https://doi.org/10.3390/rs8020108>.
- Krayenhoff, E.S., Moustaqai, M., Broadbent, A.M., Gupta, V., Georgescu, M., 2018. Diurnal interaction between urban expansion, climate change and adaptation in US cities. *Nat. Clim. Chang.* 8, 1097–1103. <https://doi.org/10.1038/s41558-018-0320-9>.
- Kwok, Y.T., de Munck, C., Schoetter, R., Ren, C., Lau, K.K.-L., 2020. Refined dataset to describe the complex urban environment of Hong Kong for urban climate modelling studies at the mesoscale. *Theor. Appl. Climatol.* 142, 129–150. <https://doi.org/10.1007/s00704-020-03298-x>.
- Kwok, Y.T., Schoetter, R., Lau, K.K., Hidalgo, J., Ren, C., Pigeon, G., Masson, V., 2019. How well does the local climate zone scheme discern the thermal environment of Toulouse (France)? An analysis using numerical simulation data. *Int. J. Climatol.* 39, 5292–5315. <https://doi.org/10.1002/joc.6140>.
- La, Y., Bagan, H., Yamagata, Y., 2020. Urban land cover mapping under the local climate zone scheme using Sentinel-2 and PALSAR-2 data. *Urban Clim.* 33, 100661. <https://doi.org/10.1016/j.ulclim.2020.100661>.
- Lao, J., Wang, C., Zhu, X., Xi, X., Nie, S., Wang, J., Cheng, F., Zhou, G., 2021. Retrieving building height in urban areas using ICESat-2 photon-counting LiDAR data. *Int. J. Appl. Earth Obs. Geoinf.* 104, 102596. <https://doi.org/10.1016/j.jag.2021.102596>.
- Lau, K.K., Ren, C., Shi, Y., Zheng, V., Yim, S., Lai, D., Ka, K., 2013. Determining the optimal size of local climate zones for spatial mapping in high-density cities. In: Proceedings of the 9th International Conference on Urban Climate Jointly with 12th Symposium on the Urban Environment, pp. 20–24.
- Lau, K.K.-L., Chung, S.C., Ren, C., 2019. Outdoor thermal comfort in different urban settings of sub-tropical high-density cities: an approach of adopting local climate zone (LCZ) classification. *Build. Environ.* 154, 227–238. <https://doi.org/10.1016/j.buildenv.2019.03.005>.
- Lau, K.K.-L., Ren, C., Shi, Y., Zheng, V., Yim, S., Lai, D., 2015. Determining the optimal size of local climate zones for spatial mapping in high-density cities. In: Proceedings of the 9th International Conference on Urban Climate Jointly with 12th Symposium on the Urban Environment, Toulouse, France, pp. 20–24.
- Leconte, F., Bouyer, J., Claverie, R., Pétrissans, M., 2017. Analysis of nocturnal air temperature in districts using mobile measurements and a cooling indicator. *Theor. Appl. Climatol.* 130, 365–376. <https://doi.org/10.1007/s00704-016-1886-7>.
- Leconte, F., Bouyer, J., Claverie, R., Pétrissans, M., 2015. Using local climate zone scheme for UHI assessment: evaluation of the method using mobile measurements. *Build. Environ.* 83, 39–49. <https://doi.org/10.1016/j.buildenv.2014.05.005>.
- Lehnert, M., Geletić, J., Dobrovolský, P., Jurek, M., 2018. Temperature differences among local climate zones established by mobile measurements in two central European cities. *Clim. Res.* 75, 53–64. <https://doi.org/10.3354/cr01508>.
- Lehnert, M., Geletić, J., Husák, J., Vysudil, M., 2015. Urban field classification by “local climate zones” in a medium-sized central European city: the case of Olomouc (Czech Republic). *Theor. Appl. Climatol.* 122, 531–541. <https://doi.org/10.1007/s00704-014-1309-6>.
- Lehnert, M., Savić, S., Milošević, D., Dunjić, J., Geletić, J., 2021. Mapping local climate zones and their applications in European urban environments: a systematic literature review and future development trends. *ISPRS Int. J. Geoinf.* 10, 260. <https://doi.org/10.3390/ijgi10040260>.
- Leichter, A., Wittich, D., Rottensteiner, F., Werner, M., Sester, M., 2018. Improved classification of satellite imagery using spatial feature maps extracted from social media. *International Archives of the Photogrammetry, Remote Sensing and Spatial Information Sciences XLII-4*, 335–342. <https://doi.org/10.5194/isprs-archives-XLII-4-335-2018>.
- Lelovics, E., Unger, J., Gál, T., Gál, C., 2014. Design of an urban monitoring network based on local climate zone mapping and temperature pattern modelling. *Clim. Res.* 60, 51–62. <https://doi.org/10.3354/cr01220>.
- Lelovics, E., Unger, J., Savić, S., Gal, T., Milošević, D., Gulyás, A., Marković, V., Arsenovic, D., Gal, C.V., 2016. Intra-urban temperature observations in two Central European cities: a summer study. *Időjárás/Q. J. Hungarian Meteorol. Serv.* 120, 283–300.
- Li, N., Yang, J., Qiao, Z., Wang, Y., Miao, S., 2021. Urban thermal characteristics of local climate zones and their mitigation measures across cities in different climate zones of China. *Remote Sens.* 13, 1468. <https://doi.org/10.3390/rs13081468>.
- Li, X., Zhou, Y., Gong, P., Seto, K.C., Clinton, N., 2020. Developing a method to estimate building height from Sentinel-1 data. *Remote Sens. Environ.* 240, 111705. <https://doi.org/10.1016/j.rse.2020.111705>.
- Liang, T., He, J., Chen, L., Yao, Z., Zhang, L., Che, H., Gong, S., 2021. Simulation of the influence of a fine-scale urban underlying surface on the urban heat island effect in Beijing. *Atmos. Atmos. Res.* 262, 105786. <https://doi.org/10.1016/j.atmosres.2021.105786>.
- Liasis, G., Stavrou, S., 2016. Satellite images analysis for shadow detection and building height estimation. *ISPRS J. Photogramm. Remote Sens.* 119, 437–450. <https://doi.org/10.1016/j.isprsjprs.2016.07.006>.
- Zhongli, Lin, Hanqiu, Xu, 2016. A study of Urban heat island intensity based on “local climate zones”: A case study in Fuzhou, China. In: Weng, Q., Gamba, P., Xian, G., Chen, J.M., Liang, S. (Eds.), 2016 4th International Workshop on Earth Observation and Remote Sensing Applications (EORSA). IEEE, pp. 250–254. <https://doi.org/10.1109/EORSA.2016.7552807>.
- Liu, L., Lin, Y., Xiao, Y., Xue, P., Shi, L., Chen, X., Liu, J., 2018. Quantitative effects of urban spatial characteristics on outdoor thermal comfort based on the LCZ scheme. *Build. Environ.* 143, 443–460. <https://doi.org/10.1016/j.buildenv.2018.07.019>.
- Liu, L., Liu, J., Jin, L., Liu, L., Gao, Y., Pan, X., 2020a. Climate-conscious spatial morphology optimization strategy using a method combining local climate zone parameterization concept and urban canopy layer model. *Build. Environ.* 185, 107301. <https://doi.org/10.1016/j.buildenv.2020.107301>.
- Liu, S., Qi, Z., Li, X., Yeh, A., 2019. Integration of convolutional neural networks and object-based post-classification refinement for land use and land cover mapping with optical and SAR data. *Remote Sens.* 11, 690. <https://doi.org/10.3390/rs11060690>.
- Liu, S., Shi, Q., 2020. Local climate zone mapping as remote sensing scene classification using deep learning: a case study of metropolitan China. *ISPRS J. Photogramm. Remote Sens.* 164, 229–242. <https://doi.org/10.1016/j.isprsjprs.2020.04.008>.
- Liu, Y., Li, Q., Yang, L., Mu, K., Zhang, M., Liu, J., 2020b. Urban heat island effects of various urban morphologies under regional climate conditions. *Sci. Total Environ.* 743, 140589. <https://doi.org/10.1016/j.scitotenv.2020.140589>.
- Lopes, P., Fonte, C., See, L., Bechtel, B., 2017. Using OpenStreetMap data to assist in the creation of LCZ maps. In: 2017 Joint Urban Remote Sensing Event (JURSE). IEEE, Dubai, United Arab Emirates, pp. 1–4. <https://doi.org/10.1109/JURSE.2017.7924630>.
- Lordan, T., Grimmond, C.S.B., 2012. Characterization of energy flux partitioning in urban environments: links with surface seasonal properties. *J. Appl. Meteorol. Climatol.* 51, 219–241. <https://doi.org/10.1175/JAMC-D-11-0381>.
- Ma, L., Yang, Z., Zhou, L., Lu, H., Yin, G., 2021a. Local climate zones mapping using object-based image analysis and validation of its effectiveness through urban surface temperature analysis in China. *Build. Environ.* 206, 108348. <https://doi.org/10.1016/j.buildenv.2021.108348>.
- Ma, L., Zhu, X., Qiu, C., Blaschke, T., Li, M., 2021b. Advances of local climate zone mapping and its practice using object-based image analysis. *Atmosphere (Basel)* 12, 1146. <https://doi.org/10.3390/atmos12091146>.
- Maharoof, N., Emmanuel, R., Thomson, C., 2020. Compatibility of local climate zone parameters for climate sensitive street design: influence of openness and surface properties on local climate. *Urban Clim.* 33, 100642. <https://doi.org/10.1016/j.ulclim.2020.100642>.
- Manandhar, P., Bande, L., Tsoupos, A., Marpu, P.R., Armstrong, P., 2019. A study of local climate zones in Abu Dhabi with urban weather stations and numerical simulations. *Sustainability* 12, 156. <https://doi.org/10.3390/su12010156>.
- Mandelman, M., Ferenz, M., Mandelman, N., Potchter, O., 2020. Urban spatial patterns and heat exposure in the Mediterranean City of Tel Aviv. *Atmosphere (Basel)* 11, 963. <https://doi.org/10.3390/atmos11090963>.
- Manoli, G., Fatici, S., Schläpfer, M., Yu, K., Crowther, T.W., Meili, N., Burlando, P., Katul, G.G., Bou-Zeid, E., 2019. Magnitude of urban heat islands largely explained by

- climate and population. *Nature* 573, 55–60. <https://doi.org/10.1038/s41586-019-1512-9>.
- Masson, V., Hidalgo, J.A.A., Belaid, F., Bocher, E., Bonhomme, M., Bourgeois, A., Bretagne, G., Caillerez, S., Cordeau, E., Demazeux, C., Faraut, S., Gallato, C., Haoues-Jouve, S., Lambert, M.-L., Lemonsu, A., Lestringant, R., Lévy, J.-P., Long, N., Lopez, C.-X., Pellegrino, M., Petit, G., Pignon, C., Plumejeaud, C., Ruff, V., Schoetter, R., Tornay, N., Vye, D., 2015. Urban climate, human behavior & energy consumption: From LCZ mapping to simulation and urban planning (the MapUCE project). In: 9th International Conference on Urban Climate. Toulouse, France.
- Masson, V., Lemonsu, A., Hidalgo, J., Voogt, J., 2020. Urban climates and climate change. *Annu. Rev. Environ. Resour.* 45, 411–444. <https://doi.org/10.1146/annurev-environ-012320-083623>.
- McRae, I., Freedman, F., Rivera, A., Li, X., Dou, J., Cruz, I., Ren, C., Dronova, I., Fraker, H., Bornstein, R., 2020. Integration of the WUDAPT, WRF, and ENVI-met models to simulate extreme daytime temperature mitigation strategies in San Jose, California. *Build. Environ.* 184, 107180. <https://doi.org/10.1016/j.buildenv.2020.107180>.
- Meier, F., Fenner, D., Grassmann, T., Otto, M., Scherer, D., 2017. Crowdsourcing air temperature from citizen weather stations for urban climate research. *Urban Clim.* 19, 170–191. <https://doi.org/10.1016/j.ulclim.2017.01.006>.
- Mhedbi, Z., Masson, V., Hidalgo, J., Haoués-Jouve, S., 2019. Collection of refined architectural parameters by crowdsourcing using Facebook social network: case of greater Tunis. *Urban Clim.* 29, 100499. <https://doi.org/10.1016/j.ulclim.2019.100499>.
- Middel, A., Häb, K., Brazel, A.J., Martin, C.A., Guhathakurta, S., 2014. Impact of urban form and design on mid-afternoon microclimate in Phoenix local climate zones. *Landsc. Urban Plan.* 122, 16–28. <https://doi.org/10.1016/j.landurbplan.2013.11.004>.
- Middel, A., Lukasczyk, J., Maciejewski, R., Demuzere, M., Roth, M., 2018. Sky view factor footprints for urban climate modeling. *Urban Clim.* 25, 120–134. <https://doi.org/10.1016/j.ulclim.2018.05.004>.
- Mills, G., Ching, J., See, L., Bechtel, B., Foley, M., 2015. An introduction to the WUDAPT project. In: Proceedings of the 9th International Conference on Urban Climate, pp. 20–24.
- Milošević, D.D., Savić, S.M., Marković, V., Arsenović, D., Šećerov, I., 2016. Outdoor human thermal comfort in local climate zones of Novi Sad (Serbia) during heat wave period. *Hungarian Geograph. Bull.* 65, 129–137. <https://doi.org/10.15201/hungeobull.65.2.4>.
- Mitraka, Z., del Frate, F., Chrysoulakis, N., Gastellu-Etchegorry, J.-P., 2015. Exploiting Earth Observation data products for mapping Local Climate Zones. In: 2015 Joint Urban Remote Sensing Event (JURSE). IEEE, Lausanne, Switzerland, pp. 1–4. <https://doi.org/10.1109/JURSE.2015.7120456>. Mar. 30 – Apr. 1.
- Molnár, G., Gyöngyösi, A.Z., Gál, T., 2019. Integration of an LCZ-based classification into WRF to assess the intra-urban temperature pattern under a heatwave period in Szeged, Hungary. *Theor. Appl. Climatol.* 138, 1139–1158. <https://doi.org/10.1007/s00704-019-02881-1>.
- Mouzourides, P., Eleftheriou, A., Kyprianou, A., Ching, J., Neophytou, M.K.-A., 2019. Linking local-climate-zones mapping to multi-resolution-analysis to deduce associative relations at intra-urban scales through an example of metropolitan London. *Urban Clim.* 30, 100505. <https://doi.org/10.1016/j.ulclim.2019.100505>.
- Mu, K., Liu, Y., Zhang, M., Han, B., Yang, L., 2019. Investigations of surface urban Heat Island effect based on local climate zone method: a case of Xi'an. *E3S Web Conf.* 136, 05011. <https://doi.org/10.1051/e3sconf/201913605011>.
- Mu, Q., Miao, S., Wang, Y., Li, Y., He, X., Yan, C., 2020. Evaluation of employing local climate zone classification for mesoscale modelling over Beijing metropolitan area. *Meteorol. Atmos. Phys.* 132, 315–326. <https://doi.org/10.1007/s00703-019-00692-7>.
- Mughal, M.O., Li, X., Yin, T., Martilli, A., Brousse, O., Dissegna, M.A., Norford, L.K., 2019. High-resolution, multilayer modeling of Singapore's urban climate incorporating local climate zones. *J. Geophys. Res. Atmos.* 124, 7764–7785. <https://doi.org/10.1029/2018JD029796>.
- Mughal, M.O., Li, X.-X., Norford, L.K., 2020. Urban heat island mitigation in Singapore: evaluation using WRF/multilayer urban canopy model and local climate zones. *Urban Clim.* 34, 100714. <https://doi.org/10.1016/j.ulclim.2020.100714>.
- Müller, N., Kuttler, W., Barlag, A.-B., 2014. Counteracting urban climate change: adaptation measures and their effect on thermal comfort. *Theor. Appl. Climatol.* 115, 243–257. <https://doi.org/10.1007/s00704-013-0890-4>.
- Mushore, T.D., Dube, T., Manjowe, M., Gumindanga, W., Chemura, A., Rousta, I., Odindi, J., Mutanga, O., 2019. Remotely sensed retrieval of local climate zones and their linkages to land surface temperature in Harare metropolitan city, Zimbabwe. *Urban Clim.* 27, 259–271. <https://doi.org/10.1016/j.ulclim.2018.12.006>.
- Nassar, A.K., Blackburn, G.A., Whyatt, J.D., 2016. Dynamics and controls of urban heat sink and island phenomena in a desert city: development of a local climate zone scheme using remotely-sensed inputs. *Int. J. Appl. Earth Obs. Geoinf.* 51, 76–90. <https://doi.org/10.1016/j.jag.2016.05.004>.
- Ndetto, E.L., Matzarakis, A., 2015. Urban atmospheric environment and human biometeorological studies in Dar Es Salaam, Tanzania. *Air Qual. Atmos. Health* 8, 175–191. <https://doi.org/10.1007/s11869-014-0261-z>.
- Nurwanda, A., 2018. City expansion and urban heat island in Bogor. *IOP Conf. Ser. Earth Environ. Sci.* 179, 012007. <https://doi.org/10.1088/1755-1315/179/1/012007>.
- Nurwanda, A., Honjo, T., 2018. Analysis of land use change and expansion of surface urban Heat Island in Bogor City by remote sensing. *ISPRS Int. J. Geoinf.* 7, 165. <https://doi.org/10.3390/ijgi7050165>.
- Ochola, E.M., Fakharizadehshirazi, E., Adimo, A.O., Mukundi, J.B., Wesonga, J.M., Soudodi, S., 2020. Inter-local climate zone differentiation of land surface temperatures for Management of Urban Heat in Nairobi City, Kenya. *Urban Clim.* 31, 100540. <https://doi.org/10.1016/j.ulclim.2019.100540>.
- Oke, T.R., 2004. Initial guidance to obtain representative meteorological observations at urban sites.
- Oliveira, A., Lopes, A., Niza, S., 2020. Local climate zones in five southern european cities: an improved GIS-based classification method based on copernicus data. *Urban Clim.* 33, 100631. <https://doi.org/10.1016/j.ulclim.2020.100631>.
- Oxoli, D., Ronchetti, G., Minghini, M., Molinari, M., Loftian, M., Sona, G., Brovelli, M., 2018. Measuring urban land cover influence on air temperature through multiple geo-data—the case of Milan, Italy. *ISPRS Int. J. Geoinf.* 7, 421. <https://doi.org/10.3390/ijgi7110421>.
- Patel, P., Jamshidi, S., Nadimpalli, R., Aliaga, D.G., Mills, G., Chen, F., Demuzere, M., Niyogi, D., 2022. Modeling large-scale heatwave by incorporating enhanced urban representation. *J. Geophys. Res. Atmos.* 127, e2021JD035316. <https://doi.org/10.1029/2021JD035316>.
- Patel, P., Karnasakar, S., Ghosh, S., Niyogi, D., 2020. Improved simulation of very heavy rainfall events by incorporating WUDAPT urban land use/land cover in WRF. *Urban Clim.* 32, 100616. <https://doi.org/10.1016/j.ulclim.2020.100616>.
- Pellegrati Franco, D.M., Andrade, M.F., Ynoue, R.Y., Ching, J., 2019. Effect of Local Climate Zone (LCZ) classification on ozone chemical transport model simulations in São Paulo, Brazil. *Urban Clim.* 27, 293–313. <https://doi.org/10.1016/j.ulclim.2018.12.007>.
- Perera, N.G.R., Emmanuel, M.P.R., Mahanama, P.K.S., 2013. Projected urban development, changing "Local Climate Zones" and relative warming effects in Colombo, Sri Lanka. In: International Conference on "Cities, People and Places". ICCPP.
- Perera, N.G.R., Emmanuel, R., 2018. A "Local climate zone" based approach to urban planning in Colombo, Sri Lanka. *Urban Clim.* 23, 188–203. <https://doi.org/10.1016/j.ulclim.2016.11.006>.
- Picone, N., Campo, A.M., 2015. Preparing urban climate maps using the LCZ methodology for improving communication with urban planners: the case of Tandil city, Argentina. In: Proceedings of the ICUC9–ICUC9. France, Toulouse.
- Plumejeaud-Perreau, C., Poitevin, C., Pignon-Mussaud, C., Long, N., 2015. Building local climate zones by using socio-economic and topographic vectorial databases. In: 9th International Conference on Urban Climate.
- Pokhrel, R., González-Cruz, J.E., 2021. Mitigation options to reduce peak air temperature and air-conditioning demand in the context of a warming climate for a tropical Coastal City. *ASME J. Eng. Sustain. Build. Cities* 2. <https://doi.org/10.1115/1.4051160>.
- Pokhrel, R., Ramírez-Beltran, N.D., González, J.E., 2019. On the assessment of alternatives for building cooling load reductions for a tropical coastal city. *Energy Build.* 182, 131–143. <https://doi.org/10.1016/j.enbuild.2018.10.023>.
- Pradhesta, Y.F., Nurjani, E., Arijuddin, B.I., 2019. Local climate zone classification for climate-based urban planning using landsat 8 imagery (A case study in Yogyakarta urban Area). *IOP Conf. Ser. Earth Environ. Sci.* 303, 012022. <https://doi.org/10.1088/1755-1315/303/1/012022>.
- Qi, F., Zhai, J.Z., Dang, G., 2016. Building height estimation using Google earth. *Energy Build.* 118, 123–132. <https://doi.org/10.1016/j.enbuild.2016.02.044>.
- Qiu, C., Liebel, L., Hughes, L.H., Schmitt, M., Korner, M., Zhu, X.X., 2022. Multitask learning for human settlement extent regression and local climate zone classification. *IEEE Geosci. Remote Sens. Lett.* 19, 1–5. <https://doi.org/10.1109/LGRS.2020.3037246>.
- Qiu, C., Mou, L., Schmitt, M., Zhu, X.X., 2020a. Fusing multisessional Sentinel-2 imagery for urban land cover classification with multibranch residual convolutional neural networks. *IEEE Geosci. Remote Sens. Lett.* 17, 1787–1791. <https://doi.org/10.1109/LGRS.2019.2953497>.
- Qiu, C., Mou, L., Schmitt, M., Zhu, X.X., 2019a. Local climate zone-based urban land cover classification from multi-seasonal Sentinel-2 images with a recurrent residual network. *ISPRS J. Photogramm. Remote Sens.* 154, 151–162. <https://doi.org/10.1016/j.isprsjprs.2019.05.004>.
- Qiu, C., Schmitt, M., Mou, L., Ghamisi, P., Zhu, X., 2018a. Feature importance analysis for local climate zone classification using a residual convolutional neural network with multi-source datasets. *Remote Sens.* 10, 1572. <https://doi.org/10.3390/rs10101572>.
- Qiu, C., Schmitt, M., Mou, L., Zhu, X., 2018. Urban local climate zone classification with a residual convolutional neural network and multi-seasonal sentinel-2 images. In: 2018 10th IAPR Workshop on Pattern Recognition in Remote Sensing (PRRS). IEEE, pp. 1–5. <https://doi.org/10.1109/PRRS.2018.8486155>.
- Qiu, C., Schmitt, M., Zhu, X.X., 2019. Fusing multi-seasonal sentinel-2 images with residual convolutional neural networks for local climate zone-derived urban land cover classification. In: IGARSS 2019 - 2019 IEEE International Geoscience and Remote Sensing Symposium. IEEE, pp. 5037–5040. <https://doi.org/10.1109/IGARSS.2019.8898223>.
- Qiu, C., Tong, X., Schmitt, M., Bechtel, B., Zhu, X., 2020b. Multilevel feature fusion-based CNN for local climate zone classification from sentinel-2 images: benchmark results on the So2Sat LCZ24 dataset. *IEEE J. Sel. Top. Appl. Earth Obs. Remote Sens.* 13, 2793–2806. <https://doi.org/10.1109/JSTARS.2020.2995711>.
- Qiu, C.P., Schmitt, M., Ghamisi, P., Zhu, X.X., 2018. Effect of the training set configuration on sentinel-2-based urban local climate zone classification. *Int. Arch. Photogramm. Remote Sens. Spatial Inform. Sci.* XLII-2, 931–936. <https://doi.org/10.5194/isprs-archives-XLII-2-931-2018>.
- Quan, J., 2019a. Enhanced geographic information system-based mapping of local climate zones in Beijing, China. *Sci. China Technol. Sci.* 62, 2243–2260. <https://doi.org/10.1007/s11431-018-9417-6>.

- Quan, J., 2019b. Multi-temporal effects of urban forms and functions on urban Heat Islands based on local climate zone classification. *Int. J. Environ. Res. Public Health* 16, 2140. <https://doi.org/10.3390/ijerph16122140>.
- Quan, S.J., Bansal, P., 2021. A systematic review of GIS-based local climate zone mapping studies. *Build. Environ.* 196, 107791 <https://doi.org/10.1016/j.buildenv.2021.107791>.
- Quan, S.J., Dutt, F., Woodworth, E., Yamagata, Y., Yang, P.P.-J., 2017. Local climate zone mapping for energy resilience: a fine-grained and 3D approach. *Energy Proc.* 105, 3777–3783. <https://doi.org/10.1016/j.egypro.2017.03.883>.
- Rathnayake, N.U., Perera, N.G.R., Emmanuel, M.P.R., 2020. Anthropogenic heat implications of Colombo core area development plan. *IOP Conf. Ser. Earth Environ. Sci.* 471, 012002 <https://doi.org/10.1088/1755-1315/471/1/012002>.
- Ren, C., Cai, M., Li, X., Zhang, L., Wang, R., Xu, Y., Ng, E., 2019. Assessment of local climate zone classification maps of cities in China and feasible refinements. *Sci. Rep.* 9, 18848. <https://doi.org/10.1038/s41598-019-55444-9>.
- Ren, C., Cai, M., Wang, M., Xu, Y., Ng, E., 2016. Local climate zone (LCZ) classification using the world urban database and access portal Tools (WUDAPT) method: A case study in Wuhan and Hangzhou. In: *The Fourth International Conference on Countermeasure to Urban Heat Islands (4th IC2UHI)*, pp. 1–12.
- Ren, C., Ng, E.Y., Katschner, L., 2011. Urban climatic map studies: a review. *Int. J. Climatol.* 31, 2213–2233. <https://doi.org/10.1002/joc.2237>.
- Ren, C., Wang, R., Cai, M., Xu, Y., Zheng, Y., Ng, E., 2016. The accuracy assessment of LCZ map generated by world urban database and access portal tools method: A case study of Hong Kong. In: *The Fourth International Conference on Countermeasure to Urban Heat Islands (4th IC2UHI)*, pp. 1–11.
- Ribeiro, I., Martilli, A., Falls, M., Zonato, A., Villalba, G., 2021. Highly resolved WRF-BEP/BEM simulations over Barcelona urban area with LCZ. *Atmos. Res.* 248, 105220 <https://doi.org/10.1016/j.atmosres.2020.105220>.
- Richard, Y., Emery, J., Dudek, J., Pergaud, J., Chateau-Smith, C., Zito, S., Rega, M., Vairet, T., Castel, T., Thévenin, T., Pohl, B., 2018. How relevant are local climate zones and urban climate zones for urban climate research? Dijon (France) as a case study. *Urban Clim.* 26, 258–274. <https://doi.org/10.1016/j.uclim.2018.10.002>.
- Rodler, A., Leduc, T., 2019. Local climate zone approach on local and micro scales: dividing the urban open space. *Urban Clim.* 28, 100457 <https://doi.org/10.1016/j.uclim.2019.100457>.
- Rosentreter, J., Hagensieker, R., Waske, B., 2020. Towards large-scale mapping of local climate zones using multitemporal sentinel 2 data and convolutional neural networks. *Remote Sens. Environ.* 237, 111472 <https://doi.org/10.1016/j.rse.2019.111472>.
- Ru, C., Duan, S.-B., Jiang, X.-G., Li, Z.-L., Jiang, Y., Ren, H., Leng, P., Gao, M., 2021. Land surface temperature retrieval from landsat 8 thermal infrared data over urban areas considering geometry effect: method and application. *IEEE Trans. Geosci. Remote Sens.* 60, 1–16. <https://doi.org/10.1109/TGRS.2021.3088482>.
- Sapena, M., Wurm, M., Taubenböck, H., Tuia, D., Ruiz, L.A., 2021. Estimating quality of life dimensions from urban spatial pattern metrics. *Comput. Environ. Urban. Syst.* 85, 101549 <https://doi.org/10.1016/j.compenvurbsys.2020.101549>.
- Savić, S., Marković, V., Šećerov, I., Pavic, D., Arsenović, D., Milošević, D., Dolinaj, D., Nagy, I., Pantelić, M., 2018. Heat wave risk assessment and mapping in urban areas: case study for a mid-sized central european city, Novi Sad (Serbia). *Nat. Hazards* 91, 891–911. <https://doi.org/10.1007/s11069-017-3160-4>.
- Savic, S., Milosevic, D., Lazic, L., Markovic, V., Arsenovic, D., Pavic, D., 2013. Classifying urban meteorological stations sites by “local climate zones”: preliminary results for the city of Novi Sad (Serbia). *Geograph. Pannon.* 17, 60–68. <https://doi.org/10.5937/GeoPan13030605>.
- Secerov, I., Savic, S., Milosevic, D., Markovic, V., Bajsanski, I., 2015. Development of an automated urban climate monitoring system in Novi Sad (Serbia). *Geograph. Pannon.* 19, 174–183. <https://doi.org/10.5937/GeoPan15041745>.
- Semenova, A.A., Konstantinov, P.I., Varentsov, M.I., Samsonov, T.E., 2019. Modeling the dynamics of comfort thermal conditions in Arctic cities under regional climate change. *IOP Conf. Ser. Earth Environ. Sci.* 386, 012017 <https://doi.org/10.1088/1755-1315/386/1/012017>.
- Shao, Y., Taff, G.N., Walsh, S.J., 2011. Shadow detection and building-height estimation using IKONOS data. *Int. J. Remote Sens.* 32, 6929–6944. <https://doi.org/10.1080/01431161.2010.517226>.
- Sharifi, A., Wu, Y., Khamchiangta, D., Yoshida, T., Yamagata, Y., 2018. Urban carbon mapping: towards a standardized framework. *Energy Proc.* 152, 799–808. <https://doi.org/10.1016/j.egypro.2018.09.193>.
- Shevchenko, O., Matvienko, M., Snizhko, S., 2020. A GIS and WUDAPT based mapping of the local climate zones in ukrainian cities. In: *Geoinformatics: Theoretical and Applied Aspects 2020*. European Association of Geoscientists & Engineers, pp. 1–5. <https://doi.org/10.3997/2214-4609.2020geo100>.
- Shi, L., Ling, F., 2021. Local climate zone mapping using multi-source free available datasets on Google earth engine platform. *Land (Basel)* 10, 454. <https://doi.org/10.3390/land10050454>.
- Shi, L., Luo, Z., Matthews, W., Wang, Z., Li, Y., Liu, J., 2019a. Impacts of urban microclimate on summertime sensible and latent energy demand for cooling in residential buildings of Hong Kong. *Energy* 189, 116208. <https://doi.org/10.1016/j.energy.2019.116208>.
- Shi, Y., Lau, K.K.-L., Ren, C., Ng, E., 2018. Evaluating the local climate zone classification in high-density heterogeneous urban environment using mobile measurement. *Urban Clim.* 25, 167–186. <https://doi.org/10.1016/j.uclim.2018.07.001>.
- Shi, Y., Ren, C., Lau, K.K.-L., Ng, E., 2019b. Investigating the influence of urban land use and landscape pattern on PM2.5 spatial variation using mobile monitoring and WUDAPT. *Landsc. Urban Plan.* 189, 15–26. <https://doi.org/10.1016/j.landurbplan.2019.04.004>.
- Shi, Y., Xiang, Y., Zhang, Y., 2019c. Urban Design factors influencing surface urban Heat Island in the high-Density City of Guangzhou based on the local climate zone. *Sensors* 19, 3459. <https://doi.org/10.3390/s19163459>.
- Shih, W., 2017. The impact of urban development patterns on thermal distribution in Taipei. In: *2017 Joint Urban Remote Sensing Event (JURSE)*. IEEE, Dubai, United Arab Emirates, pp. 1–5. <https://doi.org/10.1109/JURSE.2017.7924634>. Mar 5–7.
- Shih, W.-Y., Ahmad, S., Chen, Y.-C., Lin, T.-P., Mabon, L., 2020. Spatial relationship between land development pattern and intra-urban thermal variations in Taipei. *Sustain. Cities Soc.* 62, 102415 <https://doi.org/10.1016/j.scs.2020.102415>.
- Simanjuntak, R.M., Kuffer, M., Reckien, D., 2019. Object-based image analysis to map local climate zones: the case of Bandung, Indonesia. *Appl. Geogr.* 106, 108–121. <https://doi.org/10.1016/j.apgeog.2019.04.001>.
- Siu, L.W., Hart, M.A., 2013. Quantifying urban heat island intensity in Hong Kong SAR, China. *Environ. Monit. Assess.* 185, 4383–4398. <https://doi.org/10.1007/s10661-012-2876-6>.
- Skarbit, N., Gál, T., 2016. Projection of intra-urban modification of night-time climate indices during the 21st century. *Hungarian Geograph. Bull.* 65, 181–193. <https://doi.org/10.15201/hungeobull.65.2.8>.
- Skarbit, N., Gal, T., Unger, J., 2015. Airborne surface temperature differences of the different Local Climate Zones in the urban area of a medium sized city. In: *2015 Joint Urban Remote Sensing Event (JURSE)*. IEEE, Lausanne, Switzerland, pp. 1–4. <https://doi.org/10.1109/JURSE.2015.7120497>. Mar. 30 – Apr. 1.
- Skarbit, N., Stewart, I.D., Unger, J., Gál, T., 2017. Employing an urban meteorological network to monitor air temperature conditions in the ‘local climate zones’ of Szeged, Hungary. *Int. J. Climatol.* 37, 582–596. <https://doi.org/10.1002/joc.5023>.
- Somuncu, D.H., Yüksel, Ü., 2020. Assessment of relationship between the surface temperatures and built-up urban environment in Ankara city center. *J. Environ. Biol.* 41, 491–498. [https://doi.org/10.22438/jeb/41/2\(SI\)/JEB-30](https://doi.org/10.22438/jeb/41/2(SI)/JEB-30).
- Stehman, S.V., Foody, G.M., 2019. Key issues in rigorous accuracy assessment of land cover products. *Remote Sens. Environ.* 231, 111199 <https://doi.org/10.1016/j.rse.2019.05.018>.
- Stewart, I.D., Oke, T., 2019. Classifying URBAN climate field sites by “LOCAL climate ZONES”: the CASE of Nagano, Japan. *Rev. Formacao Online* 26, 220–229.
- Stewart, I.D., Oke, T.R., 2012. Local climate zones for urban temperature studies. *Bull. Am. Meteorol. Soc.* 93, 1879–1900. <https://doi.org/10.1175/BAMS-D-11-00019.1>.
- Stewart, I.D., Oke, T.R., 2009. Newly developed “thermal climate zones” for defining and measuring urban heat island “magnitude” in the canopy layer. In: *AMS Eighth Symposium on the Urban Environment* p. J8.2A.
- Stewart, I.D., Oke, T.R., Krayenhoff, E.S., 2014. Evaluation of the ‘local climate zone’ scheme using temperature observations and model simulations. *Int. J. Climatol.* 34, 1062–1080. <https://doi.org/10.1002/joc.3746>.
- Středová, H., Chuchma, F., Rožnovský, J., Středa, T., 2021. Local climate zones, land surface temperature and air temperature interactions: case study of Hradec Králové, the Czech Republic. *ISPRS Int. J. Geoinf.* 10, 704. <https://doi.org/10.3390/ijgi10100704>.
- Sukhanov, S., Tankoyeu, I., Louradour, J., Heremans, R., Trofimova, D., Debes, C., 2017. Multilevel ensembling for local climate zones classification. In: *2017 IEEE International Geoscience and Remote Sensing Symposium (IGARSS)*. IEEE, Texas, USA, pp. 1201–1204. <https://doi.org/10.1109/IGARSS.2017.8127173>.
- Sun, Y., Mou, L., Wang, Y., Montazeri, S., Zhu, X.X., 2022. Large-scale building height retrieval from single SAR imagery based on bounding box regression networks. *ISPRS J. Photogramm. Remote Sens.* 184, 79–95. <https://doi.org/10.1016/j.isprsjprs.2021.11.024>.
- Sun, Y., Zhang, X., Ren, G., Zwiers, F.W., Hu, T., 2016. Contribution of urbanization to warming in China. *Nat. Clim. Chang.* 6, 706–709. <https://doi.org/10.1038/nclimate2956>.
- Taubenböck, H., Debray, H., Qiu, C., Schmitt, M., Wang, Y., Zhu, X.X., 2020. Seven city types representing morphological configurations of cities across the globe. *Cities* 105, 102814. <https://doi.org/10.1016/j.cities.2020.102814>.
- Thomas, G., Sherin, A.P., Ansar, S., Zachariah, E.J., 2014. Analysis of urban Heat Island in Kochi, India, using a modified local climate zone classification. *Proc. Environ. Sci.* 21, 3–13. <https://doi.org/10.1016/j.proenv.2014.09.002>.
- Tong, Z., Luo, Y., Zhou, J., 2021. Mapping the urban natural ventilation potential by hydrological simulation. *Build. Simul.* 14, 351–364. <https://doi.org/10.1007/s12273-020-0755-6>.
- Top, S., Milošević, D., Caluwaerts, S., Hamdi, R., Savić, S., 2020. Intra-urban differences of outdoor thermal comfort in Ghent on seasonal level and during record-breaking 2019 heat wave. *Build. Environ.* 185, 107103 <https://doi.org/10.1016/j.buldev.2020.107103>.
- Tse, J.W.P., Yeung, P.S., Fung, J.C.-H., Ren, C., Wang, R., Wong, M.M.-F., Cai, M., 2018. Investigation of the meteorological effects of urbanization in recent decades: A case study of major cities in Pearl River Delta. *Urban Clim.* 26, 174–187. <https://doi.org/10.1016/j.uclim.2018.08.007>.
- Tu, W., Hu, Z., Li, L., Cao, J., Jiang, J., Li, Q., Li, Q., 2018. Portraying urban functional zones by coupling remote sensing imagery and human sensing data. *Remote Sens.* 10, 141. <https://doi.org/10.3390/10010141>.
- Tuholske, C., Caylor, K., Funk, C., Verdin, A., Sweeney, S., Grace, K., Peterson, P., Evans, T., 2021. Global urban population exposure to extreme heat. *Proc. Natl. Acad. Sci.* 118 (41), e2024792118 <https://doi.org/10.1073/pnas.2024792118>.
- Tuia, D., Moser, G., le Saux, B., Bechtel, B., See, L., 2017a. 2017 IEEE GRSS data fusion contest: open data for global multimodal land use classification [Technical Committees]. *IEEE Geosci. Remote Sens. Mag.* 5, 70–73. <https://doi.org/10.1109/MGRS.2016.2645380>.
- Tuia, D., Moser, G., Wurm, M., Taubenbock, H., 2017. Land use modeling in North Rhine-Westphalia with interaction and scaling laws. In: *2017 Joint Urban Remote*

- Sensing Event (JURSE). IEEE, Dubai, United Arab Emirates, pp. 1–4. <https://doi.org/10.1109/JURSE.2017.7924542>.
- Tuia, D., Persello, C., Bruzzone, L., 2016. Domain adaptation for the classification of remote sensing data: an overview of recent advances. *IEEE Geosci. Remote Sens. Mag.* 4, 41–57. <https://doi.org/10.1109/MGRS.2016.2548504>.
- Unal Cilek, M., Cilek, A., 2021. Analyses of land surface temperature (LST) variability among local climate zones (LCZs) comparing Landsat-8 and ENVI-met model data. *Sustain. Cities Soc.* 69, 102877 <https://doi.org/10.1016/j.scs.2021.102877>.
- Unger, J., Gál, T., Csépe, Z., Lelovics, E., Gulyás, Á., 2015. Development, data processing and preliminary results of an urban human comfort monitoring and information system. *IDÓJÁRÁS/Q. J. Hungarian Meteorol. Serv.* 119, 337–354.
- Unger, J., Lelovics, E., Gál, T., 2014. Local Climate Zone mapping using GIS methods in Szeged. *Hungarian Geograph. Bull.* 63, 29–41. <https://doi.org/10.15201/hungebull.63.1.3>.
- Unger, J., Skarbit, N., Gál, T., 2018. Evaluation of outdoor human thermal sensation of local climate zones based on long-term database. *Int. J. Biometeorol.* 62, 183–193. <https://doi.org/10.1007/s00484-017-1440-z>.
- United Nations, 2019. *World Urbanization Prospects: The 2018 Revision*. United Nations, New York.
- van de Walle, J., Brousse, O., Arnalsteen, L., Byarugaba, D., Ddumba, D.S., Demuzere, M., Iwasa, S., Nsangi, G., Sseviri, H., Thiery, W., Vanhaeren, R., Wouters, H., van Lipzig, P.M., N., 2021. Can local fieldwork help to represent intra-urban variability of canopy parameters relevant for tropical African climate studies? *Theor. Appl. Climatol.* 146, 457–474. <https://doi.org/10.1007/s00704-021-03733-7>.
- Vandamme, S., Demuzere, M., Verdonck, M.-L., Zhang, Z., van Coillie, F., 2019. Revealing Kunming's (China) historical urban planning policies through local climate zones. *Remote Sens.* 11, 1731. <https://doi.org/10.3390/rs11141731>.
- Varentsov, M., Samonov, T., Demuzere, M., 2020. Impact of urban canopy parameters on a Megacity's modelled thermal environment. *Atmosphere (Basel)* 11, 1349. <https://doi.org/10.3390/atmos11121349>.
- Verdonck, M., Demuzere, M., Bechtel, B., Beck, C., Brousse, O., Droste, A., Fenner, D., Leconte, F., van Coillie, F., 2019a. The human influence experiment (Part 2): guidelines for improved mapping of local climate zones using a supervised classification. *Urban Sci.* 3, 27. <https://doi.org/10.3390/urbansci3010027>.
- Verdonck, M.-L., Demuzere, M., Hooyberghs, H., Priem, F., van Coillie, F., 2019b. Heat risk assessment for the Brussels capital region under different urban planning and greenhouse gas emission scenarios. *J. Environ. Manag.* 249, 109210 <https://doi.org/10.1016/j.jenvman.2019.06.111>.
- Verdonck, M.-L., Okujeni, A., van der Linden, S., Demuzere, M., de Wulf, R., van Coillie, F., 2017. Influence of neighbourhood information on 'Local climate zone' mapping in heterogeneous cities. *Int. J. Appl. Earth Obs. Geoinf.* 62, 102–113. <https://doi.org/10.1016/j.jag.2017.05.017>.
- Villadiego, K., Velay-Dabat, M.A., 2014. Outdoor thermal comfort in a hot and humid climate of Colombia: a field study in Barranquilla. *Build. Environ.* 75, 142–152. <https://doi.org/10.1016/j.buildenv.2014.01.017>.
- Vogel, J., Afshari, A., Chockalingam, G., Stadler, S., 2022. Evaluation of a novel WRF/PALM-4U coupling scheme incorporating a roughness-corrected surface layer representation. *Urban Clim.* 46, 101311 <https://doi.org/10.1016/j.uclim.2022.101311>.
- Wang, C., Middel, A., Myint, S.W., Kaplan, S., Brazel, A.J., Lukasczyk, J., 2018a. Assessing local climate zones in arid cities: the case of Phoenix, Arizona and Las Vegas, Nevada. *ISPRS J. Photogramm. Remote Sens.* 141, 59–71. <https://doi.org/10.1016/j.isprsjprs.2018.04.009>.
- Wang, Q., Zhang, C., Ren, C., Hang, J., Li, Y., 2020. Urban heat island circulations over the Beijing-Tianjin region under calm and fair conditions. *Build. Environ.* 180, 107063 <https://doi.org/10.1016/j.buildenv.2020.107063>.
- Wang, R., Cai, M., Ren, C., Bechtel, B., Xu, Y., Ng, E., 2019. Detecting multi-temporal land cover change and land surface temperature in Pearl River Delta by adopting local climate zone. *Urban Clim.* 28, 100455 <https://doi.org/10.1016/j.uclim.2019.100455>.
- Wang, R., Gao, W., Zhou, N., Kammen, D.M., Peng, W., 2021a. Urban structure and its implication of heat stress by using remote sensing and simulation tool. *Sustain. Cities Soc.* 65, 102632 <https://doi.org/10.1016/j.scs.2020.102632>.
- Wang, R., Ren, C., Xu, Y., Lau, K.K.-L., Shi, Y., 2018b. Mapping the local climate zones of urban areas by GIS-based and WUDAPT methods: a case study of Hong Kong. *Urban Clim.* 24, 567–576. <https://doi.org/10.1016/j.uclim.2017.10.001>.
- Wang, T., Dong, J., Xu, S., Tong, Z., 2018. Comparative study of urban forms on macro scale. In: Hu, S., Ye, X., Yang, K., Fan, H. (Eds.), 2018 26th International Conference on Geoinformatics. IEEE, pp. 1–6. <https://doi.org/10.1109/GEOINFORMATICS.2018.8557163>.
- Wang, Y., Ni, Z., Hu, M., Chen, S., Xia, B., 2021b. A practical approach of urban green infrastructure planning to mitigate urban overheating: a case study of Guangzhou. *J. Clean. Prod.* 287, 124995 <https://doi.org/10.1016/j.jclepro.2020.124995>.
- Wang, Y., Zhan, Q., Ouyang, W., 2017. Impact of urban climate landscape patterns on land surface temperature in Wuhan, China. *Sustainability* 9, 1700. <https://doi.org/10.3390/su9101700>.
- Wang, Z., Xing, W., Huang, Y., Xie, T., 2016. Studying the urban Heat Island using a local climate zone scheme. *Pol. J. Environ. Stud.* 25, 2609–2616. <https://doi.org/10.1524/pjoes/63672>.
- Wei, C.Z., Blaschke, T., 2016. Identifying local scale climate zones of urban heat island from HJ-1B satellite data using self-organizing maps. *International Archives of the Photogrammetry, Remote Sensing and Spatial Information Sciences XLI-B8*, 1431–1436. <https://doi.org/10.5194/isprs-archives-XLI-B8-1431-2016>. Mar 5-7.
- Wicki, A., Parlow, E., 2017. Attribution of local climate zones using a multitemporal land use/land cover classification scheme. *J. Appl. Remote. Sens.* 11, 026001 <https://doi.org/10.1117/1.JRS.11.026001>.
- Wu, Y., Sharifi, A., Yang, P., Borjigin, H., Murakami, D., Yamagata, Y., 2018. Mapping building carbon emissions within local climate zones in Shanghai. *Energy Proc.* 152, 815–822. <https://doi.org/10.1016/j.egypro.2018.09.195>.
- Xing, H., Meng, Y., 2018. Integrating landscape metrics and socioeconomic features for urban functional region classification. *Comput. Environ. Urban. Syst.* 72, 134–145. <https://doi.org/10.1016/j.compenvurbsys.2018.06.005>.
- Xu, C., Hystad, P., Chen, R., van den Hoek, J., Hutchinson, R.A., Hankey, S., Kennedy, R., 2021. Application of training data affects success in broad-scale local climate zone mapping. *Int. J. Appl. Earth Obs. Geoinf.* 103, 102482 <https://doi.org/10.1016/j.jag.2021.102482>.
- Xu, G., Zhu, X., Tapper, N., Bechtel, B., 2019. Urban climate zone classification using convolutional neural network and ground-level images. *Progr. Phys. Geogr. Earth Environ.* 43, 410–424. <https://doi.org/10.1177/030913319837711>.
- Xu, Y., Ma, F., Meng, D., Ren, C., Leung, Y., 2017. A co-training approach to the classification of local climate zones with multi-source data. In: 2017 IEEE International Geoscience and Remote Sensing Symposium (IGARSS). IEEE, Texas, USA, pp. 1209–1212. <https://doi.org/10.1109/IGARSS.2017.8127175>. July 23–28.
- Xu, Y., Ren, C., Cai, M., Edward, N.Y.Y., Wu, T., 2017b. Classification of local climate zones using ASTER and Landsat data for high-density cities. *IEEE J. Sel. Top. Appl. Earth Obs. Remote Sens.* 10, 3397–3405. <https://doi.org/10.1109/JSTARS.2017.2683484>.
- Xu, Y., Ren, C., Cai, M., Wang, R., 2017. Issues and challenges of remote sensing-based local climate zone mapping for high-density cities. In: 2017 Joint Urban Remote Sensing Event (JURSE). IEEE, Dubai, United Arab Emirates, pp. 1–4. <https://doi.org/10.1109/JURSE.2017.7924558>. Mar 5–7.
- Xu, Z., Chen, J., Xia, J., Du, P., Zheng, H., Gan, L., 2018. Multisource earth observation data for land-cover classification using random Forest. *IEEE Geosci. Remote Sens. Lett.* 15, 789–793. <https://doi.org/10.1109/LGRS.2018.2806223>.
- Yan, Y., Huang, B., 2022. Estimation of building height using a single street view image via deep neural networks. *ISPRS J. Photogramm. Remote Sens.* 192, 83–98. <https://doi.org/10.1016/j.isprsjprs.2022.08.006>.
- Yang, G., Fu, Y., Yan, M., Zhang, J., 2020a. Exploring the distribution of energy consumption in a northeast Chinese city based on local climate zone scheme: Shenyang city as a case study. *Energy Explor. Exploit.* 38, 2079–2094. <https://doi.org/10.1177/0144598720950465>.
- Yang, J., Jin, S., Xiao, X., Jin, C., Xia, J., Li, X., Wang, S., 2019. Local climate zone ventilation and urban land surface temperatures: Towards a performance-based and wind-sensitive planning proposal in megacities. *Sustain. Cities Soc.* 47, 101487 <https://doi.org/10.1016/j.scs.2019.101487>.
- Yang, J., Ren, J., Sun, D., Xiao, X., Xia, J., Jin, C., Li, X., 2021. Understanding land surface temperature impact factors based on local climate zones. *Sustain. Cities Soc.* 69, 102818 <https://doi.org/10.1016/j.scs.2021.102818>.
- Yang, J., Wang, Y., Xiu, C., Xiao, X., Xia, J., Jin, C., Li, X., 2020b. Optimizing local climate zones to mitigate urban heat island effect in human settlements. *J. Clean. Prod.* 275, 123767 <https://doi.org/10.1016/j.jclepro.2020.123767>.
- Yang, J., Zhan, Y., Xiao, X., Xia, J.C., Sun, W., Li, X., 2020c. Investigating the diversity of land surface temperature characteristics in different scale cities based on local climate zones. *Urban Clim.* 34, 100700 <https://doi.org/10.1016/j.uclim.2020.100700>.
- Yang, R., Zhang, Y., Zhao, P., Ji, Z., Deng, W., 2019. MSPPF-nets: a deep learning architecture for remote sensing image classification. In: IGARSS 2019 - 2019 IEEE International Geoscience and Remote Sensing Symposium. IEEE, pp. 3045–3048. <https://doi.org/10.1109/IGARSS.2019.8899068>.
- Yang, X., Peng, L.L.H., Chen, Y., Yao, L., Wang, Q., 2020d. Air humidity characteristics of local climate zones: a three-year observational study in Nanjing. *Build. Environ.* 171, 106661 <https://doi.org/10.1016/j.buildenv.2020.106661>.
- Yokoya, N., Ghamisi, P., Xia, J., 2017. Multimodal, multitemporal, and multisource global data fusion for local climate zones classification based on ensemble learning. In: 2017 IEEE International Geoscience and Remote Sensing Symposium (IGARSS). IEEE, Texas, USA, pp. 1197–1200. <https://doi.org/10.1109/IGARSS.2017.8127172>. July 23–28.
- Yokoya, N., Ghamisi, P., Xia, J., Sukhanov, S., Heremans, R., Tankoyeu, I., Bechtel, B., le Saux, B., Moser, G., Tuia, D., 2018. Open data for global multimodal land use classification: outcome of the 2017 IEEE GRSS data fusion contest. *IEEE J. Sel. Top. Appl. Earth Obs. Remote Sens.* 11, 1363–1377. <https://doi.org/10.1109/JSTARS.2018.2799698>.
- Yoo, C., Han, D., Im, J., Bechtel, B., 2019. Comparison between convolutional neural networks and random forest for local climate zone classification in mega urban areas using landsat images. *ISPRS J. Photogramm. Remote Sens.* 157, 155–170. <https://doi.org/10.1016/j.isprsjprs.2019.09.009>.
- Yoo, C., Lee, Y., Cho, D., Im, J., Han, D., 2020. Improving local climate zone classification using incomplete building data and sentinel 2 images based on convolutional neural networks. *Remote Sens.* 12, 3552. <https://doi.org/10.3390/rs12213552>.
- Yu, Y., Li, J., Yuan, Q., Shi, Q., Shen, H., Zhang, L., 2021. Coupling dual graph convolution network and residual network for local climate zone mapping. *IEEE J. Sel. Top. Appl. Earth Obs. Remote Sens.* 15, 1221–1234. <https://doi.org/10.1109/JSTARS.2021.3123294>.
- Zhan, Q., Fan, Y., Xiao, Y., Ouyang, W., Lan, Y., Jin, Z., Yin, J., Zhang, L., 2018. Sustainable strategy: comprehensive computational approach for wind path planning in dense urban area. *Int. Rev. Spatial Plann. Sustain. Dev.* 6, 148–164. [https://doi.org/10.14246/irspsd.6.4\\_148](https://doi.org/10.14246/irspsd.6.4_148).

- Zhang, G., Ghamsi, P., Zhu, X.X., 2019a. Fusion of heterogeneous earth observation data for the classification of local climate zones. *IEEE Trans. Geosci. Remote Sens.* 57, 7623–7642. <https://doi.org/10.1109/TGRS.2019.2914967>.
- Zhang, R., Wang, Y., Hu, J., Yang, W., Chen, J., Zhu, X., 2021a. SAR4LCZ-net: A complex-valued convolutional neural network for local climate zones classification using Gaofen-3 quad-pol SAR data. *IEEE Trans. Geosci. Remote Sens.* 60, 1–16. <https://doi.org/10.1109/TGRS.2021.3137911>.
- Zhang, Y., Li, D., Liu, L., Liang, Z., Shen, J., Wei, F., Li, S., 2021b. Spatiotemporal Characteristics of the Surface Urban Heat Island and Its Driving Factors Based on Local Climate Zones and Population in Beijing, China. *Atmosphere (Basel)* 12, 1271. <https://doi.org/10.3390/atmos12101271>.
- Zhang, Y., Li, Q., Tu, W., Mai, K., Yao, Y., Chen, Y., 2019b. Functional urban land use recognition integrating multi-source geospatial data and cross-correlations. *Comput. Environ. Urban. Syst.* 78, 101374 <https://doi.org/10.1016/j.compenvurbsys.2019.101374>.
- Zhao, C., Jensen, J., Weng, Q., Currit, N., Weaver, R., 2019a. Application of airborne remote sensing data on mapping local climate zones: cases of three metropolitan areas of Texas, U.S. *Comput. Environ. Urban. Syst.* 74, 175–193. <https://doi.org/10.1016/j.compenvurbsys.2018.11.002>.
- Zhao, C., Jensen, J.L.R., Weng, Q., Currit, N., Weaver, R., 2020a. Use of local climate zones to investigate surface urban heat islands in Texas. *Glsci. Remote Sens.* 57, 1083–1101. <https://doi.org/10.1080/15481603.2020.1843869>.
- Zhao, J., Chen, G., Yu, L., Ren, C., Xie, J., Chung, L., Ni, H., Gong, P., 2023. Mapping urban morphology changes in the last two decades based on local climate zone scheme: a case study of three major urban agglomerations in China. *Urban Clim.* 47, 101391 <https://doi.org/10.1016/j.uclim.2022.101391>.
- Zhao, L., Oleson, K., Bou-Zeid, E., Krayenhoff, E.S., Bray, A., Zhu, Q., Zheng, Z., Chen, C., Oppenheimer, M., 2021. Global multi-model projections of local urban climates. *Nat. Clim. Chang.* 11, 152–157. <https://doi.org/10.1038/s41558-020-00958-8>.
- Zhao, Ma., Zhong, Zhao, Cao, 2019. Self-training classification framework with spatial-contextual information for local climate zones. *Remote Sens. (Basel)* 11, 2828. <https://doi.org/10.3390/rs11232828>.
- Zhao, N., Zhong, Y., Ma, A., 2020. Mapping local climate zones with circled similarity propagation based domain adaptation. In: IGARSS 2020 - 2020 IEEE International Geoscience and Remote Sensing Symposium. IEEE, pp. 1377–1380. <https://doi.org/10.1109/IGARSS39084.2020.9323191>.
- Zhao, Z., Shen, L., Li, L., Wang, H., He, B.-J., 2020c. Local climate zone classification scheme can also indicate local-scale urban ventilation performance: an evidence-based study. *Atmosphere (Basel)* 11, 776. <https://doi.org/10.3390/atmos11080776>.
- Zheng, Y., Ren, C., Shi, Y., Lau, K.K.-L., Yim, S.H.L., Lai, D.Y.F., Ho, J., Ng, E., 2015. Applying “local climate zone (LCZ)” into a high-density high-rise cities - A pilot study in Hong Kong. In: ICUC9-9th International Conference on Urban Climate Jointly with 12th Symposium on the Urban Environment, pp. 1–6.
- Zheng, Y., Ren, C., Xu, Y., Wang, R., Ho, J., Lau, K., Ng, E., 2018. GIS-based mapping of local climate zone in the high-density city of Hong Kong. *Urban Clim.* 24, 419–448. <https://doi.org/10.1016/j.uclim.2017.05.008>.
- Zhou, X., Okaze, T., Ren, C., Cai, M., Ishida, Y., Mochida, A., 2020a. Mapping local climate zones for a Japanese large city by an extended workflow of WUDAPT level 0 method. *Urban Clim.* 33, 100660 <https://doi.org/10.1016/j.uclim.2020.100660>.
- Zhou, X., Okaze, T., Ren, C., Cai, M., Ishida, Y., Watanabe, H., Mochida, A., 2020b. Evaluation of urban heat islands using local climate zones and the influence of sea-land breeze. *Sustain. Cities Soc.* 55, 102060 <https://doi.org/10.1016/j.scs.2020.102060>.
- Zhou, X., Yamamoto, M., Yan, S., Ishida, Y., Cai, M., Ji, Q., Makvandi, M., Li, C., 2022. Exploring the impacts of heat release of vehicles on urban heat mitigation in Sendai, Japan using WRF model integrated with urban LCZ. *Sustain. Cities Soc.* 82, 103922 <https://doi.org/10.1016/j.scs.2022.103922>.
- Zhou, Y., Wei, T., Zhu, X., Collin, M., 2021a. A parcel-based deep-learning classification to map local climate zones from Sentinel-2 images. *IEEE J. Sel. Top. Appl. Earth Obs. Remote Sens.* 14, 4194–4204. <https://doi.org/10.1109/JSTARS.2021.3071577>.
- Zhou, Y., Zhang, G., Jiang, L., Chen, X., Xie, T., Wei, Y., Xu, L., Pan, Z., An, P., Lun, F., 2021b. Mapping local climate zones and their associated heat risk issues in Beijing: based on open data. *Sustain. Cities Soc.* 74, 103174 <https://doi.org/10.1016/j.scs.2021.103174>.
- Zhu, X.X., Hu, J., Qiu, C., Shi, Y., Kang, J., Mou, L., Bagheri, H., Haberle, M., Hua, Y., Huang, R., Hughes, L., Li, H., Sun, Y., Zhang, G., Han, S., Schmitt, M., Wang, Y., 2020. So2Sat LCZ42: a benchmark data set for the classification of global local climate zones [Software and data Sets]. *IEEE Geosci. Remote Sens. Mag.* 8, 76–89. <https://doi.org/10.1109/MGRS.2020.2964708>.
- Zhu, X.X., Qiu, C., Hu, J., Shi, Y., Wang, Y., Schmitt, M., Taubenböck, H., 2022. The urban morphology on our planet – global perspectives from space. *Remote Sens. Environ.* 269, 112794 <https://doi.org/10.1016/j.rse.2021.112794>.
- Ziaul, Sk, Pal, S., 2018. Analyzing control of respiratory particulate matter on land surface temperature in local climatic zones of english bazar municipality and surroundings. *Urban Clim.* 24, 34–50. <https://doi.org/10.1016/j.uclim.2018.01.006>.
- Zonato, A., Martilli, A., di Sabatino, S., Zardi, D., Giovannini, L., 2020. Evaluating the performance of a novel WUDAPT averaging technique to define urban morphology with mesoscale models. *Urban Clim.* 31, 100584 <https://doi.org/10.1016/j.uclim.2020.100584>.